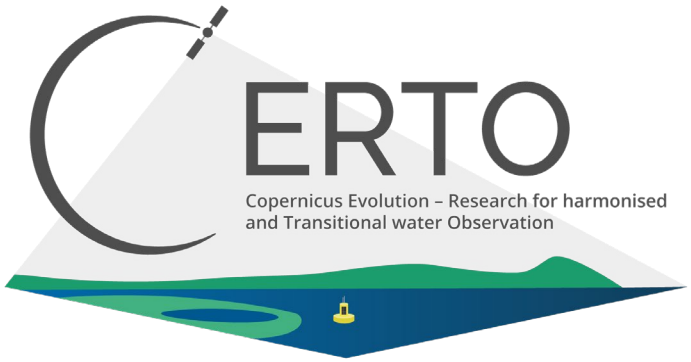

Horizon 2020

H2020 LC-SPACE-04-EO-2019-2020

Copernicus Evolution – Research for harmonised and Transitional-water Observation (CERTO)

Project Number: 870349

Deliverable No: D3.3		Work Package: 3	
Date:	18-MAY-2021	Contract delivery due date	31-MAY-2021
Title:	In situ sampling plan for years 2 and 3: characterisation of case study sites		
Lead Partner for Deliverable	University of Stirling		
Author(s):	Veloisa Mascarenhas, Dalin Jiang, Andrew Tyler, Peter Hunter, Evangelos Spyrakos, Mortimer Werther, Thomas Jackson, Liz Atwood, Victor Martinez Vicente, Gaia Gleratti, Steve Groom, Adriana Maria Constantinescu, Adrian Stanica, Vittorio Brando, Federica Braga, Gian Marco Scrapa, Federico Falcini, Vanda Brotas, Ana Brito, Giulia Sent, Federico Ienna, Carole Lebreton, Kerstin Stelzer, Mariano Bresciani, Monica Pinardi, Diana Vaiciute, Ruediger Roettgers, Hajo Krasemann		
Dissemination level (PU=public, RE=restricted, CO=confidential)			PU
Report Status (DR = Draft, FI = FINAL)			FI

Acknowledgements

This project has received funding from the European Union's Horizon 2020 research and innovation programme grant agreement N° 870349

Table of Contents

List of Acronyms

CERTO	Copernicus Evolution: Research for harmonised Transitional water Observation
USTIR	University of Stirling
USTIR*	Participation in campaign subject to covid19 travel restrictions
BC	Brockmann Consult
PML	Plymouth Marine Laboratory
FC.ID	FCiencias.ID, University of Lisbon
HZ Hereon	Centre for Materials and Coastal Research, Germany
CNR	The National Research Council of Italy
CNR*	Participation in campaign subject to covid19 travel restrictions
GeoEcoMar	The National Institute for Research and Development of Marine Geology and Geo-Ecology, Romania
OLCI	Optical Land and Cloud Imager
MSI	Multi Spectral Imager
OWT	Optical Water Type
WP	Work Package
PC	Phycocyanin Concentration
HPLC	High Performance Liquid Chromatography
CTD	Conductivity, Temperature, and Depth
Chl-*a*	Chlorophyll-*a*
IOP	Inherent Optical Properties
IS	Integrating Sphere
ISM	Inorganic Suspended Matter
CDOM	Coloured Dissolved Organic Material
AOP	Apparent Optical Properties
AOT	Aerosol Optical Thickness
NIR	Near Infrared
TSM	Total Suspended Matter
PSICAM	Point-source Integrating Cavity Absorption Meter
EO	Earth Observation
D3.3	Deliverable 3.3
GMT	Greenwich Mean Time
UTC	Coordinated Universal Time
WGS	World Geodetic System
OACs	Optically Active Constituents

1 Executive Summary

Objective 3 (In situ water characterisation) of the CERTO project aims to obtain new data from targeted in situ campaigns for key relevant transitional waters around Europe where data gaps are evident. Owing to spatial and temporal heterogeneity in regard to their optical properties, it is widely recognised that there is a significant lack in high quality data for calibration, validation and uncertainty characterisation activities in transitional environments.

The validation of satellite products and services is fundamental to characterising product uncertainties (required by modelers), building confidence in the products within the user community and influencing behavioural change that results in the wider adoption and exploitation of Copernicus Services. Whilst much effort has been invested in the calibration and validation of Earth Observation data from inland and coastal waters, the inherent temporal and spatial variability in the optical properties of the transitional environments lacks comprehensive coverage.

Deliverable 3.3 (D3.3) is a design plan for sampling the case study sites (Razelm-Sinoe Lagoon, Venice Lagoon, Tagus estuary, Plymouth Sound, Elbe estuary and Curonian Lagoon) that has been put together with local partners (GeoEcoMar, CNR, FC.ID, PML and BC and additional local practitioners where appropriate). Based on the expertise of local partners the sites are studied in terms of processes (tides, bathymetry, algal blooms, resuspension etc.) that influence the water optical properties in the systems.

The objective of the planned sampling campaigns is to characterise the case study sites with regard to their bio-optical properties. The strategy first employs an initial OWT classification (WP4) using time series of satellite imagery of case study sites to identify optical water classes and secondly identifies under sampled regions so as to better characterise the OWTs in terms of their biogeochemical and bio-optical properties. In order to identify the under sampled regions efforts have been made to gather information on the existing in situ databases for each of the sites and assess the need to sample areas that need more coverage. The plan prioritises the time of sampling campaigns in the contrasting locations to capture the maximum range in OWTs in each case study site.

The sampling plans for years 2 (2021) and 3 (2022) also aim to cover seasonal variations in the case study sites. Sampling time is scheduled to match satellite passes over the study sites to minimise time gaps between satellite imageries and in situ measured parameters. For year 2, we have taken account of the latest local intelligence on the progress of the Covid-19 situation and its mitigation. The plan for year 2 is the minimum that can be perceived to be achievable with existing logistical and other restrictions. The underlying assumption remains that travel will be more easily facilitated for year 3 (2022).

Chapters 3 to 8 are dedicated to each of the study sites and cover each of the sites in detail. Sections x.1 present an overview of existing bio-optical databases and information on the ongoing and historical data availability. Sections x.2 and x.3 involve results obtained from OWT analysis using Sentinel 3 and Sentinel 2 respectively, the optical water types identified, and spatial and temporal variability in the observed OWTs. Sections x.4 detail the various processes that influence the water optics in the systems. Sections x.5 identify the under sampled regions in the study sites based on existing bio-optical databases. Sections x.6 present proposed sampling times based on the local expertise and OWT analyses. Sections x.7 include proposed essential measurements and USTIR support as part of COVID19 mitigation. Chapter 9 presents an overview of the proposed sampling campaigns and USTIR support across all sites for years 2 (2021) and 3 (2021) in terms of instrumentation and post sampling analyses.

2 Introduction

CERTO (Copernicus Evolution: Research for harmonised Transitional water Observation) aims to provide solutions to harmonised water quality products in the three Copernicus services (C3S, CMEMS, CLMS) across a continuum of oceans, seas, coasts, estuaries, lagoons, rivers and lakes, to support industry, policy-makers and academia. This will be achieved by creating a prototype system that would be implemented in all the relevant Copernicus services. The system incorporates research on harmonised water optical classification approaches, improved atmospheric correction in optically complex waters and environmental indicators that can be applied to all these waters.

The existing data from Copernicus services have helped to define statistically Optical Water Types (OWTs) for lakes, off-shore and ocean waters at the global scale. It also demonstrates that many of these OWTs remain poorly characterised in terms of their biogeochemical and bio-optical properties and lack description of the most complex coastal and transitional water bodies. The available data are also compromised further by issues of data quality due to differences in sample and data collection and processing. CERTO will deliver timely innovation in the targeting of in situ data requirements by using an initial OWT classification (from WP4) in case study regions and the implementation of standardised protocols of in situ data collection. This will provide more tightly controlled data for better calibration and validation (cal/val) activities.

The main objectives of the in situ campaigns are to: (1) provide the biogeochemical and bio-optical data to characterise and validate the OWT definition and characterise the atmospheric aerosols at different times of the year, and validate the OWT classification and association algorithm validation work (WP4); and (2) provide data to validate and understand the atmospheric and adjacency effect corrections (WP5) across a range of atmospheric profiles and contrasting adjacent land-use types and water body characteristics. The sampling strategy is designed to provide a targeted approach to the in situ campaigns (through initial classification of OWT in WP4) to optimise data collection (in WP3) towards under-represented OWTs, coincident with Sentinel 2 and 3 data collection, thereby maximising the value of the data collected.

Given the impact on year 1 of the sampling campaign, we have taken account of the latest local intelligence on the progress of the Covid-19 virus and its mitigation for each site. With this in mind, the plan for year 2 is the minimum that can be perceived to be achievable with existing resources and logistical restrictions. The underlying assumption remains that travel will be more easily facilitated for year 3 (2022). In any case, the OWT approach does also provide the opportunity to share data between sites across common OWTs, which provides the opportunity to optimise sampling campaign strategies to maximise the return on sampling effort.

3 Case Study Area 1: Razelm-Sinoe Lagoon System

Razelm-Sinoe Lagoon System (Danube Delta – Black Sea)

Located in the southeast part of Romania, the Razelm-Sinoe Lagoon System represents the southernmost part of the Danube Delta Biosphere Reserve (North Long 44º 54' 6"; East Lat 28º 55' 19"). It is the largest lagoon in Romania, with an area of around 1000 km^2. The lagoon system is divided in two main units, Razelm and Sinoe, consisting of semi-independent lakes. Razelm has an area of 415 km^2 and a maximum depth of 3.2 m and Sinoe has 171 km^2 and a maximum depth of 2.2 m. Regarding the physical and administrative boundaries, the lagoon shares its southern, western and eastern limits with the Danube Delta Biosphere Reserve boundaries, the northwestern limit being represented by transitional areas (ponds, marshes, wetlands and channels). The lagoon was almost closed from the sea in the 1970's, to be a strategic resource of freshwater.

Nowadays, there is only one inlet, at Edighiol, that insures exchanges with the sea. Water level in the lagoon fluctuates with the Danube water level. Due to its hydrology and morphology, Razelm-Sinoe behaves like a large, eutrophic lake. Eutrophication, also enhanced by inputs from agricultural activities inland, affects water quality, mainly in the spring and summer, leading to a decrease in fish stocks. Fishing is one of the traditional occupations in the region and traditional food is one of the main tourist attractions in villages bordering the lagoon, along with ancient sites located in the west, and fishing and boat trips all around the lagoon. GeoEcoMar has been performing systematic water quality measurements beginning in 2010. So far, there is very little knowledge about the eutrophication phenomenon, its phenology and controlling factors in the Razelm lagoon and its effects on the ecosystem.

3.1 Current sampling locations and bio-optical monitoring

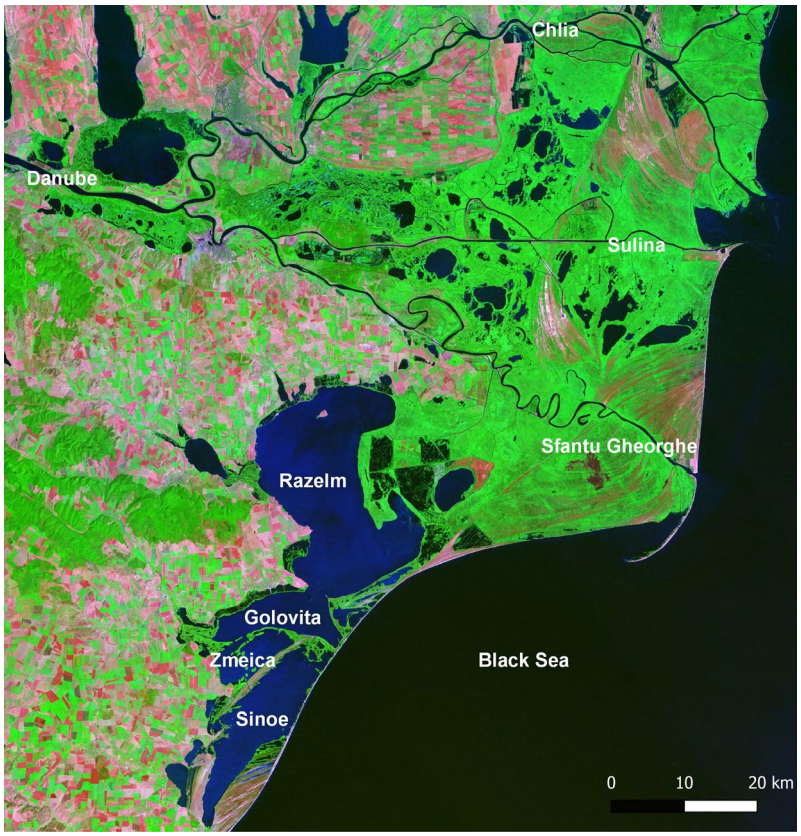

Figure 3.1: The Danube Delta and the Black Sea area with the Razelm-Sinoe lagoon system in the south.

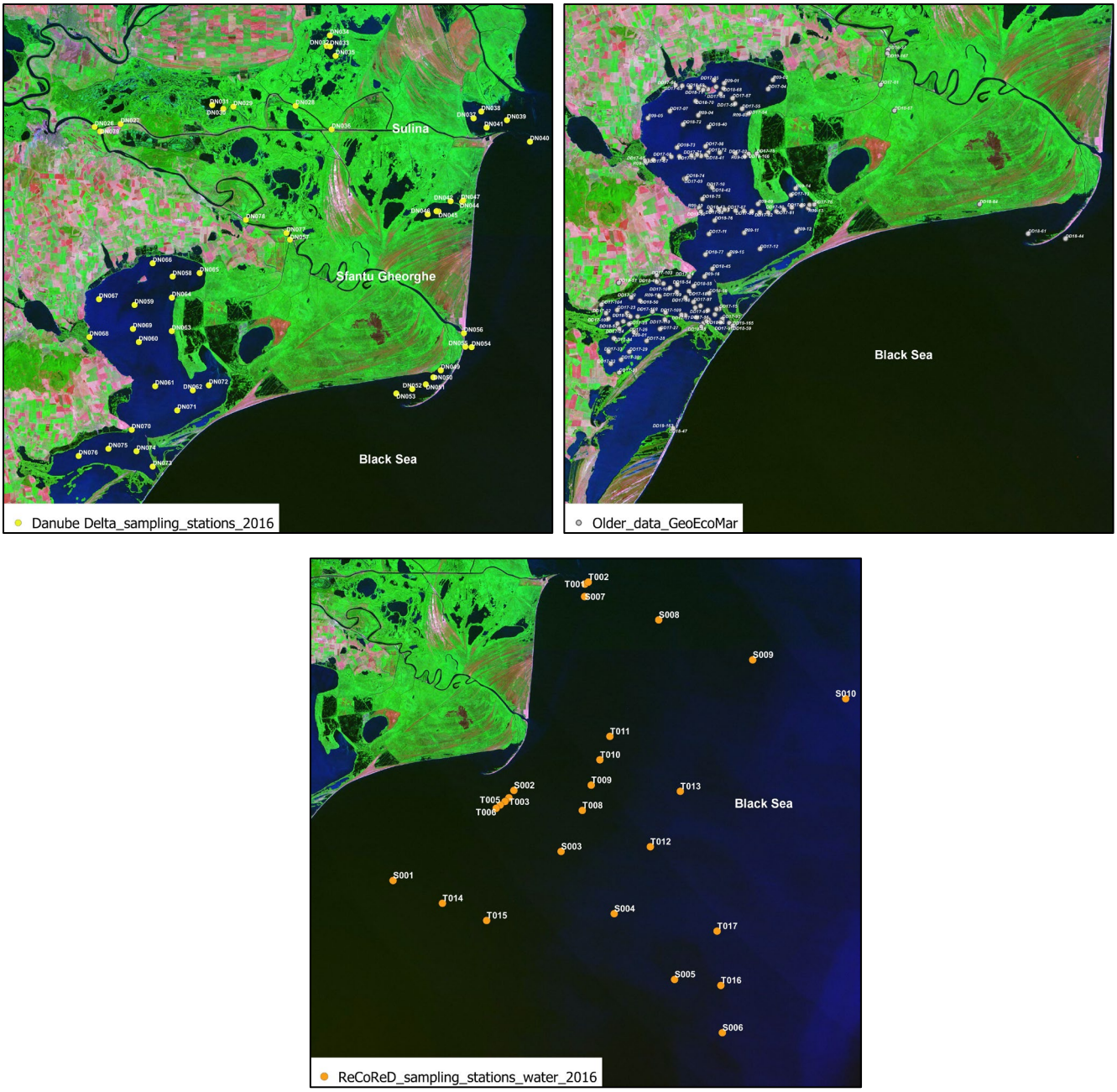

Figure 3.2: Sampling stations in the Danube Delta in 2016 (including Razelm and Golovita), sampling points in Razelm, Golovita and Zmeica (2009-2018) and the sampling points in the Black Sea during the ReCoReD project (2016).

3.1.1 Recent field campaigns

A field campaign was carried out in 2016 (23.05-03.06.2016), on board RV Istros, at high water levels. Water samples were collected from all the areas of the Danube Delta, from the main branches to lakes and lagoons. The locations in the Danube Delta that were chosen to sample include: the main channels (Sulina and Sfantu Ghoerghe), cut meanders (Old Danube on Sulina, Mahmudia and Dunavat), secondary channels or canals, lakes of different sizes and different degree of connectivity to the main hydrographic network (Matita, Fortuna, Rosu and Rosulet), and lagoons (Musura, Sahalin, Razelm and Golovita).

The Black Sea marine cruise was carried out in May 2016 (4-12.05.2016), on board RV Mare Nigrum, as part of the EuroFleets 2 funded project ReCoReD (Reconstructing the Changing Impact of the Danube on the Black Sea and Coastal Region). During the cruise the water discharge of the Danube was close to annual. Average wind conditions were stable, with dominant direction from N-NE or N-NW, with a low average speed (<10 m/s). Surface samples were collected from all stations (T or S stations). Water at different depth were collected in all S stations. The locations in the Black Sea were chosen to sample the Danube plume, in both its lateral and longitudinal extent to the east and south, respectively, and the extent in depth, from the surface, down to -80 m.

In the Danube Delta, the surface waters were sampled from boats, directly into plastic bottles. Water sampling in the Black sea was done with a 5 litre Niskin bottle system, equipped with a CTD, at depths were the chl-a and turbidity values were changing. Sub-samples were then filtered for Total Suspended Matter (TSM), chlorophyll-a, phycocyanin, particulate absorption, CDOM and particle size. All samples were preserved at appropriate temperatures for analysis. Both AOPs and IOPs were measured (details in the table 3.1).

3.1.2 Historical bio-optical data from GeoEcoMar

Data on chlorophyl-a, TSM, turbidity, Secchi depth and physical parameters of the water, were measured in Razelm, Golovita and Zmeica (Razelm-Sinoe lagoon system) by GeoEcoMar since 2009, but mostly from 2017 to 2019.

Table 3.1: Summary of in situ bio-optical data available in the Danube

Campaign	Area sampled	Sampling platform	OACs	IOPs	AOPs
23 May - 03 June 2016	Danube Delta, including Razelm, Golovita	RV Istros, small boats	Chl-a, PC, TSM, CDOM, particle size	$a_{CDOM}(\lambda)$, $a_{NAP}(\lambda)$, $a_{ph}(\lambda)$, c (z, λ), a (λ), bp (z, λ), b_{bp} (z, λ)	$R_{rs}(\lambda)$, $L_u(\lambda)$, $L_{sky}(\lambda)$, $E_d(\lambda)$, SZ Secchi depth
4 – 12 May 2016	Black Sea, offshore Danube Delta	RV Mare Nirum	Chl-a, PC, TSM, CDOM, particle size	$a_{CDOM}(\lambda)$, $a_{NAP}(\lambda)$, $a_{ph}(\lambda)$, c (z, λ), a(λ), bp (z, λ), b_{bp} (z, λ)	$R_{rs}(\lambda)$, $L_u(\lambda)$, $L_{sky}(\lambda)$, $E_d(\lambda)$, SZ Secchi depth
August 2009	Razelm, Golovita, Zmeica	RV Istros, small boats	TSM, turbidity		
May - June 2017	Razelm, Golovita, Zmeica	RV Istros, small boats	Chl-a , TSM, turbidity		Secchi depth
May 2018	Razelm, Golovita	RV Istros, small boats	Chl-a , TSM, turbidity		
Sptember 2019	Connecting channels	RV Istros, small boats	TSM		

3.2 Sentinel 3 OWT Analysis

3.2.1 Sentinel 3 OLCI dataset

- OLCI 300m data (2019-2021) processed with the POLYMER processor and selected pixels as the training dataset
- These were selected using a regular subsampling of the 300m data in the along scan and cross scan directions
- All visible wavelengths were used (400, 412, 443, 490, 510, 560, 620, 665, 674, 681 and 709nm)
- Prior to clustering the data, the spectra were standardised using a standard scalar and then applied a principal component analysis (PCA) to reproject the spectra
- Clusters created using Euclidian distance in principle-component-space

3.2.2 Sentinel 3 OWT classes

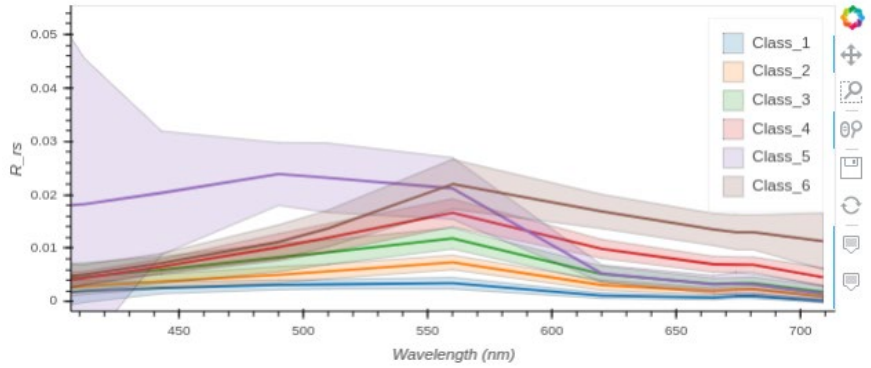

Figure 3.3: Derived optical water classes for the Danube using Sentinel 3.

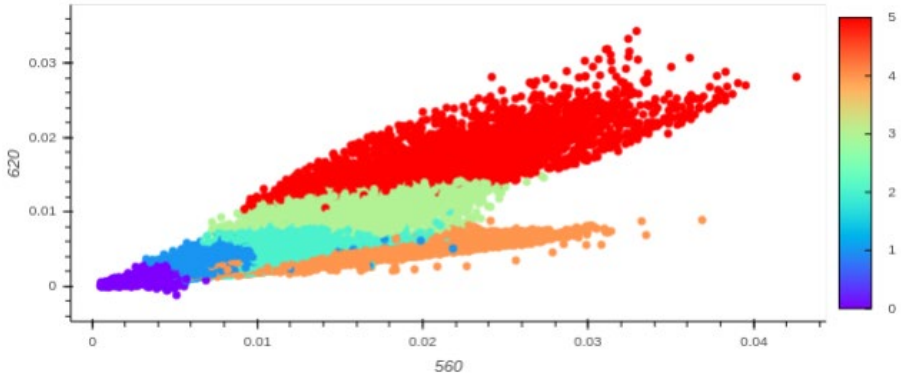

Figure 3.4: Dominant optical water class for each training data point in 2-band Rrs space for the Danube using Sentinel 3. Add one to the colourbar values for the OWT (colourbar is 0 indexed).

3.2.3 Sentinel 3 OWT spatial analysis

This class set was then applied to OLCI data from 2019 to 2021. The resulting memberships (daily products) were then used for a number of different types of analysis.

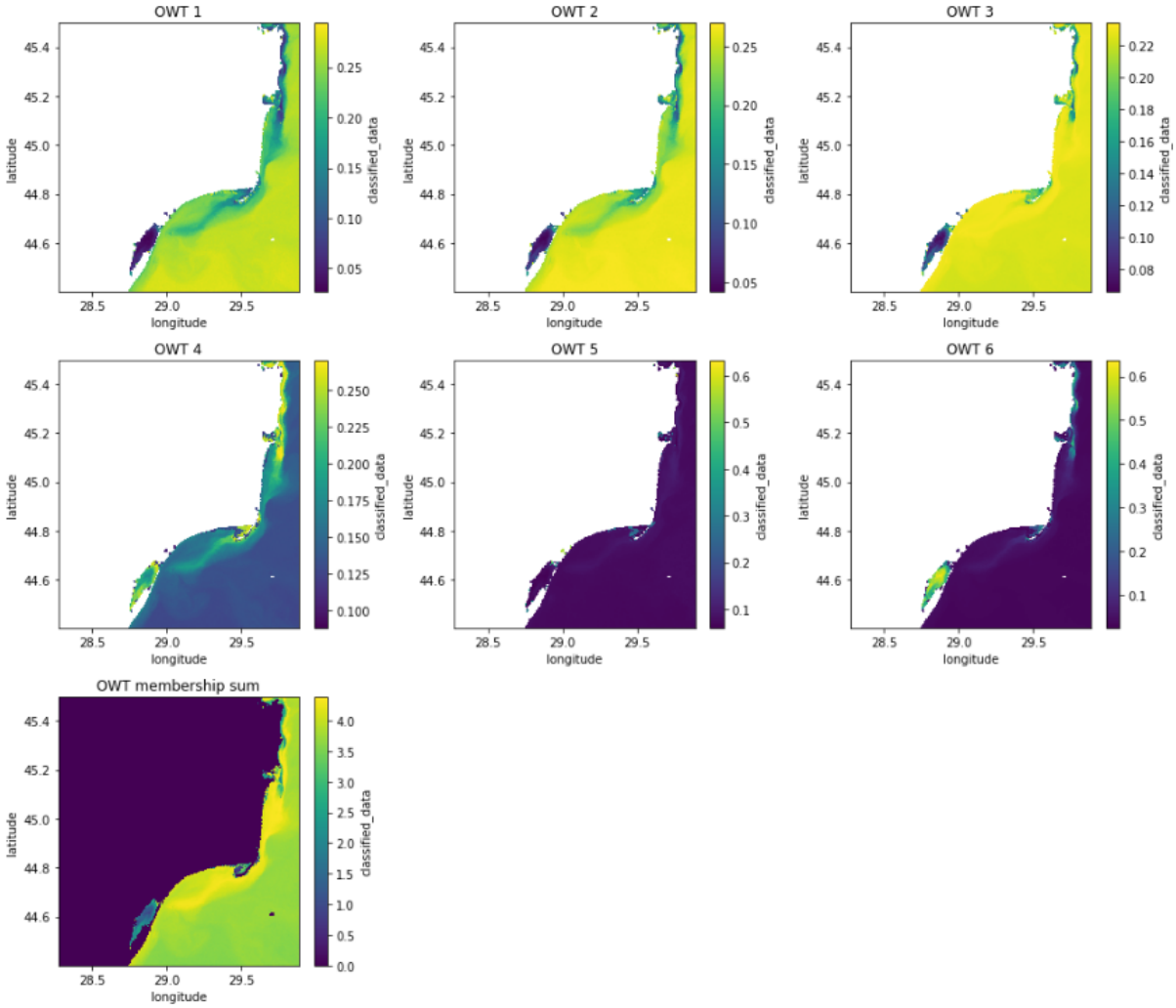

Figure 1.5: Example of clusters applied to data from 2020-08-08 for the Danube using Sentinel 3. Membership values to each class are shown normalised to the total pixel membership (which is also shown in the last plot).

3.2.4 Sentinel 3 entropy filter and edge detection

The first analysis combines entropy filter and edge detection to try to locate the boundaries between regions of change in the optical water type structure. Where boundaries occur for more than one water class, we consider this to be a 'strong edge' that is then stored as a variable. An example of this for a single image is shown in Figure 3.6.

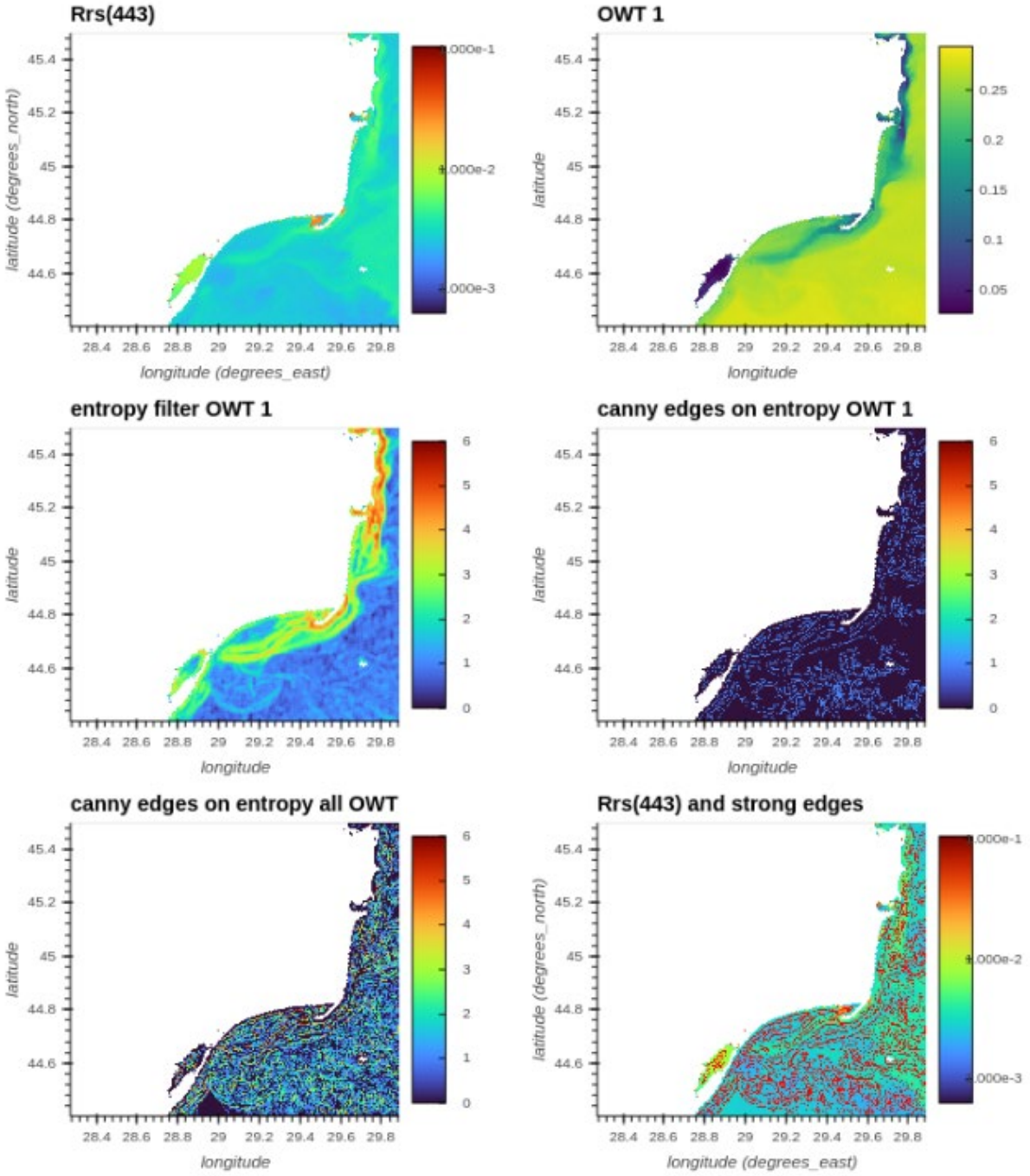

Figure 3.6: Example of entropy filter and edge detection application to data from 2018-08-08 in the Danube using Sentinel 3.

Stacking these results across all data available for each month we can look for persistent regions of change in optical water type membership structure (Figure 3.7).

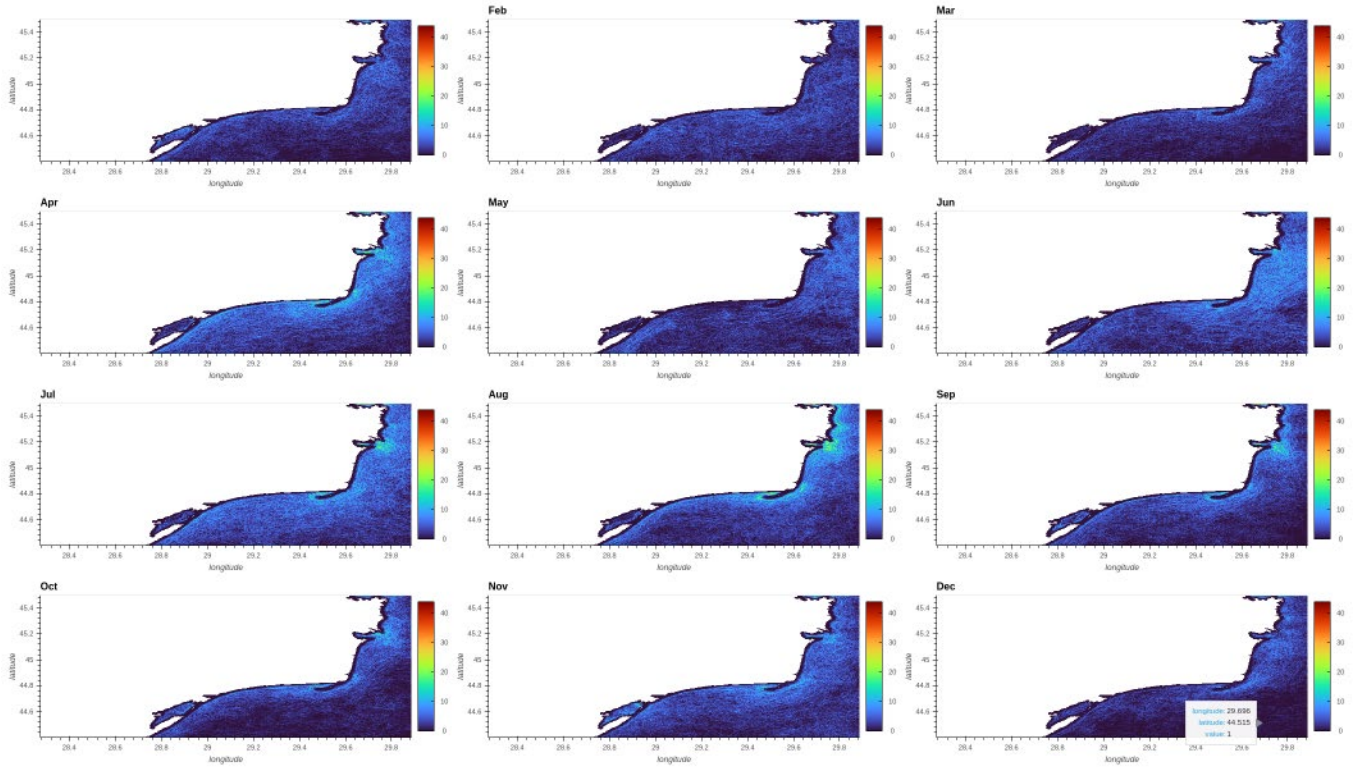

Figure 3.7: Stacked strong front incidence across all data available for a given month (across all years)

The strongest front incidence (could have some sampling bias due to clearer skies) appears to be in April, July, August and September. There are regions of interest highlighted around the St. George river branch mouth and Laguna Sacalin, as well as Danube-Sulina branch flowing into Musura Bay.

We can then stack this information across all available times (Figure 3.8) and by month (Figure 3.9) and visualise as maps. The colour bar does not line up properly (to be fixed) but it is interesting to see the regions of change /dominance.

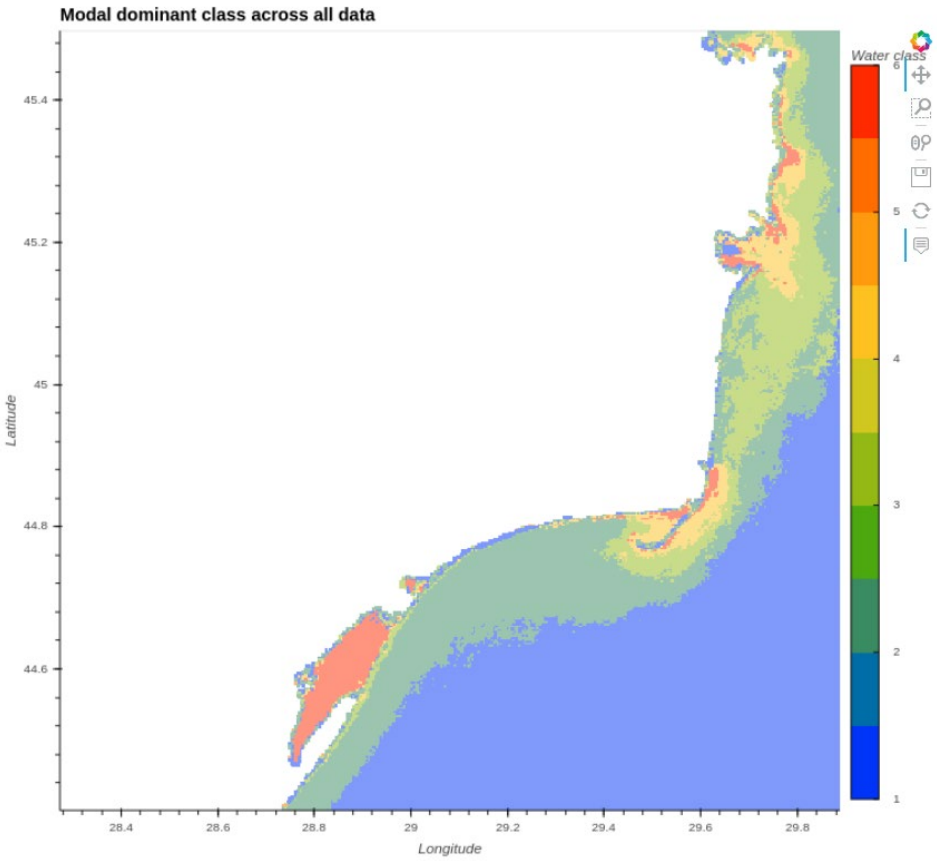

Figure 3.8: Dominant optical water class across all data in the Danube using Sentinel 3.

3.2.5 Sentinel 3 OWT temporal analysis

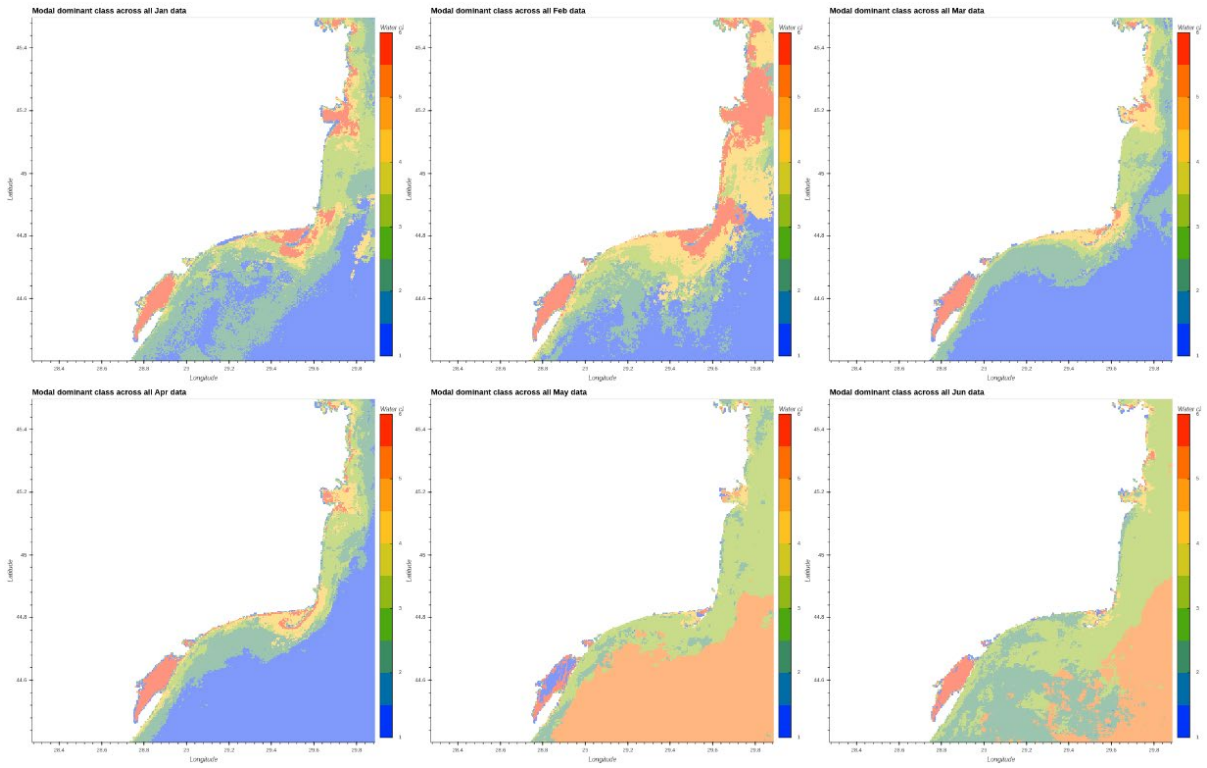

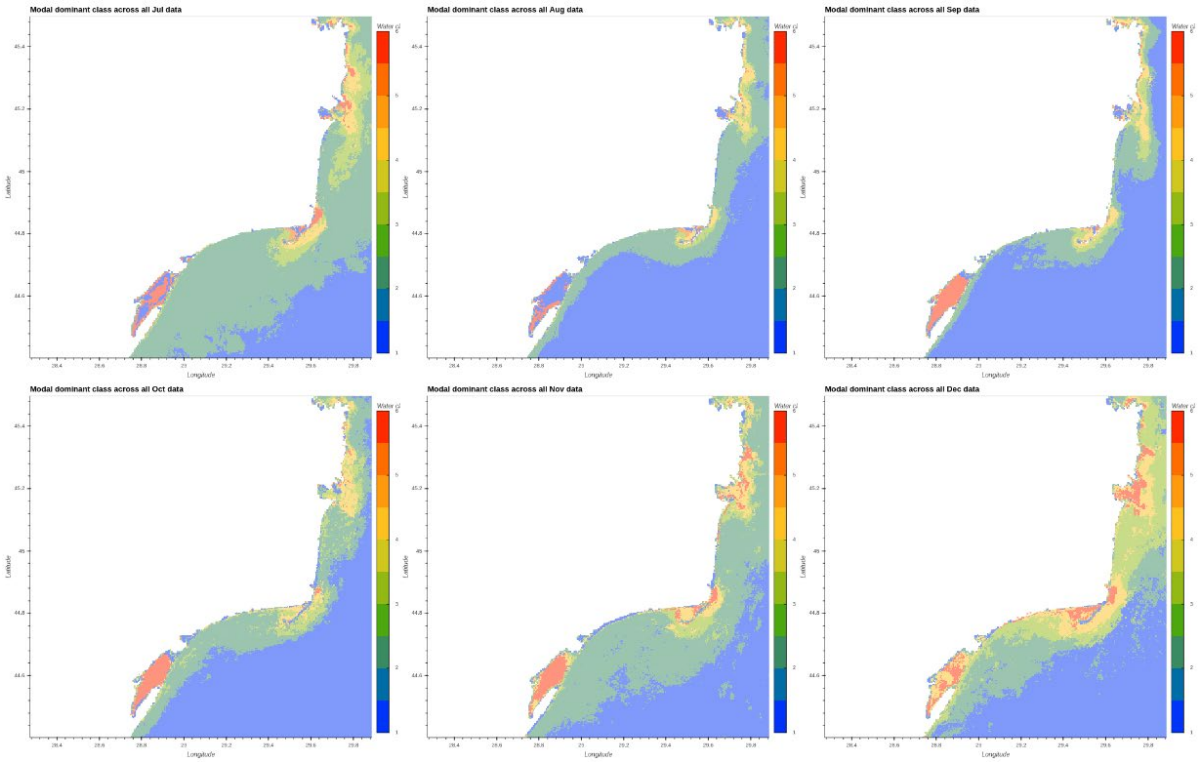

Figure: 3.9: (rows, left to right) Temporal analysis of OWT in the Danube from January to December

3.2.6 Revised Sentinel 3 OWT Analysis

The OLCI dataset has been updated to cover a longer time period that better matches that of the Sentinel 2 MSI dataset, thus cluster analyses for the OLCI dataset is being updated as follows:

- OLCI 300m data processed with the POLYMER processor: 2016-04-26 to 2021-03-08
- Training dataset built using regular subsampling along scan and cross scan directions, wavelengths used were: 400, 412, 443, 490, 510, 560, 620, 665, 674, 681, 709, 754, 779, 865 and 885 nm
- Winter month exclusion from training dataset (based on incident light level <30° calculated using NOAA solcalc): November-January

Analysis on the new OLCI dataset is ongoing and will be made available to the Danube teams.

3.3 Sentinel 2 OWT analysis

3.3.1 Sentinel 2 MSI dataset

- MSI 60m data processed with POLYMER processor: 2016-11-01 to 2020-12-31
- Training dataset built using regular subsampling along scan and cross scan directions, wavelengths used were: 443, 490, 560, 665, 705, 740, 783, 865, 1610 and 2190 nm
- Winter month exclusion from training dataset (based on incident light level <30° calculated using NOAA solcalc): November-January
- Prior to clustering, spectra were standardised using a standard scalar and then principal component analysis (PCA)
- Clusters created using Euclidian distance in principle-component-space

3.3.2 Sentinel 2 OWT classes

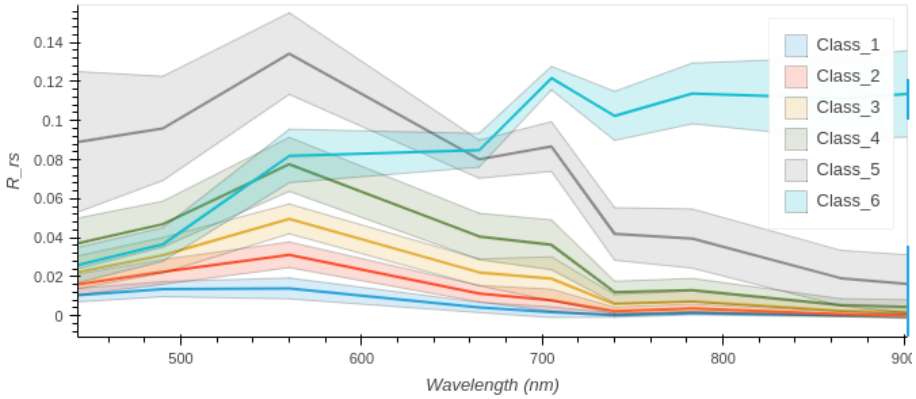

Figure 3.10: Optical Water Classes obtained in the Danube using Sentinel 2

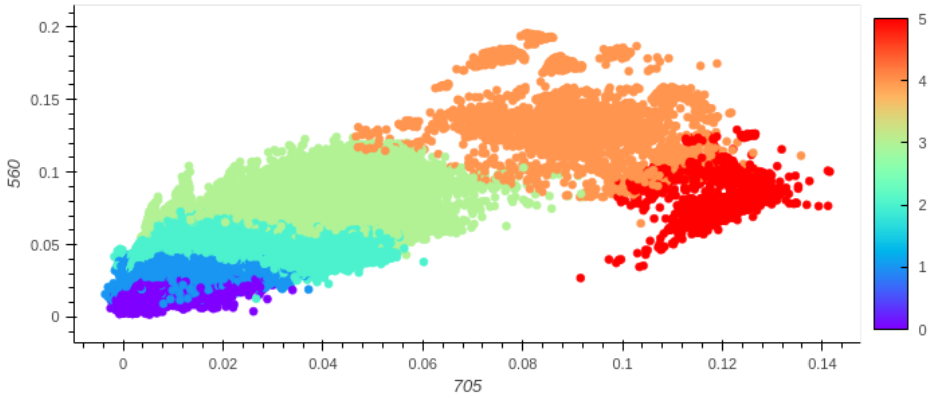

Figure 3.11: Optical Water Classes in 2 dimensional space using Sentinel 2. Add one to the colourbar values for the OWT (colourbar is 0 indexed).

3.3.3 Sentinel 2 OWT Spatial analysis

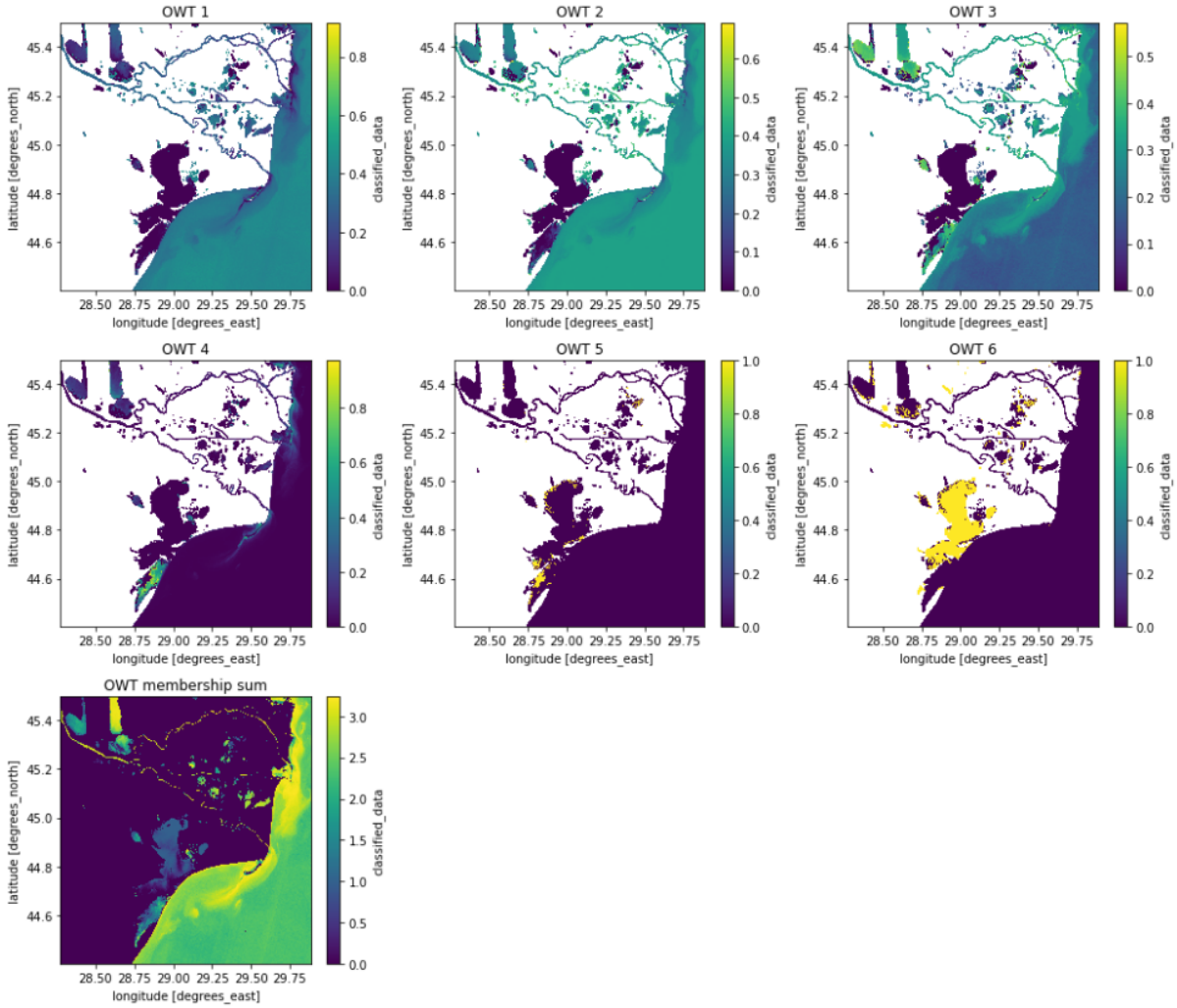

Figure 3.12: Spatial distribution of OWT classes for 2020-09-14 using Sentinel 2

3.4 Influence of local processes

The Razelm-Sinoe Lagoon system is not subject to tides. The Black Sea is a micro-tidal sea, with a maximum tide of 12 cm. The climate in the area is temperate continental, with Pontic influences and temperatures typically ranging from -20°C in winter to 36°C in summer (recorded at Gura Portitei meteorological station, on the shores of the lagoon). Annual rainfall ranges from 350 to 400mm/year, as recorded at the same station.

Usually, water bodies within the lagoon are partly or entirely frozen during winter due to long periods with negative temperatures in the months of December – February. Characteristic for the area are strong winds from a N and NE direction that are predominant from September to May and winds from the S and SE that are predominant in the summer months, such that exposed lagoon shores experience considerable waves generated over fetch distances of several kilometers.

Water depths within the lagoon system have been measured as < 2.2 m in Sinoe and < 3.2 m in Razelm (see bathymetry map, Figure 3.13) and varies with the water level of the Danube river. Maximum depth in Razelm reaches 3 m approximately 750 m offshore of the Cape Dolosman site, and at Histria the maximum depth offshore reaches 1.75 m at approximately 2 km offshore (see bathymetry map). Wind-driven resuspension is a very common phenomenon in the Razelm-Sinoe Lagoon, as well as in other near coast areas of the Danube Delta. Algal blooms occur from spring until Autumn, with a maximum in September.

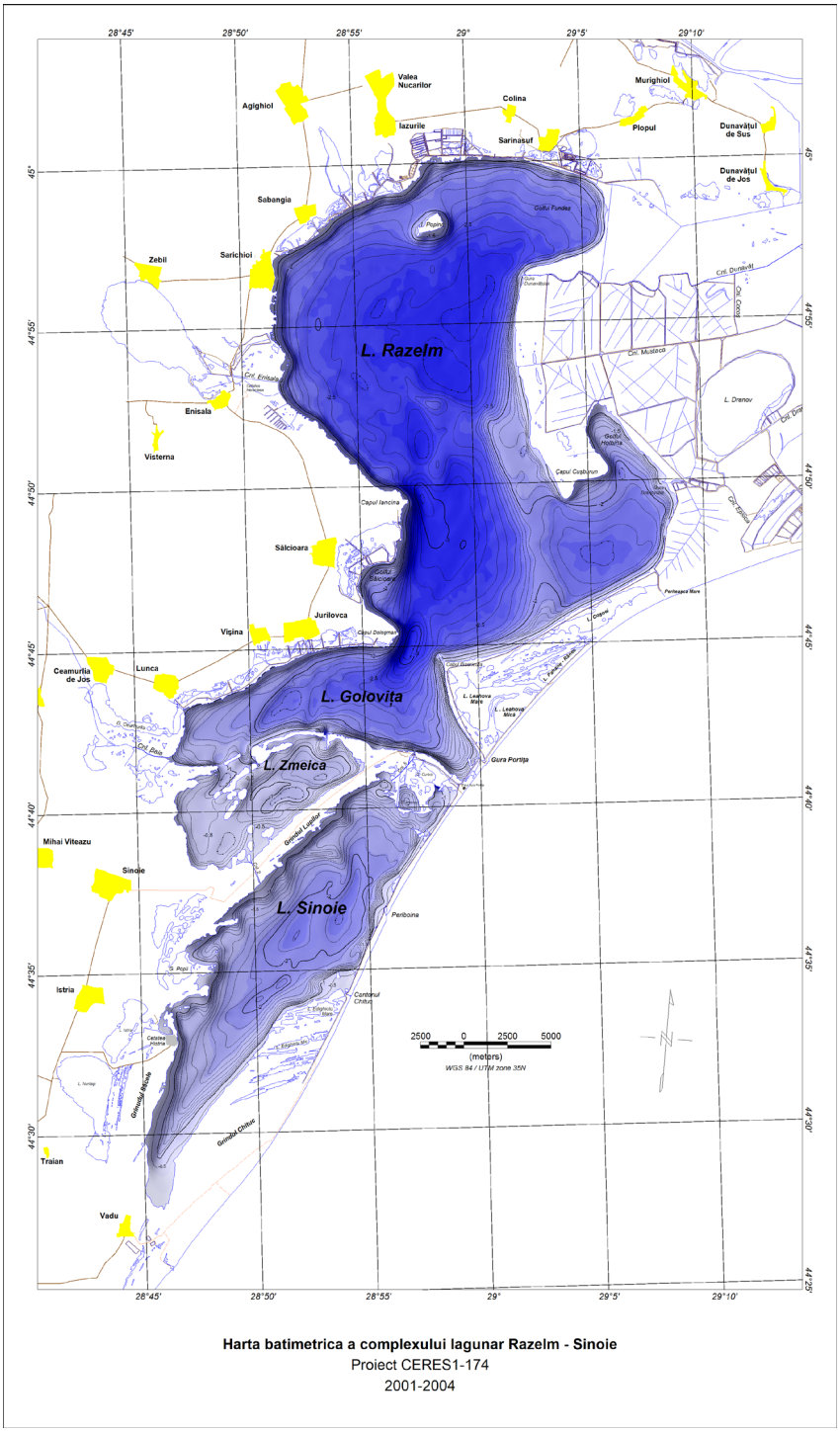

Harta batimetrica a complexului lagunar Razelm - Sinoie
Proiect CERES1-174
2001-2004

Figure 3.13: Bathymetry map of Razelm-Sinoe Lagoon system (from Dimitriu et al., 2008)

Figure 3.14: (left) Wind driven resuspension in the shallow waters of the Razelm-Sinoe Lagoon system and water and sediment inputs from the Danube through channels in the east (8th April 2018) and (right) algal blooms (21st August 2019) – Sentinel 2 images

3.5 Identification of under sampled regions

3.5.1 Satellite (Sentinel 2) and in situ match up analysis

Based on historical sampling locations and bio-optical data availability, the in situ bio-optical data available in the Danube area was insufficient (evident in table 3.1) to produce any matchups.

3.6 Proposed ideal sampling time for year 2 (2021) in Danube

For aiding the validation and interpretation of satellite data, the ideal sampling time would be at the same moment as the satellite overpass. This is not possible in most cases so we propose that the in situ measurements should be taken within a 3-hour window either side of the satellite overpass so that the influence of tides and weather changes are reduced.

- Time of sampling – May/June 2021
- Sampling duration – 1 week
- Sampling platform availability – logistics arranged
    - RV ISTROS – with the SO-RAD system
    - IRIS research boat - to go inside the lagoon
    - Catamaran - to go inside the lagoon
- Campaign participants – GeoEcoMar, USTIR*

Table 3.2: Sentinel 3 passes over Danube in May and June 2021

	May (date)	May (time) UTC	June (date)	June (time) UTC
SENTINEL 3	daily	07:45 - 08:45	daily	07:45 - 08:45

Table 3.3: Sentinel 2 passes over Danube in May and June 2021

Satellite platform	Orbit	Date	Time (UTC)
SENTINEL2A	30606	2021/05/02	9:07
SENTINEL2A	30749	2021/05/12	9:07
SENTINEL2A	30892	2021/05/22	9:07
SENTINEL2A	31035	2021/06/01	9:07
SENTINEL2A	31178	2021/06/11	9:07
SENTINEL2A	31321	2021/06/21	9:07
SENTINEL2B	21769	2021/05/07	9:07
SENTINEL2B	21912	2021/05/17	9:07
SENTINEL2B	22055	2021/05/27	9:07
SENTINEL2B	22198	2021/06/06	9:07
SENTINEL2B	22341	2021/06/16	9:07
SENTINEL2B	22484	2021/06/26	9:07

3.7 Covid19 Mitigation: proposed essential measurements and USTIR support

University of Stirling will provide support in terms of instrumentation and post-sampling analysis (for sites that need support). In year 2 (2021) participation by USTIR in the sampling campaigns will be subjected to Covid19 travel restrictions. However, the plan is to replicate a small percentage of samples for Chl-a, TSM, PC and particulate absorption from all sites. Shipping of the samples to USTIR will be arranged accordingly. USTIR will arrange a shipment and a rota of required instrumentation, in association with FC.ID, across the different sites in Europe. Intercomparison experiments therefore are planned in year 3 (2022) with a possibility to participate onboard with a suite of USTIR instrumentation across the sites in the UK and Europe.

Table 3.4: Proposed essential measurements and USTIR support for year 2 (2021) and 3 (2022) in Danube GeoEcoMar-USTIR indicates GeoEcoMar will collect samples and USTIR will analyse them.

	Parameters to be measured (essentials in bold)	**Instrumentation/ Sample Analysis 2021**	**Instrumentation/ Sample Analysis 2022**
Biogeochemistry	Chlorophyll a, Chl-a	GeoEcoMar	GeoEcoMar
	Phycocyanin, PC	GeoEcoMar-USTIR	GeoEcoMar-USTIR
	Total Suspended Matter, TSM	GeoEcoMar	GeoEcoMar
AOPs	**Remote sensing reflectance, R_{rs}**	GeoEcoMar	GeoEcoMar
	Diffuse attenuation coefficient, K_d	USTIR (USSIMO)	USTIR (USSIMO)
	Secchi Disk Depth, Z_{SD}	GeoEcoMar	GeoEcoMar
IOPs	**Total absorption coefficient, a**	---	USTIR (ac-s)
	Absorption coefficient of phytoplankton, a_{ph}	GeoEcoMar-USTIR	GeoEcoMar-USTIR
	Absorption coefficient of non-algal particles, a_{nap}	GeoEcoMar-USTIR	GeoEcoMar-USTIR

	Coloured dissolved organic matter, CDOM	GeoEcoMar	GeoEcoMar
	Backscattering coefficient, b_b	USTIR (sc-6)	USTIR (sc-6)
	Beam attenuation coefficient, c	---	USTIR (ac-s)
Physical Parameters	Water temperature	GeoEcoMar	GeoEcoMar
	Salinity	GeoEcoMar	GeoEcoMar
	Turbidity	GeoEcoMar	GeoEcoMar
	Water depth	GeoEcoMar	GeoEcoMar
Atmospheric parameters	Wind speed	GeoEcoMar	GeoEcoMar
	AOT	USTIR (Microtops)	USTIR (Microtops)

3.8 References

Dimitriu, R.G., Oaie, G., Gomoiu, M.T., Begun, T., Szobotka, S., Radan, S., C., Fulga, C., 2008, O Caracterizare interdisciplinară a stării geoecologice a complexului lagunar Razelm - Sinoie la începutul secolului XXI, GEO-ECO-MARINA 14/2008 – SUPLIMENT NR. 1

4 Case Study Area 2: Venice Lagoon

Venice Lagoon (Northern Adriatic)

The Venice Lagoon with a total surface of ca. 550 km^2 is a very shallow coastal environment with a mean depth of 1 m and a spring-tidal range up to 1 m (Figure 4.2). It maintains a connection to the northern Adriatic Sea through the inlets of Lido, Malamocco, and Chioggia, and the exchange of water through the inlets in each tidal cycle is about a third of the total volume of the lagoon. The northern Adriatic Sea is a shallow and semi-enclosed regional sea, influenced by the plumes of large rivers (Po, Adige, Piave, Tagliamento). The Venice Lagoon constitutes a complex system of major historical and environmental interests that is under the pressure of anthropogenic factors and global scale processes bringing about noticeably rapid changes to the environment. Its heterogeneous morphology is characterised by a complex pattern of major (navigable) and minor channels, salt marshes, tidal flats and islands, which have been artificially modified by man throughout the centuries. In response to the increasing frequency of floods determined by natural and anthropogenic subsidence and sea level rise, the last significant intervention is the construction of a system of mobile barriers at the tidal inlets, known by the acronym of MoSE.

The project entails building mobile barriers at the bottom of each inlet that will rise and separate the lagoon from the sea when the expected tidal elevation becomes critical. In a future scenario of rising sea level, the MoSE will then transform the lagoon in a regulated system, due to the intensification of management actions, which will result in changes in hydrodynamics and in the transport of sediments, contaminants and organisms. Like all shallow water transitional areas, the Venice Lagoon is a constantly evolving environment, where the exchanges at the tidal inlets drive biogeochemical and morphological processes in dynamic key areas such as mudflats, wetlands, and the dense network of channels influencing coastal erosion and accretion patterns. The knowledge of the processes at the lagoon-sea interface represents a focal point for the safeguard of Venice, the lagoon and the functionality of the ecosystem.

In situ monitoring in the lagoon, the inlets and the coastal waters is carried out by several agencies and a regional observing system to support environmental monitoring and reporting is being currently setup. In the framework of national and international projects, CNR-ISMAR has been involved in the integration of large

dataset of experimental observations (hydrodynamics, sediment transport, optical water characterisation) with analytical and numerical models able to provide a synthetic vision and to predict the evolutionary trends in the medium and long term. ISMAR is also supporting the management, monitoring and definition of strategies for the safeguard of the lagoon during the operational phase of the mobile gates.

Figure 4.2: Case study area – the Lagoon of Venice.

4.1 Current sampling locations and bio-optical monitoring

During the last years, a sampling monitoring programme has been set up and carried out in the Lagoon of Venice with the aim of investigating radiometric and biogeophysical variability of optically deep and shallow waters. The surveys were perfomed mainly during the overpasses of Landsat 8 and Sentinel-2 to gather data for cal/val activities. Ancillary data from monitoring stations (tidal level, wind speed and direction, water quality, etc.) were also considered in the analysis. In the next paragraphs, an overview of the main types of fieldwork activities (sampling locations, measured parameters, etc.) are reported.

4.1.1 ACQUA ALTA Oceanographic Tower

The Acqua Alta Oceanographic Tower (AAOT lat. 45.314° N and lon. 12.508° E) is located 8 nautical miles off the Lagoon of Venice, Italy, in the northern Adriatic Sea. The site is characterised by optically complex waters, moderately dominated by sediments. It is a steel tower with a platform containing an instrument house to facilitate the measurement of meteo-climatic parameters and ocean colour properties under exceptionably stable conditions. Since 1995 has been used to support ocean colour validation activities through a comprehensive collection of bio-optical data (Zibordi et al. 2002, 2006). It is included in the AERONET and AERONET-OC networks (Figure 4.3), which respectively perform atmospheric measurements for retrieving aerosol optical properties and marine radiometric measurements for determining normalised water-leaving radiances $L_{WN}(\lambda)$, at various center wavelengths in the visible and near-infrared spectral (Holben et al. 2001; Zibordi et al. 2009).

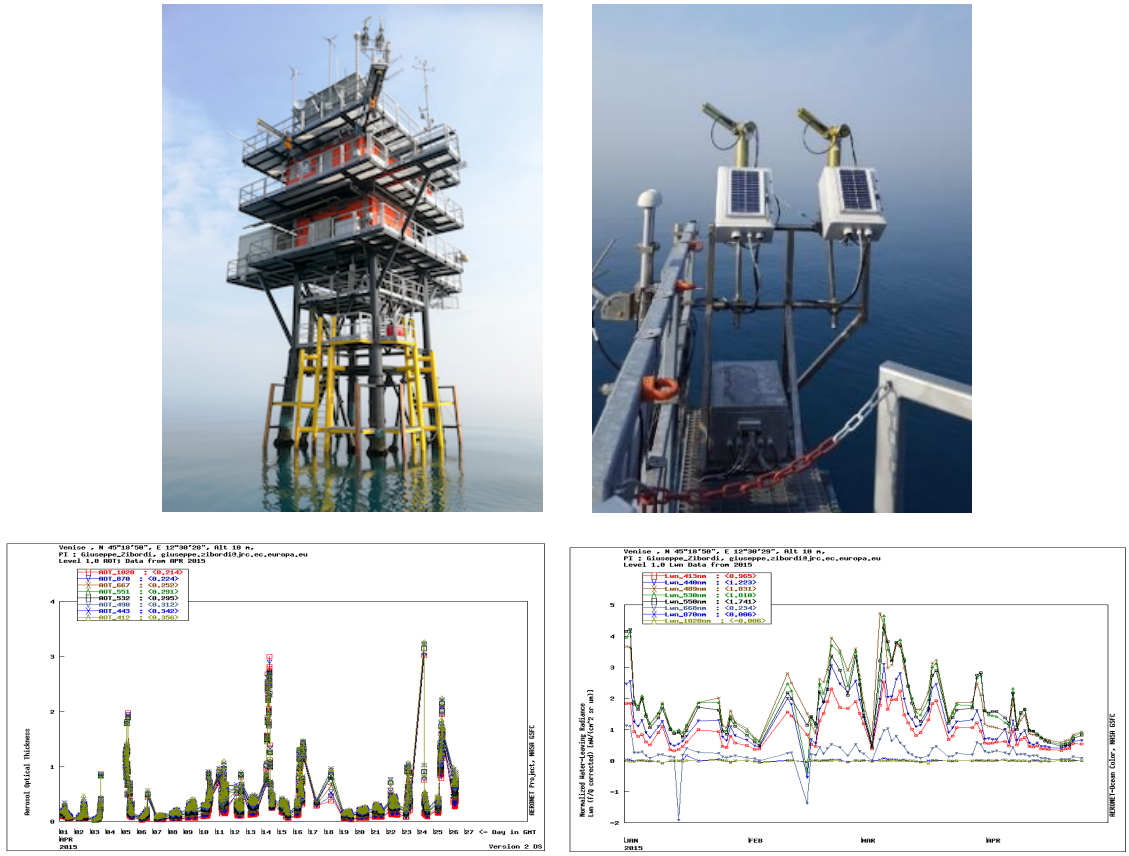

Figure 4.3: a) Acqua Alta Oceanographic tower, b) CIMEL Electronique (Paris, France) CE-318 automated sun photometers of the AERONET and AERONET-OC systems; c) aerosol optical properties and d) normalised water-leaving radiances $L_{WN}(\lambda)$, measured at AAOT.

4.1.2 Expeditive daily stations

Starting from 2017, expeditive campaigns have been performed in the Lido tidal inlet at the time of Sentinel-2 overpasses. The 8 stations are distributed along a transect from the lagoon to the open sea, through the channel network, with water depth ranging from 6 to 12 meters (Figure 4.4). The measurements are acquired in different meteorological and tidal conditions and provide sufficient spatial resolution to investigate the suspended sediment transport. The transect could be considered as a reference area: inside the inlets water velocities are high (over 1 m s^{-1}) and the vertical shear creates enough turbulence to mix the water column. The main circulation forcing factors are the tide (± 50 cm during spring tide) and the wind.

Each campaign is carried out within 1 hour and the total distance between the 8 stations is about 4 km: this permits to maintain a maximum time difference of 1 h between satellite and *in situ* data collection. At each station, above water remote sensing reflectances were measured with the WISP-3 spectroradiometer (Water Insight), CTD profiles were performed with Ocean Seven 316Plus multi-parameter probe (Idronaut) equipped with optical backscattering sensor for the measurement of turbidity at 880 nm (Seapoint) and water transparency was assessed with a Secchi Disk. Discrete surface water samples were also collected and subsequently filtered in the laboratory, to estimate the concentration of chlorophyll-a (chl-a) and Total Suspended Matter (TSM) with the determination of the organic and inorganic components.

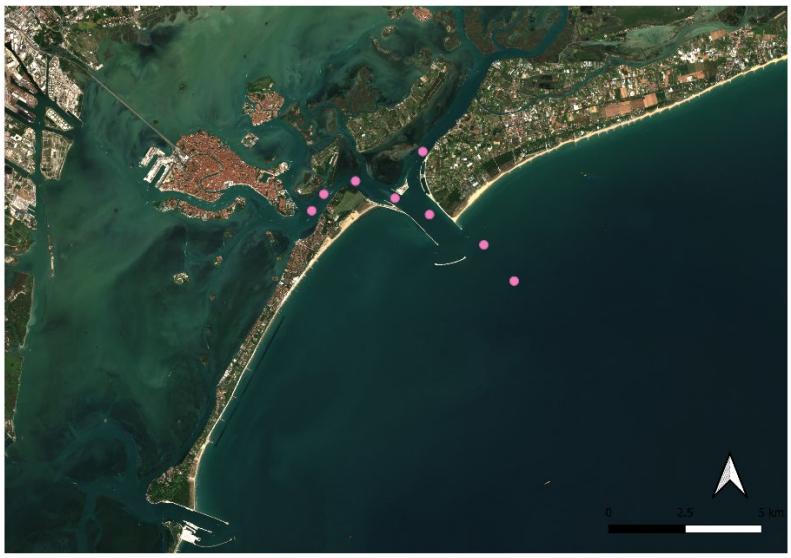

Figure 4.4: Study area with location of the expeditive daily sampling points at the Lido inlet.

4.1.3 Other daily surveys, summer

During the summer, the inner parts of the lagoon are usually affected by phytoplankton blooms and excessive growth of nuisance macroalgae with a consequent worsening of the trophic conditions. The intensity of these phenomena mainly depends on nutrient concentrations, which may be related to river discharges and the amount of rainfall during the previous weeks, and on the lower water exchanges and dynamics in the shallow areas of the lagoon. The selected areas (Figure 5) exhibit a mean deep of about 80–100 cm on the mean water level, but the bottom is not always visible. Bottom visibility is mainly influenced by seasonal and meteorological environmental conditions, as well as by anthropogenic activities (clam harvesting, boat traffic, etc).

The stations in the central part of the lagoon show poor water renewal due to limited hydrodynamics and the water quality usually depends on macroalgal cycles. The excessive growth of macroalgae and their decomposition during the warmer period affect dissolved oxygen and the sulphide cycle, lowering water clarity. The stations in the northern basin are placed near the mainland and are influenced by freshwater inflow of tributaries, which drains the sewage of the hinterland. Frequent phytoplankton blooms during the summer, sediment resuspension due to wind-induced wave and anthropogenic activities, such as clam harvesting and boat traffic, influence water clarity and bottom visibility.

At each station, above water remote sensing reflectances were measured with the WISP-3 spectroradiometer (Water Insight), CTD time series were performed with SBE-19 (SeaBird Electronics) multi-parameter probe, equipped with Dissolved Oxygen sensor SBE 43, pH/Redox sensor SBE27 and turbidity sensor OBS3plus. Backscattering coefficients were measured with HydroScat-6 (HOBILabs). Fluerescence (chl-a and CDOM) and backscattering were acquired with ECOTriplet (WteLabs). Discrete surface water samples were also collected and subsequently filtered in the laboratory, to estimate the concentration of chlorophyll-a (chl-a) and suspended particulate matter (SPM) with the determination of the organic and inorganic components.

Figure 5.4: Fieldwork activities in the areas affected by phytoplankton and macroalgae bloom.

4.1.4 CoastObs 2018 campaign

In the framework of CoastObs H2020 project, two joint sampling campaigns were undertaken by CNR and USTIR in May and June 2018 for collection of biogeochemical data (Chloroplastic pigments, TSM, CDOM), IOPs (particulate absorption, AC-S and Eco-BB3), AOPs (WISP-3 and TriOS Ramses), seagrass and macro-algae survey, particle size distribution (LISST), phytoplankton abundance and taxonomy, AOT (Microtops) and temperature and depth (CTD). The sampling stations included sites inside the lagoon of Venice in optically shallow and deep waters and along the coastal waters. Regarding coastal stations, they were distributed parallel to coastline of the lagoon of Venice.

Figure 4.6: Sampling locations in the Venice Lagoon and Adriatic Sea for CoastObs 2018 campaigns.

4.1.5 CoastObs 2019 campaign

In the framework of CoastObs H2020 project, a joint sampling campaign was undertaken by CNR and USTIR in July 2019 for collection of biogeochemical data (Chloroplastic pigments, TSM, CDOM), IOPs (particulate absorption), AOPs (WISP-3), AOT (Microtops) and temperature and depth (CTD).

The sampling stations included sites inside the lagoon of Venice in optically shallow and deep waters and along the coastal waters.

Figure 4.7: Sampling locations in the Venice Lagoon and Adriatic Sea for CoastObs 2019 campaigns.

4.2 Sentinel 3 OWT Analysis

4.2.1 Sentinel 3 OLCI dataset

- OLCI 300m data (2019-2021) processed with the POLYMER processor and selected pixels as the training dataset
- These were selected using a regular subsampling of the 300m data in the along scan and cross scan directions
- All visible wavelengths were used (400, 412, 443, 490, 510, 560, 620, 665, 674, 681 and 709nm)
- Prior to clustering the data, the spectra were standardised using a standard scalar and then applied a principal component analysis (PCA) to reproject the spectra
- Clusters created using Euclidian distance in principle-component-space

4.2.2 Sentinel 3 OWT classes

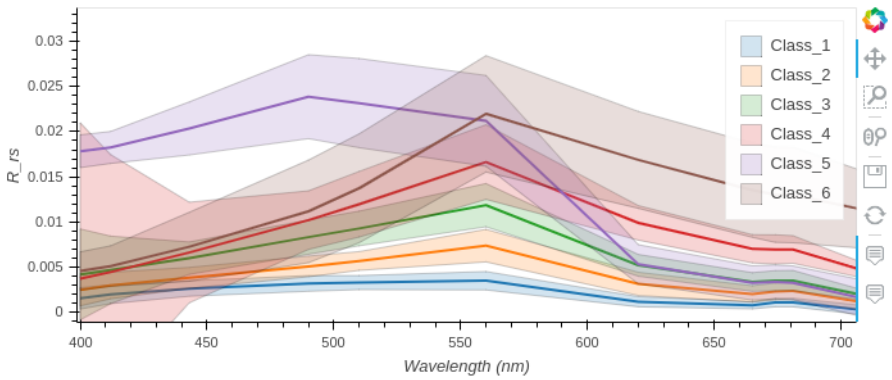

Figure 4.7: Derived optical water classes for the Venice lagoon using Sentinel 3

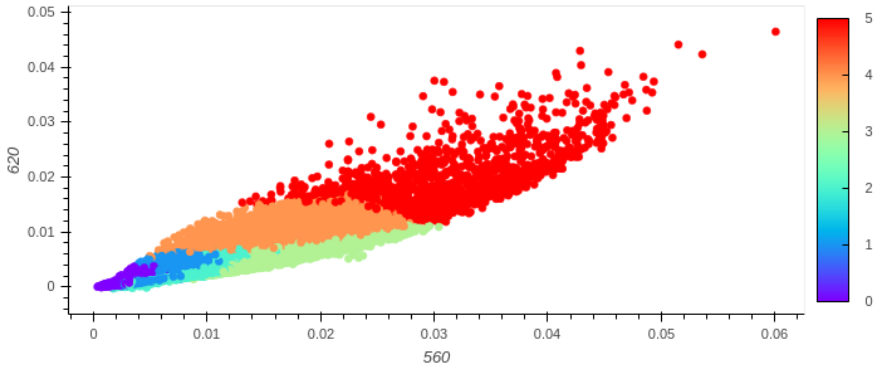

Figure 4.8: Dominant optical water class for each training data point in 2-band Rrs space for the Venice lagoon using Sentinel 3. Add one to the colourbar values for the OWT (colourbar is 0 indexed).

4.2.3 Sentinel 3 OWT Spatial analysis

This class set was then applied to OLCI data from 2019 to 2021. The resulting memberships (daily products) were then used for a number of different types of analysis.

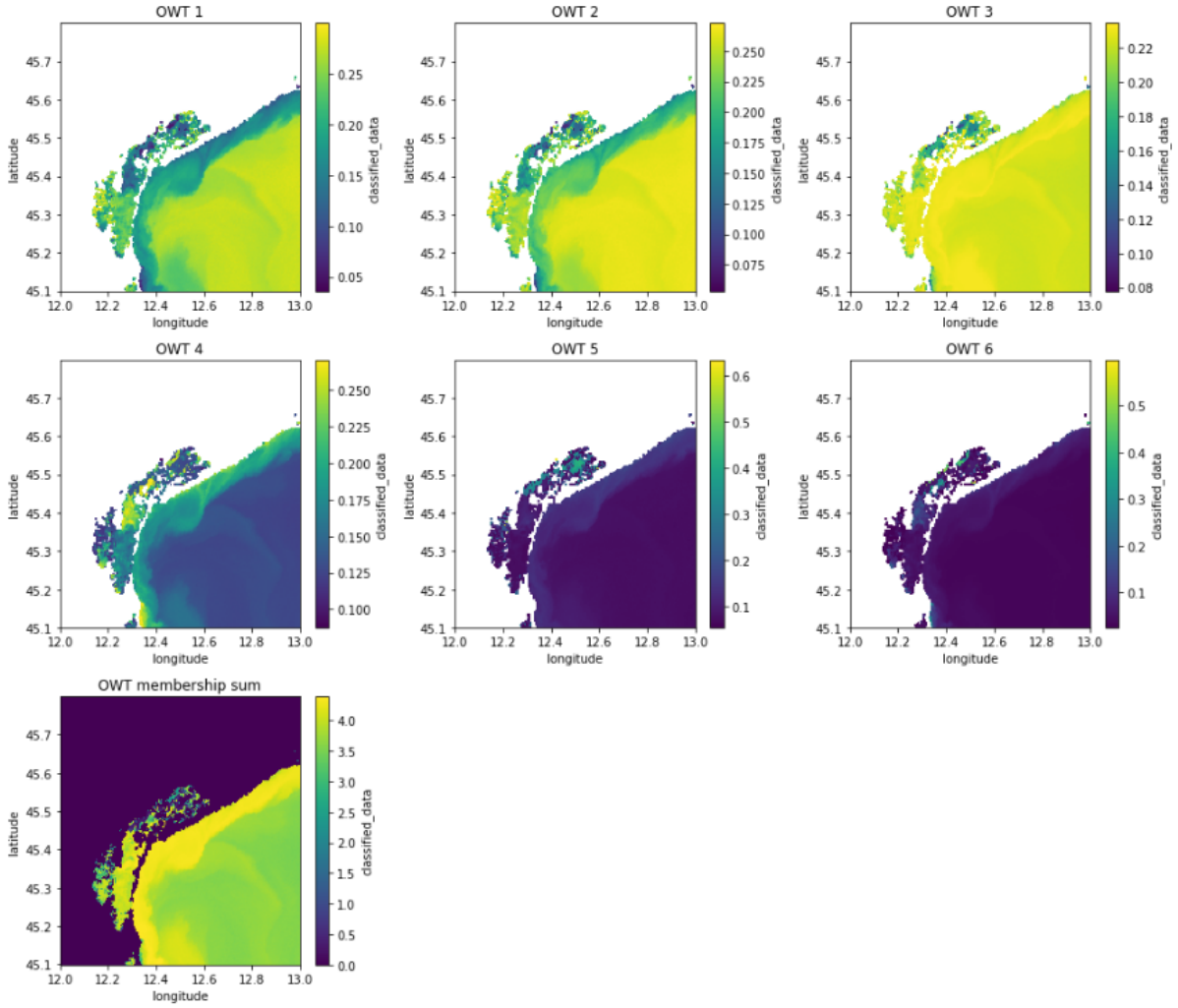

Figure 8.9: Example of clusters applied to data from 2018-08-25 for the Venice Lagoon using Sentinel 3. Membership values to each class are shown normalised to the total pixel membership (which is also shown in the last plot).

4.2.4 Sentinel 3 entropy filter and edge detection

The first analysis combines entropy filter and edge detection to try to locate the boundaries between regions of change in the optical water type structure. Where boundaries occur for more than one water class, we consider this to be a 'strong edge' that is then stored as a variable. An example of this for a single image is shown in Figure 4.10.

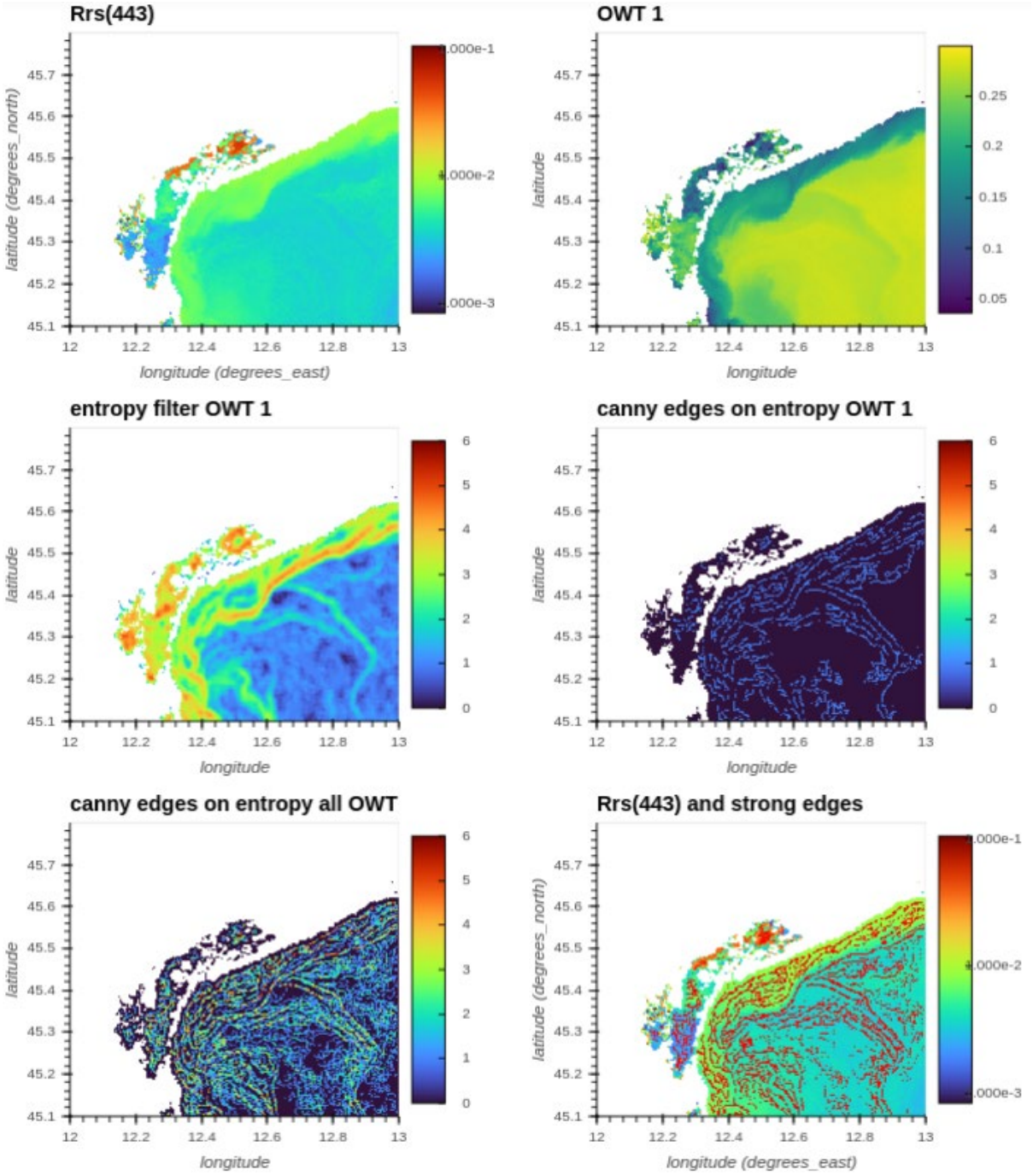

Figure 4.10: Example of entropy filter and edge detection application to data from 2018-08-25 for the Venice Lagoon using Sentinel 3.

Stacking these results across all data available for each month we can look for persistent regions of change in optical water type membership structure (Figure 4.11).

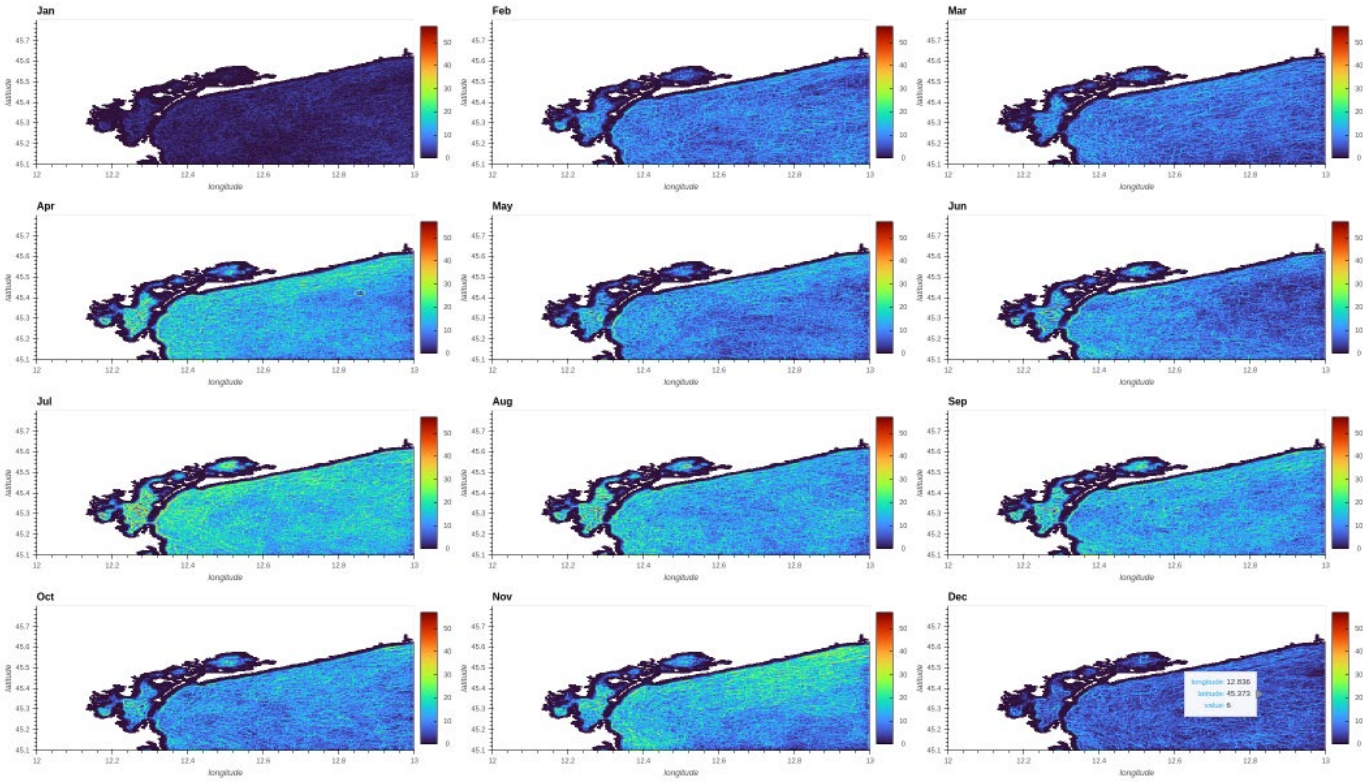

Figure 4.11: Stacked strong front incidence across all data available for a given month (across all years)

The strongest front incidence (could have some sampling bias due to clearer skies) appears to be in April, July, August and November. There are regions of interest highlighted along much of the coastline, of particular note the apparent ring in the northeast quadrant.

We can then stack this information across all available times (Figure 4.12) and by month (Figure 4.13) and visualise as maps. The colour bar does not line up properly (to be fixed) but for now it is interesting to see the regions of change /dominance.

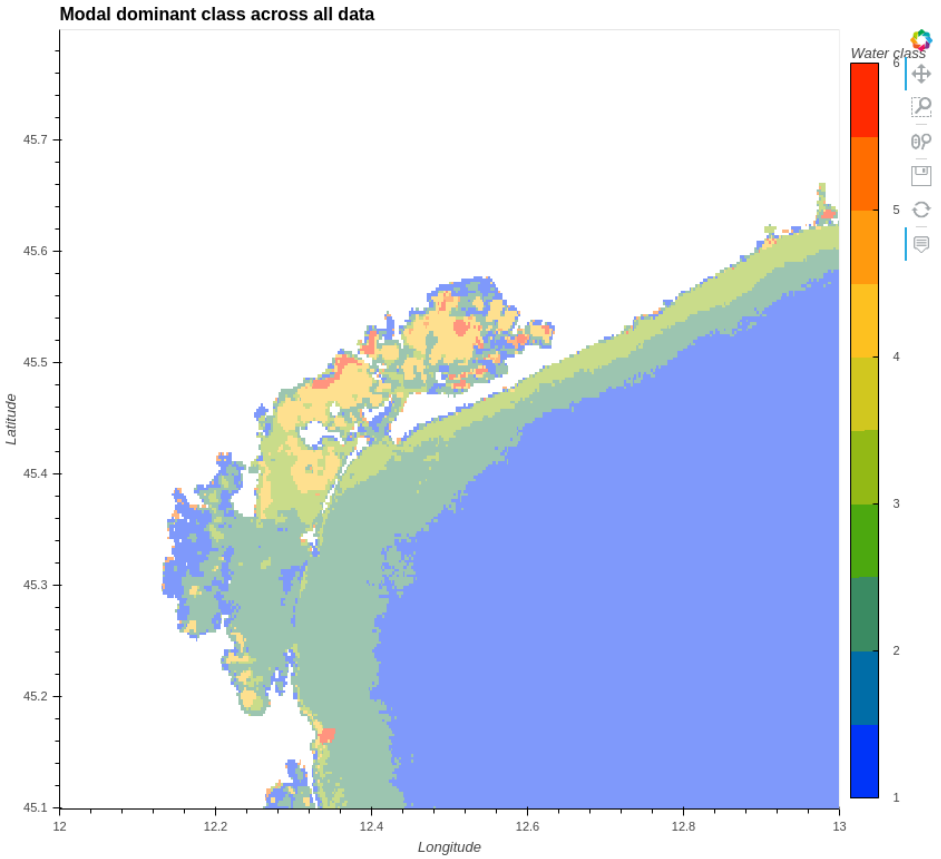

Figure 4.12: Dominant optical water class across all data in the Venice using Sentinel 3.

4.2.5 Sentinel 3 OWT temporal analysis

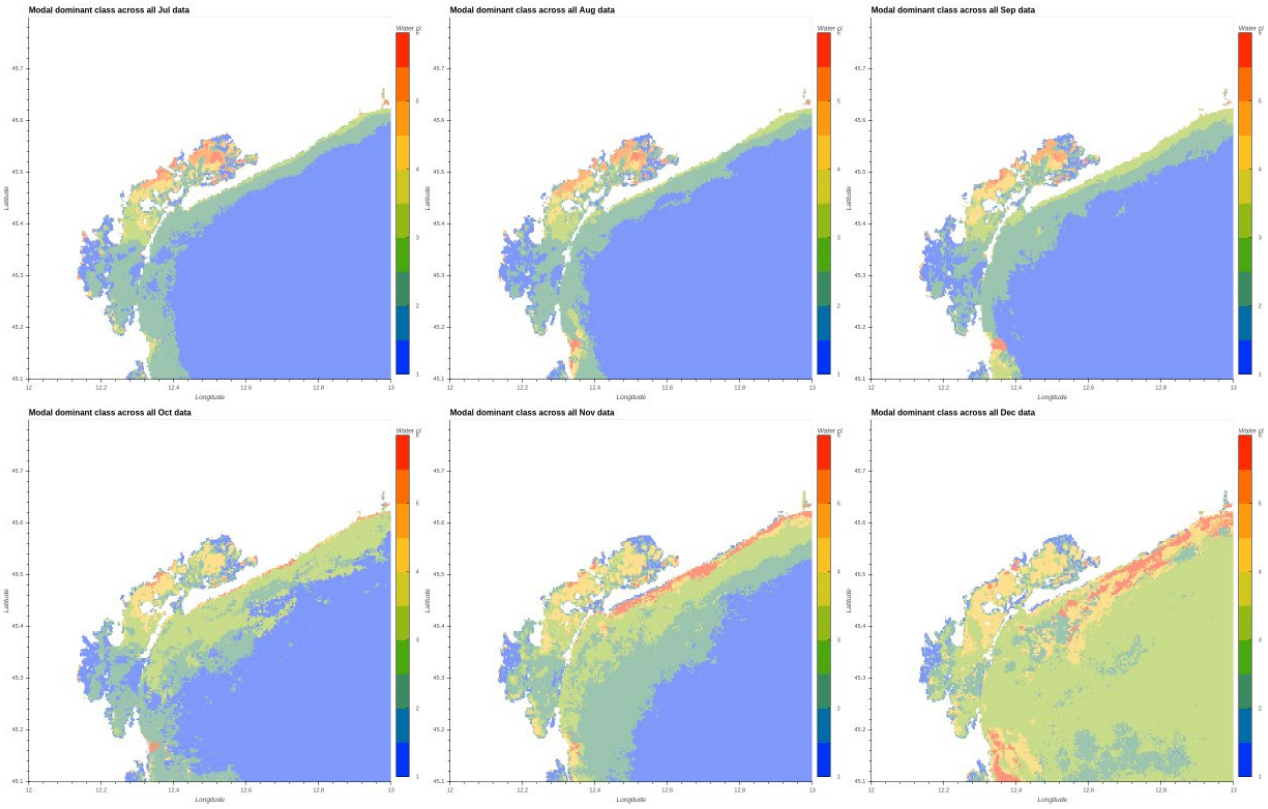

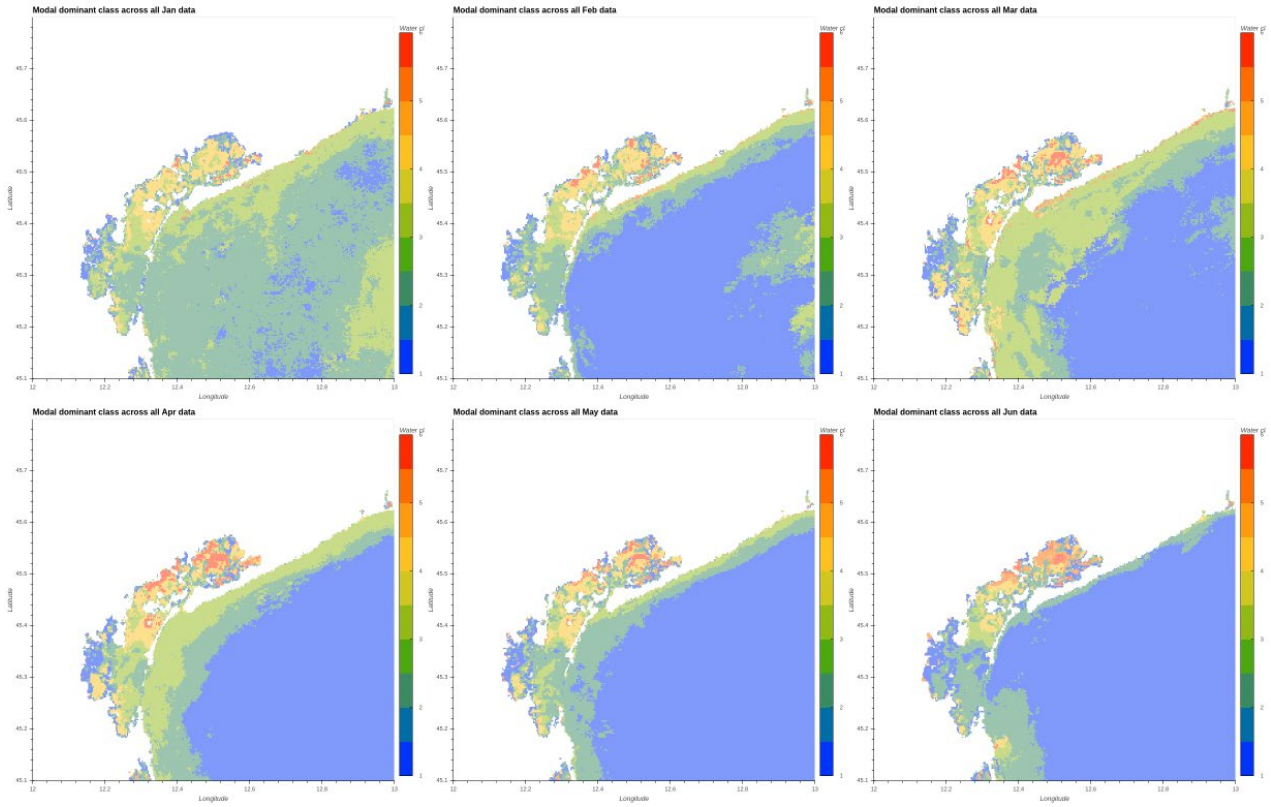

Figure 4.13: Temporal analysis of OWT in Venice Lagoon from January to December using Sentinel 3

4.2.6 Revised Sentinel 3 OWT Analysis

The OLCI dataset has been updated to cover a longer time period that better matches that of the Sentinel 2 MSI dataset, thus cluster analyses for the OLCI dataset is being updated as follows:

- OLCI 300m data processed with the POLYMER processor: 2016-04-26 to 2021-03-08
- Training dataset built using regular subsampling along scan and cross scan directions, wavelengths used were: 400, 412, 443, 490, 510, 560, 620, 665, 674, 681, 709, 754, 779, 865 and 885 nm
- No winter month exclusion from training dataset (based on incident light level <30° calculated using NOAA solcalc would be November-January, but regional leads requested that these months be included in training data

Analysis on the new OLCI dataset is ongoing and will be made available to the Venice teams.

4.3 Sentinel 2 OWT Analysis

4.3.1 Sentinel 2 MSI dataset

- MSI 60m data processed with POLYMER processor: 2016-11-02 to 2020-12-29
- Training dataset built using regular subsampling along scan and cross scan directions, wavelengths used were: 443, 490, 560, 665, 705, 740, 783, 865, 1610 and 2190 nm
- Winter month exclusion from training dataset (based on incident light level <30° calculated using NOAA solcalc): November - January
- Prior to clustering, spectra were standardised using a standard scalar and then principal component analysis (PCA)
- Clusters created using Euclidian distance in principle-component-space

4.3.2 Sentinel 2 OWT classes

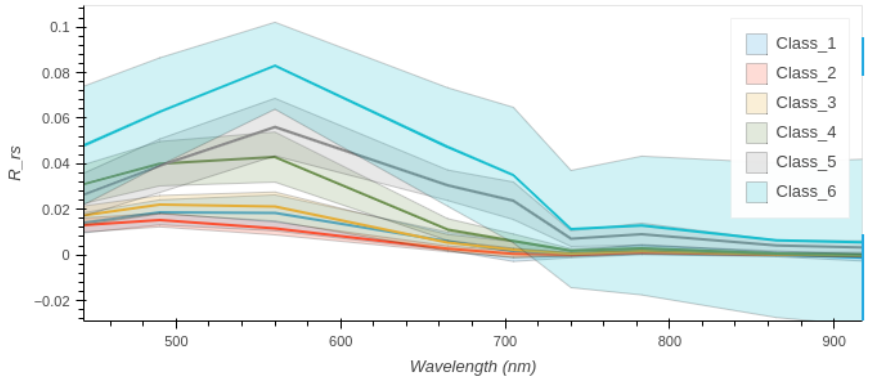

Figure 4.14: Derived optical water classes for the Venice Lagoon using Sentinel 2

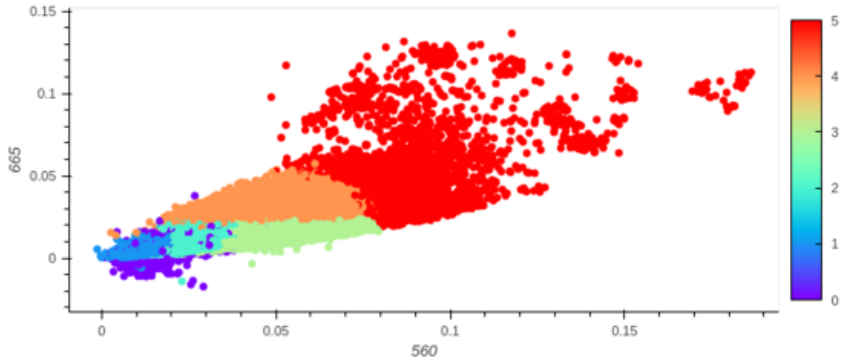

Figure 4.15: Dominant optical water class for the Venice Lagoon using Sentinel 2. Add one to the colourbar values for the OWT (colourbar is 0 indexed).

4.3.3 Sentinel 2 OWT Spatial analysis

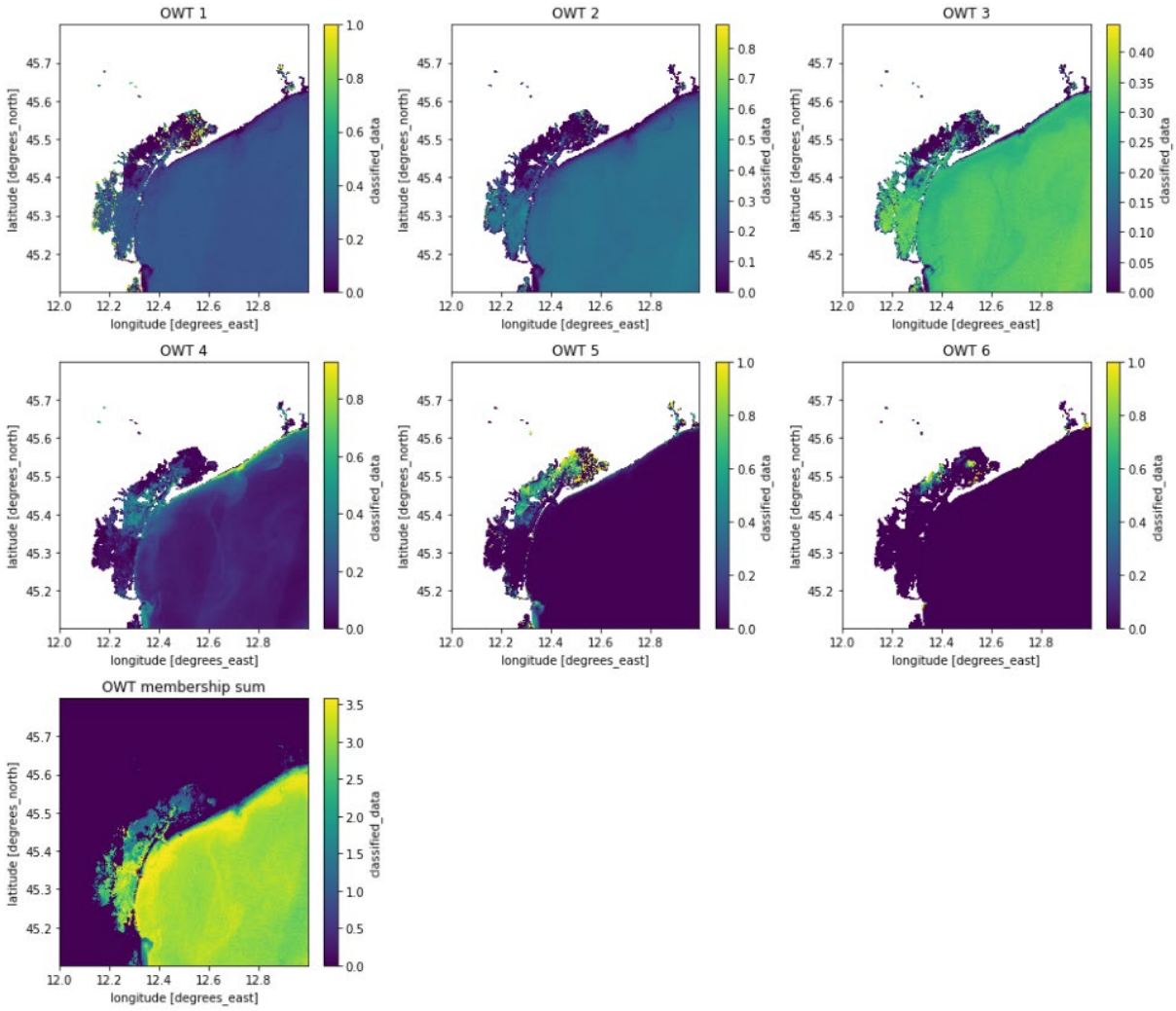

Figure 4.16: OWT spatial distribution for 2020-09-15 for the Venice Lagoon using Sentinel 2

4.4 Influence of local processes

As with most coastal lagoons, the Lagoon of Venice is formed by a complex system of channels, coastal barriers, salt marshes, tidal flats and wetlands. Most of the lagoon is very shallow, with average depths in the order of 1 m, but there are also a few deep channels (maximum depth around 15 m) leading inwards from each inlet and branching inside the basin. Traditionally the lagoon is subdivided into three sub-basins, one for each inlet, separated by two watersheds through which the residual flow is minimum.

The lagoon receives variable amounts of terrestrial and freshwater inputs and maintains a connection to the open sea through the tidal inlets. Hydrodynamics is controlled by marine and freshwater inputs and natural exchanges between them cause wide fluctuations of hydrological parameters at different temporal scales according to daily, seasonal and annual cycles. In turn, geomorphological features and seafloor topography strongly condition water circulation and residence time. Overall, hydrodynamics and geomorphology closely interact promoting the onset of gradients and patchiness of biotic and abiotic parameters.

Several processes influence the amount of dissolved and suspended matter in the water column affecting water quality in the lagoon (Figure 4.): wind, and wave, driven resuspension and erosion, redistribution of suspended sediments by tidal currents, freshwater runoff and associated sediment delivery from the drainage basin, and the primary producers growth cycle. Localised sediment mobilisation is induced by ship and boat wakes, coastal engineering works and clam harvesting. Moreover, the natural settling of suspended matter may be delayed by turbulence induced by water traffic. Within and around the historical city, wastewater discharge is also a source of dissolved and suspended matter due to the lack of a sewage system.

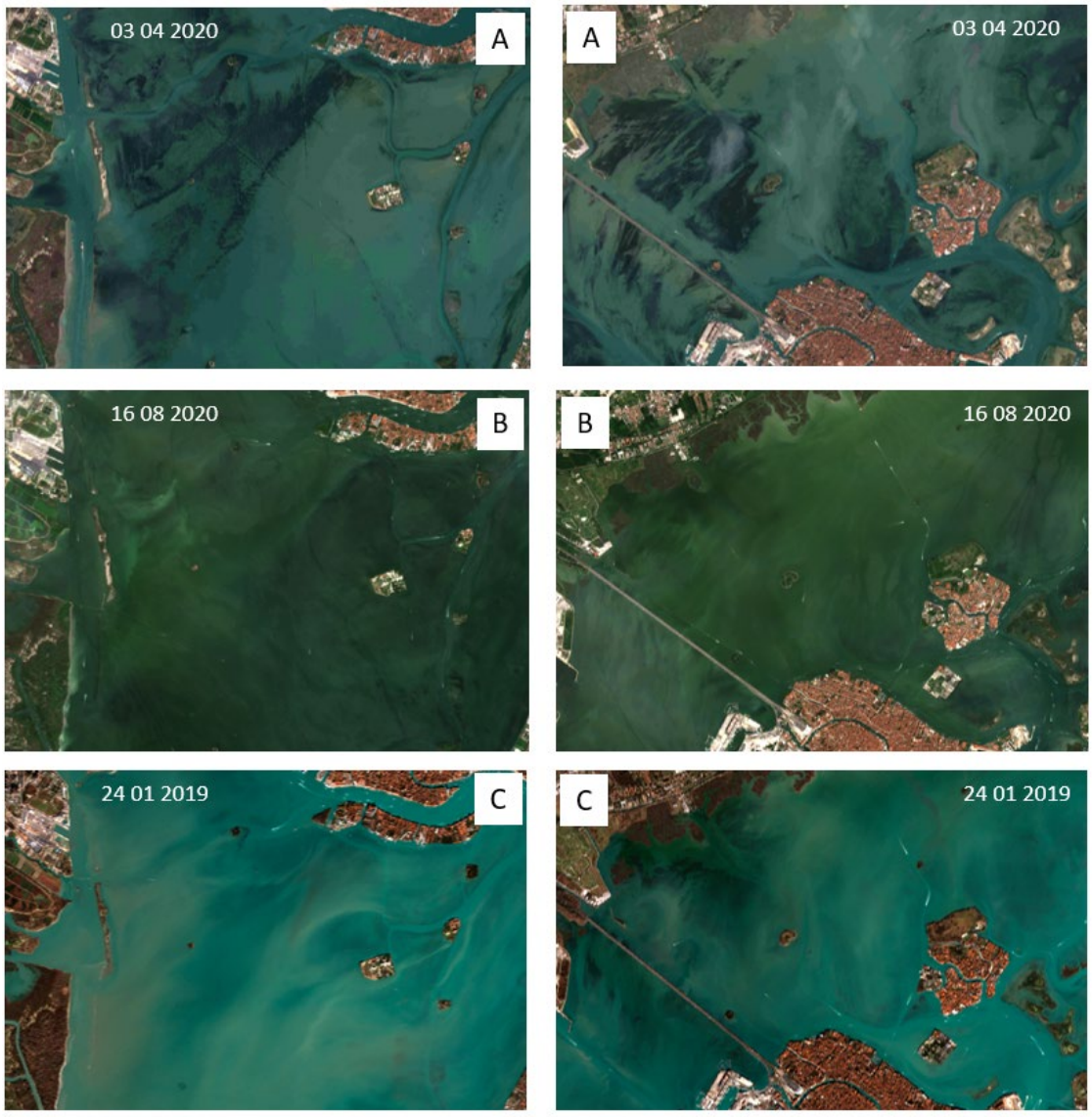

Figure 4.17: Shallow waters in the central and northern basins of the Lagoon of Venice under different environmental conditions. A) clear water, B) eutrophication due to phytoplankton blooms and decomposition of macroalgae, C: high turbidity due to wind resuspension.

The coastal zone in front of the Lagoon of Venice is influenced by wind and wave forcing. Two distinct wind regimes control sea conditions and influence basin-wide circulation: the northeasterly Bora, blowing off the Balkanic peninsula, and the southeasterly Scirocco. Both Bora and Scirocco generate energetic waves in the western Adriatic, which cause a significant resuspension of bottom sediments in waters shallower than 15 m, while coastal circulation moves the resuspended sediments offshore and/or along the coasts. Patterns of suspended sediments caused by strong wind and wave conditions and transported by coastal currents are visible in satellite images.

Figure 4.18: Sentinel-2 image acquired on 12 July 2020. Strong Bora conditions (wind speed about 15 ms^{-1}) associated with wind-driven currents and waves, induce sediment resuspension from the seabed and determine sustained southward fluxes. The effects of tidal currents, which move turbid water from the sea to the lagoon, are also visible at the Lido inlet.

4.5 Identification of under sampled regions

4.5.1 Satellite (Sentinel 2) and in situ match up analysis

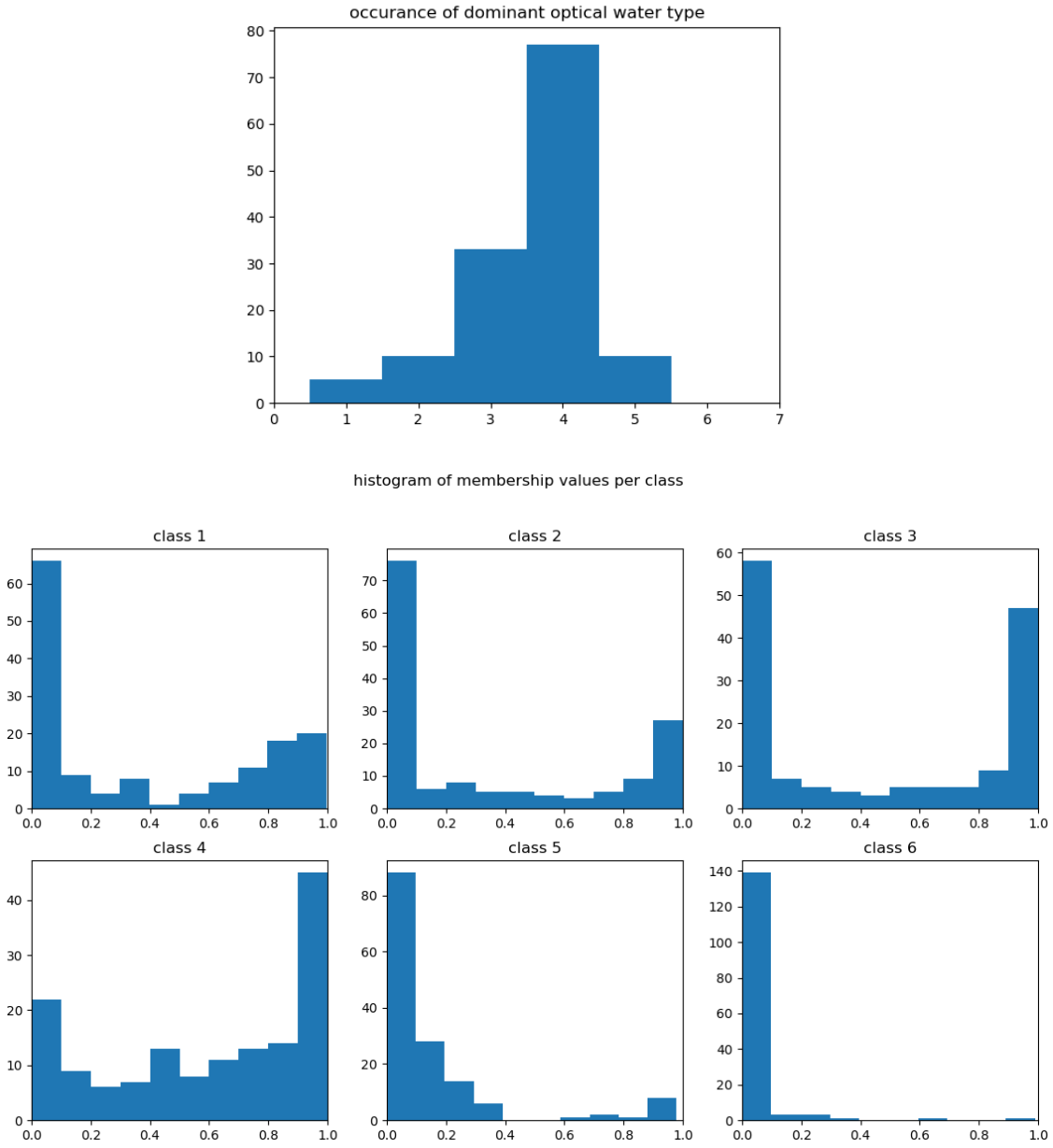

Figure 4.19: (top) Dominant optical water type and (bottom) histogram of membership values per class in the Venice using Sentinel 2.

By matching existing in situ data in time and space to available satellite data that has been classified using the optical water type approach we can see which optical water classes we might already be able to characterise. The in situ database was matched to the nearest pixel location on the day of sampling to check for a match-up. This is not ideal as there can be large changes over the diurnal cycle, particularly associated with tides, but for now we are looking to include as much data as possible. From the matchups we can see (top panel of figure 4.19) that thus far the majority of the samples have been collected in waters dominated by waterclass 4 and no samples have been collected in waters dominated by waterclass 6. The histograms per waterclass plots (bottom panel in figure 4.19) show that most of the pixel memberships for classes 1-3 tend to have either a high or low membership (bi-modal) which means that we can consider these classes as distinct (not just a constant background contribution to spectra). Class 4 (which is the most commonly dominant) seems to have a contribution to most of the matchup pixels and Classes 5 and 6 are very rarely sampled with a high membership. We would therefore recommend trying to ensure that some waters dominated by waterclasses 1,2,5 and 6 are sampled during the CERTO field work, if possible.

4.6 Proposed ideal sampling time for year 2 (2021) in Venice Lagoon

For aiding the validation and interpretation of satellite data, the ideal sampling time would be at the same moment as the satellite overpass. This is not possible in most cases so we propose that the in situ measurements should be taken within a 3-hour window either side of the satellite overpass so that the influence of tides and weather changes are reduced.

- Time of sampling – July/August 2021
- Sampling duration - 1 week
- Sampling platform availability – CNR, logistics arranged, Litus, Aretusa and Boston boats
- Campaign participants - CNR

Table 4.1: Sentinel 3 passes over Venice in July-August 2021

	July (date)	July (time) UTC	August (date)	August (time) UTC
SENTINEL 3	daily	08:50-09:50	daily	08:50-09:50

Table 4.2: Sentinel 2 passes over Venice Lagoon in July-August 2021

Satellite platform	Orbit	Date	Time (UTC)
S2A	R022_T32TQR	2-Jul	10:10
S2B	R122_T32TQR	4-Jul	10:00
S2B	R022_T32TQR	7-Jul	10:05
S2A	R122_T32TQR	9-Jul	10:00
S2A	R022_T32TQR	12-Jul	10:10
S2B	R122_T32TQR	14-Jul	10:00
S2B	R022_T32TQR	17-Jul	10:05
S2A	R122_T32TQR	19-Jul	10:00
S2A	R022_T32TQR	22-Jul	10:10
S2B	R122_T32TQR	24-Jul	10:00
S2B	R022_T32TQR	27-Jul	10:05
S2A	R122_T32TQR	29-Jul	10:00
S2A	R022_T32TQR	1-Aug	10:10
S2B	R122_T32TQR	3-Aug	10:00
S2B	R022_T32TQR	6-Aug	10:05
S2A	R122_T32TQR	8-Aug	10:00
S2A	R022_T32TQR	11-Aug	10:10
S2B	R122_T32TQR	13-Aug	10:00
S2B	R022_T32TQR	16-Aug	10:05
S2A	R122_T32TQR	18-Aug	10:00
S2A	R022_T32TQR	21-Aug	10:10
S2B	R122_T32TQR	23-Aug	10:00
S2B	R022_T32TQR	26-Aug	10:05
S2A	R122_T32TQR	28-Aug	10:00
S2A	R022_T32TQR	31-Aug	10:10

4.7 Covid19 Mitigation: proposed essential measurements and USTIR support

University of Stirling will provide support in terms of instrumentation and post-sampling analysis (for sites that need support). In year 2 (2021) participation by USTIR in the sampling campaigns will be subjected to Covid19 travel restrictions. However, the plan is to replicate a small percentage of samples for Chl-a, TSM, PC and particulate absorption from all sites. Shipping of the samples to USTIR will be arranged accordingly.

USTIR will arrange a shipment and a rota of required instrumentation, in association with FC.ID, across the different sites in Europe. Intercomparison experiments therefore are planned in year 3 (2022) with a possibility to participate onboard with a suite of USTIR instrumentation across the sites in the UK and Europe.

Table 4.3: Proposed essential measurements and USTIR support. CNR-USTIR indicates CNR will collect samples and USTIR will analyse them.

	Parameters to be measured (essentials in bold)	**Instrumentation/ Sample Analysis 2021**	**Instrumentation/ Sample Analysis 2022**
Biogeochemistry	Chlorophyll a, Chl-a	CNR	CNR
	Phycocyanin, PC	-	-
	Total Suspended Matter, TSM	CNR	CNR
AOPs	**Remote sensing reflectance, R_{rs}**	CNR	CNR
	Diffuse attenuation coefficient, K_d	USTIR (USSIMO)	USTIR (USSIMO)
	Secchi disk depth, Z_{SD}	CNR	CNR
IOPs	**Total absorption coefficient, a**	---	CNR (ac-9) USTIR (ac-s)
	Absorption coefficient of phytoplankton, a_{ph}	CNR- USTIR	CNR- USTIR
	Absorption coefficient of non-algal particles, a_{nap}	CNR- USTIR	CNR- USTIR
	Coloured dissolved organic matter, CDOM	CNR	CNR
	Backscattering coefficient, b_b	CNR (Hydroscat-6)	CNR (Hydroscat-6)
	Beam attenuation coefficient, c	---	CNR (ac-9) USTIR (ac-s)
Physical Parameters	Water temperature	CNR	CNR
	Salinity	CNR	CNR
	Turbidity	CNR	CNR
	Water depth	CNR	CNR
Atmospheric parameters	Wind speed	CNR	CNR
	AOT	CNR	CNR

4.8 References

Holben, B. N., Tanre, D., Smirnov, A., Eck, T. F., Slutsker, I., Abuhassan, N., ... & Zibordi, G. (2001). An emerging ground based aerosol climatology: Aerosol optical depth from AERONET. Journal of Geophysical Research: Atmospheres, 106(D11), 12067-12097.

Zibordi, G., Hooker, S. B., Berthon, J. F., & D'Alimonte, D. (2002). Autonomous above-water radiance measurements from an

offshore platform: a field assessment experiment. Journal of Atmospheric and Oceanic Technology, 19(5), 808-819.

Zibordi, G., Mélin, F., & Berthon, J. F. (2006). A time-series of above-water radiometric measurements for coastal water monitoring and remote sensing product validation. IEEE Geoscience and Remote Sensing Letters, 3(1), 120-124.

Zibordi, G., Berthon, J. F., Mélin, F., D'Alimonte, D., & Kaitala, S. (2009). Validation of satellite ocean color primary products at optically complex coastal sites: Northern Adriatic Sea, Northern Baltic Proper and Gulf of Finland. Remote Sensing of Environment, 113(12), 2574-2591.

5 Case Study Area 3: Tagus Estuary

Tagus Estuary (Atlantic)

The Tagus estuary is a good example for the need to achieve sustainable use of a coastal ecosystem, as it is located next to Lisbon, the capital city of Portugal. It provides a diversity of services, including the Port of Lisbon, industrial, agricultural, fisheries and tourism activities, whilst encompassing a natural reserve where waters are an iconic feature. Upstream waters from the Tagus river have their origin in Spain, with freshwater flowing through the Tagus Estuary before outflowing into the Atlantic Ocean in large plumes. The outflowing waters bring a mix of nutrients into the Atlantic affecting primary production off the Portuguese coast. The estuary itself is one of the largest in Europe, with a broad shallow bay, covering an area of about 320 km^2 (APA, 2016), and semi-diurnal tides. The morphology of the Tagus estuary is characterised by a deep, long and narrow inlet that connects the Atlantic Ocean to the interior of the estuary, which consists in a shallow basin that has extensive tidal flats and marshes. Water quality in the Tagus is of great importance to several entities in Portugal due to its complex natural ecosystem, its proximity to the city of Lisbon and the upstream industrial sites. Therefore, continuous monitoring is essential and is performed by several institutes.

An in situ monitoring programme with monthly sampling at 4 sites (blue pins in Figure 5.1) has taken place since January 1999, focusing on phytoplankton and nutrients concentration. The average Chlorophyll-a is 3.8 µg L^{-1} in these 4 sites, with a wide range of 0.5–24 µg L^{-1}, during the period 1999-2020. The maximum values are observed during spring/summer, and the minima in winter. Several publications have identified the driving forces which control phytoplankton biomass and productivity (Gameiro & Brotas, 2010; Gameiro et al., 2011) and characterised seasonal and interannual patterns (Brito et al, 2015).

5.1 Current sampling locations and bio-optical monitoring

In situ monitoring in the Tagus estuary is currently carried out in the framework of several national and international on-going projects. Furthermore, a comprehensive dataset of *in situ* biogeochemical measurements is available from completed projects. The location of the sampling sites within the Tagus estuary is presented in Figure 5.1.

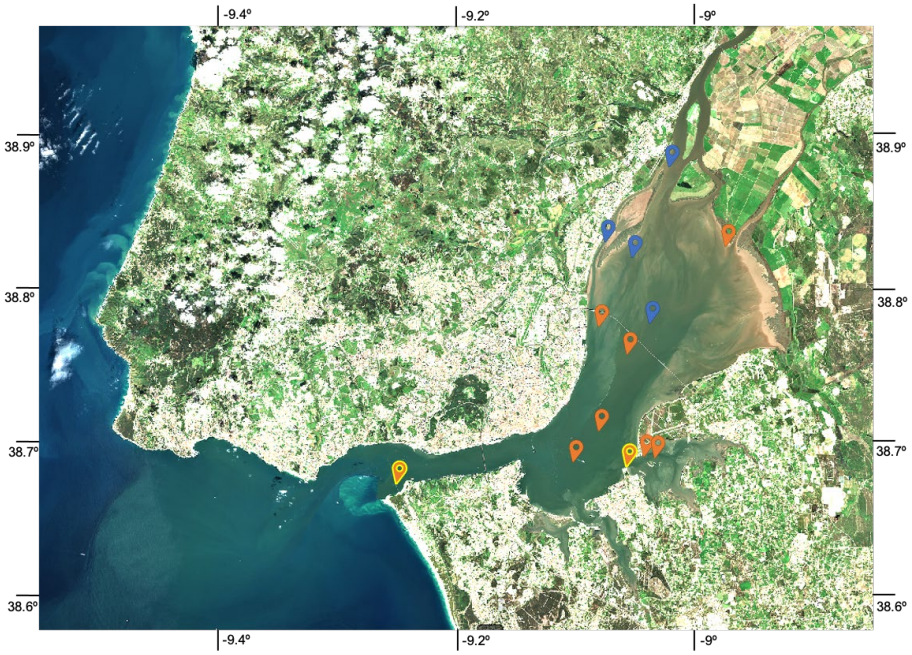

Figure 5.1: Sampling stations in the Tagus estuary. Blue pins correspond to on-going sampling programmes sampling stations; orange pins correspond to historical stations. The sampling locations where Remote sensing reflectance data are available are highlighted with yellow outline.

For the case study focused on the Tagus estuary, 13 sampling points from 3 different projects are considered, from both on-going (blue pins in Figure 5.1) and completed (orange pins in Figure 5.1) projects. The on-going project providing biogeochemical observations is the Valorsul project (see section 3.1.1). The other two projects that provide bio-optical and biogeochemical data are PLATAGUS and NIPOGES (described in section 3.1.2), both recently concluded. All these projects have adjusted dates of sampling to guarantee Sentinel-2 and/or Sentinel-3 passages. A list of parameters collected by each project is shown in Table 5.1.

Table 5.1: List of biogeochemical and physical parameters collected by the different projects along the Tagus estuary.

	ValorSul	Nipoges	Platagus
Chlorophyll-a, Chl-a	X	X	X
Phytoplankton pigments	X	X	X
TSM	X	X	X
Nutrients	X	X	
Particulate Absorption	X		X
Colored dissolved organic matter, CDOM	X		
Water temperature	X	X	X
Salinity	X	X	X
pH	X		
Turbidity	X	X	X
Diffuse attenuation, K_d	X		

Secchi Depth, Z_{sd}	X		X
Remote sensing reflectance, R_{rs}			X

5.1.1 Time series stations

For the Tagus estuary, a temporally extensive dataset of biogeochemical observations is made available by the VALORSUL project led by FC.ID, focusing on the mid and upstream region of the estuary. Since 1999, VALORSUL project provides monthly observations of several biogeochemical parameters. Sampling is carried out monthly or bimonthly during ebb tide of neap tides, to avoid the tidal influence on the temporal variability. Samplings are performed at 4 sampling stations located in the mid and upper estuary (blue pins in Figure 5.1). Furthermore, since 2018, dates of sampling were adjusted to guarantee coincident Sentinel-2 and/or Sentinel-3 passages. Each station includes the determination of physical parameters of the water (*i.e.* temperature, salinity, and in-water light penetration profiles) and water collection for posterior laboratory analysis of dissolved nutrient concentration, chlorophyll-*a*, photosynthetic pigments and suspended matter concentration. The list of parameters sampled within the VALORSUL project is shown in Table 5.1.

5.1.2 Other surveys/campaigns

To complement the long-term dataset of *in situ* observations provided by the VALORSUL project, data collected within the context of additional data-gathering projects such as the recently concluded PLATAGUS and NIPOGES will be combined, thereby extending the available data for CERTO. The PLATAGUS project's main objective was to validate satellite products such as turbidity and TSM in estuarine systems (Tagus estuary and Río de la Plata) and is the only project providing Remote sensing reflectance (R_{rs}) observations (Figure 5.1). Two sampling campaigns were performed on the Tagus estuary, one at the inlet of the estuary in August-September 2018 and one performed in the middle basin during June 2019. Both sampling sites are located close to the coastline and are highlighted in Figure 5.1 with a yellow outline on the corresponding pin. These samplings covered a wide range of tidal conditions.

Of the currently available data sets in the Tagus, the most spatially extensive is the NIPOGES project. This project was started in 2017 studying the variability of biogeochemical properties along the Tagus estuary. Therefore, an extensive range of biogeochemical conditions is available, making it particularly useful in the context of the CERTO project even if no in situ radiometric measurements were collected. As part of the planned activities aiming to gather new in situ data, transects will be performed within the Tagus estuary collecting continuous bio-optical data. This will be allowed by the installation of instrumentation on a tourist boat that performs daily transects along the estuary. Furthermore, specific campaigns will be performed to sample spatial gradients, tidal cycles and specific events of interest.

5.2 Sentinel 3 OWT Analysis

5.2.1 Sentinel 3 OLCI dataset

- OLCI 300m data (2019-2021) processed with the POLYMER processor and selected pixels as the training dataset
- These were selected using a regular subsampling of the 300m data in the along scan and cross scan directions
- All visible wavelengths were used (400, 412, 443, 490, 510, 560, 620, 665, 674, 681 and 709nm)
- Prior to clustering the data, the spectra were standardised using a standard scalar and then applied a principal component analysis (PCA) to reproject the spectra
- Clusters created using Euclidian distance in principle-component-space
- The resulting cluster set is shown below:

5.2.2 Sentinel 3 OWT classes

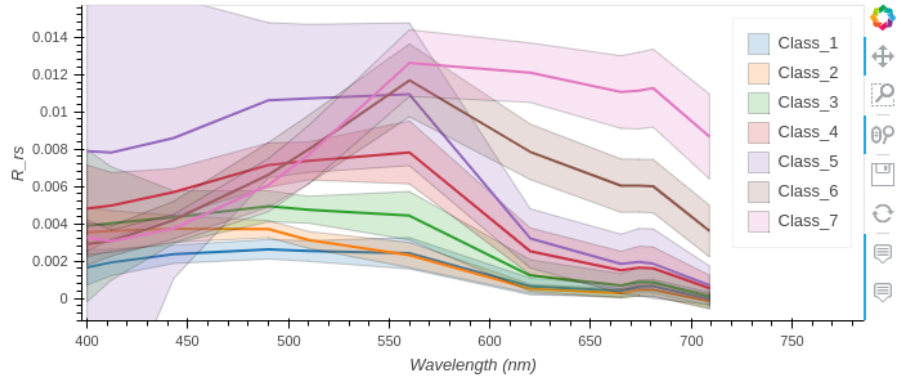

Figure 5.2: Derived optical water classes for the Tagus using Sentinel 3

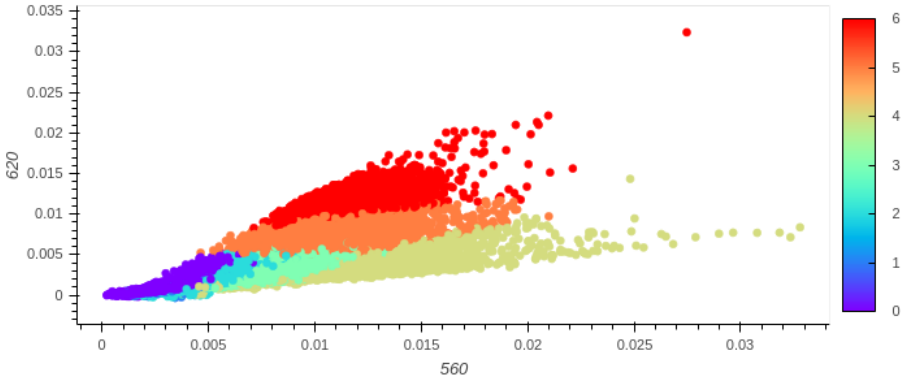

Figure 5.3: Dominant optical water class for each training data point in 2-band Rrs space. Add one to the colour bar values for the OWT (colour bar is 0 indexed) for the Tagus using Sentinel 3.

5.2.3 Sentinel 3 OWT Spatial analysis

This class set was then applied to OLCI data from 2019 to 2021. The resulting memberships (daily products) were then used for a number of different types of analysis.

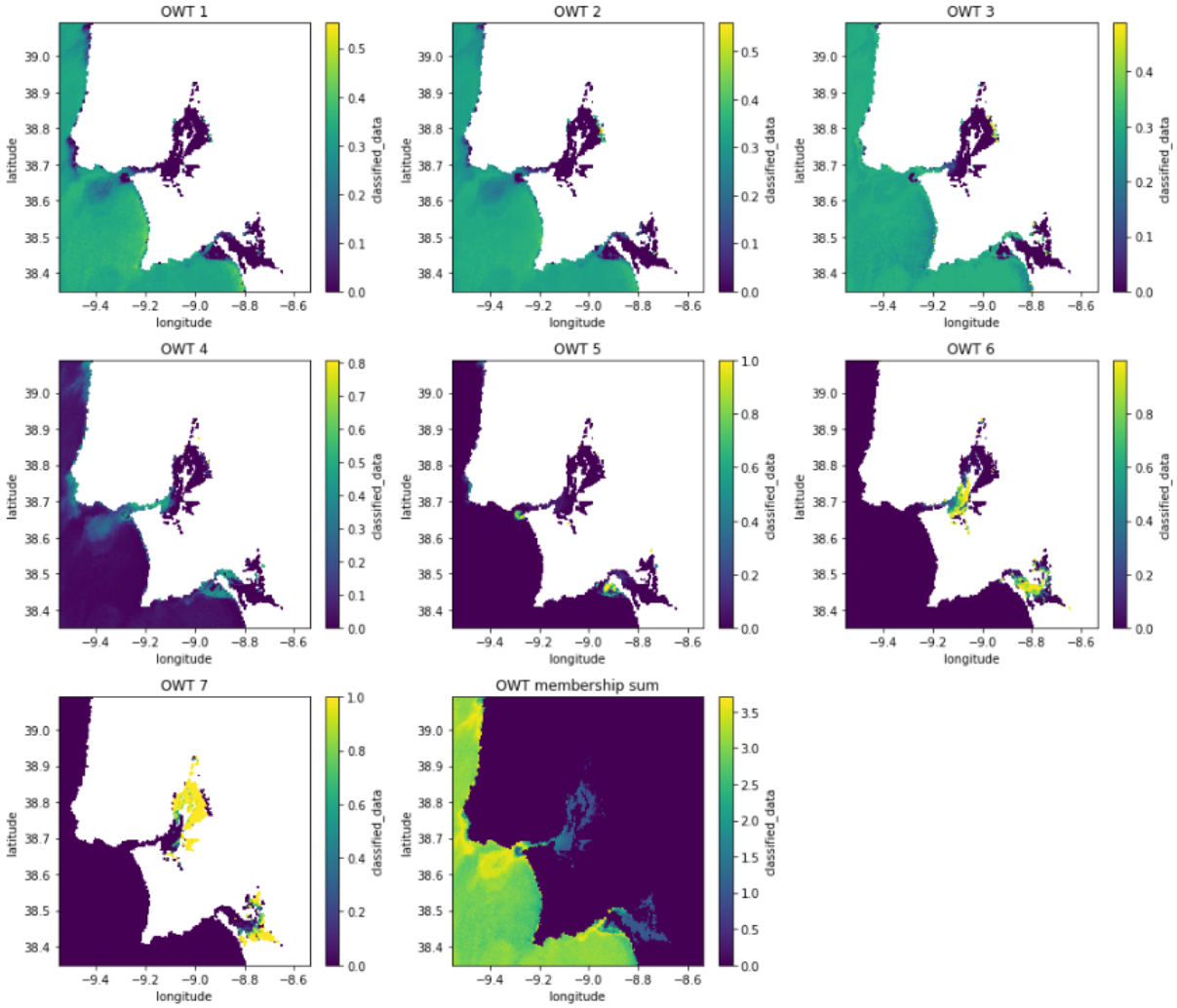

Figure 5.4: Example of clusters applied to data from 2020-07-03 for the Tagus using Sentinel 3. Membership values to each class are shown normalised to the total pixel membership (which is also shown in the last plot).

5.2.4 Sentinel 3 entropy filter and edge detection

The first analysis combines entropy filter and edge detection to try to locate the boundaries between regions of change in the optical water type structure. Where boundaries occur for more than one water class, we consider this to be a 'strong edge' that is then stored as a variable. An example of this for a single image is shown in Figure 5.5.

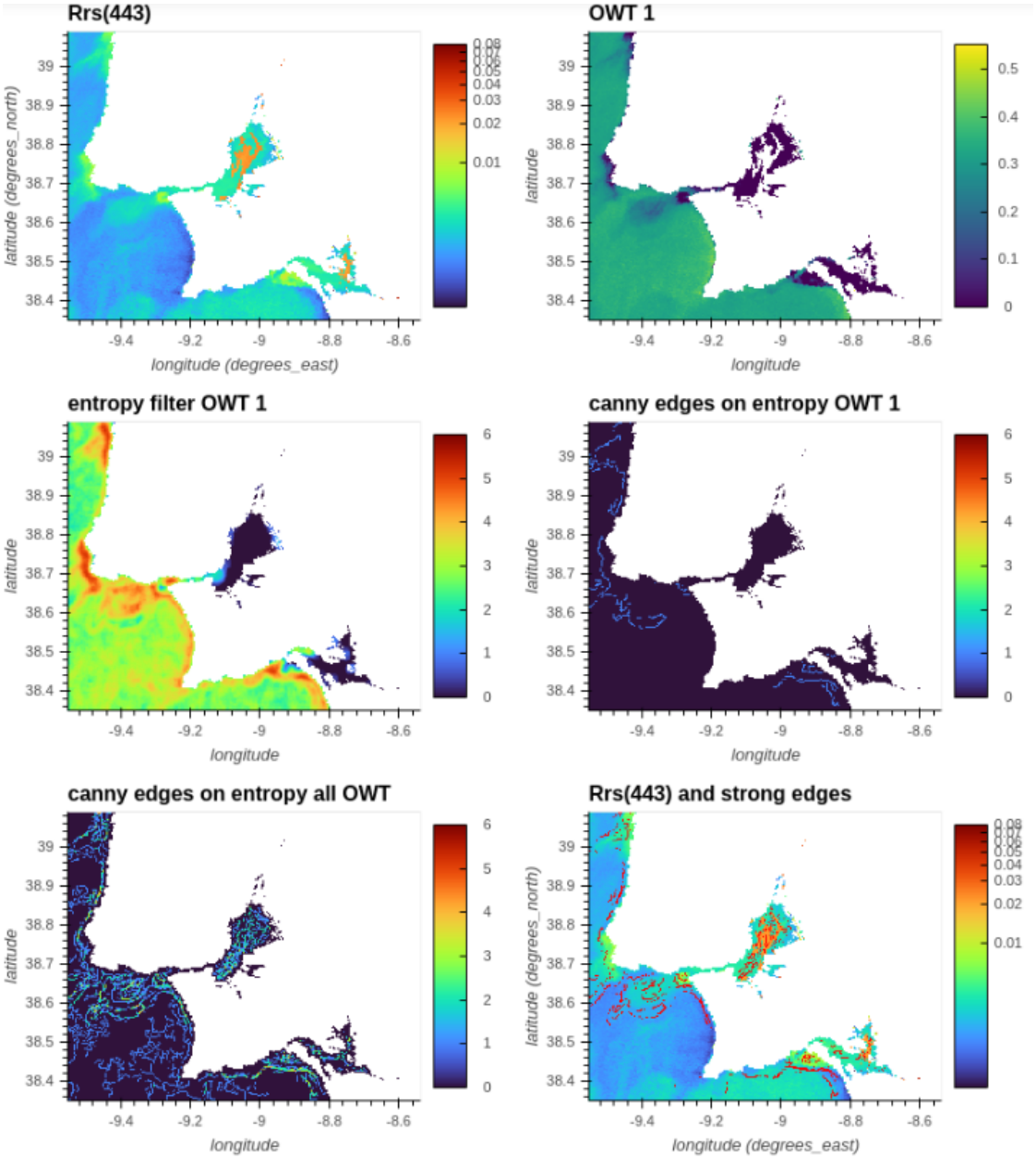

Figure 5.5: Example of entropy filter and edge detection application to data from 2020-07-03 for the Tagus using Sentinel 3.

Stacking these results across all data available for each month we can look for persistent regions of change in optical water type membership structure. This is shown below:

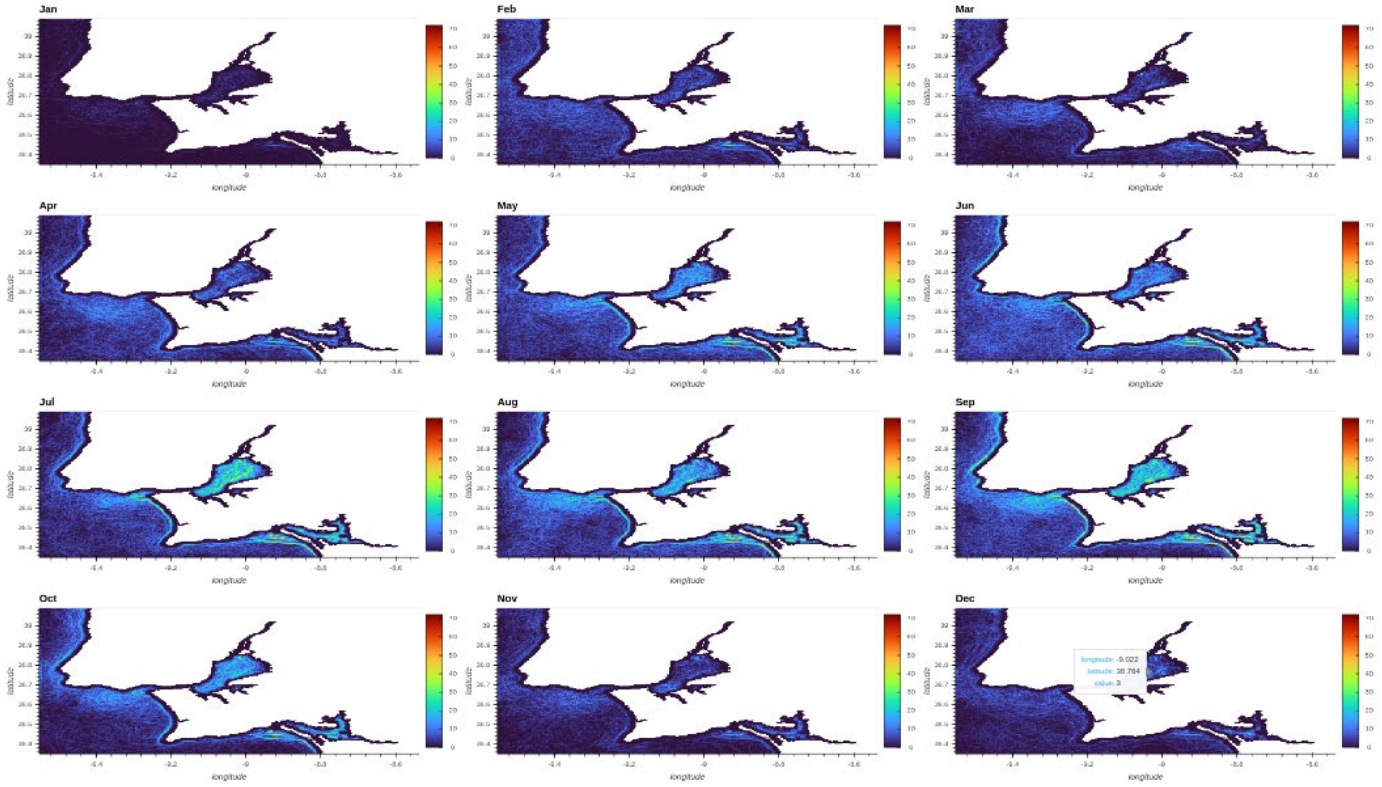

Figure 5.6: Stacked strong front incidence across all data available for a given month for the Tagus using Sentinel 3 (across all years)

The strongest front incidence (could have some sampling bias due to clearer skies) appears to be in May through September, with July and September both showing the strongest front incidence inside of the lagoon. There are regions of interest highlighted around the coasts to the North and South of the Tagus Lagoon mouth, as well as where the Sado river flows out near Costa de Galé.

We can then stack this information across all available times (Figure 5.7) and by month (Figure 5.8) and visualise as maps. The colour bar does not line up properly (to be fixed) but for now it is interesting to see the regions of change /dominance.

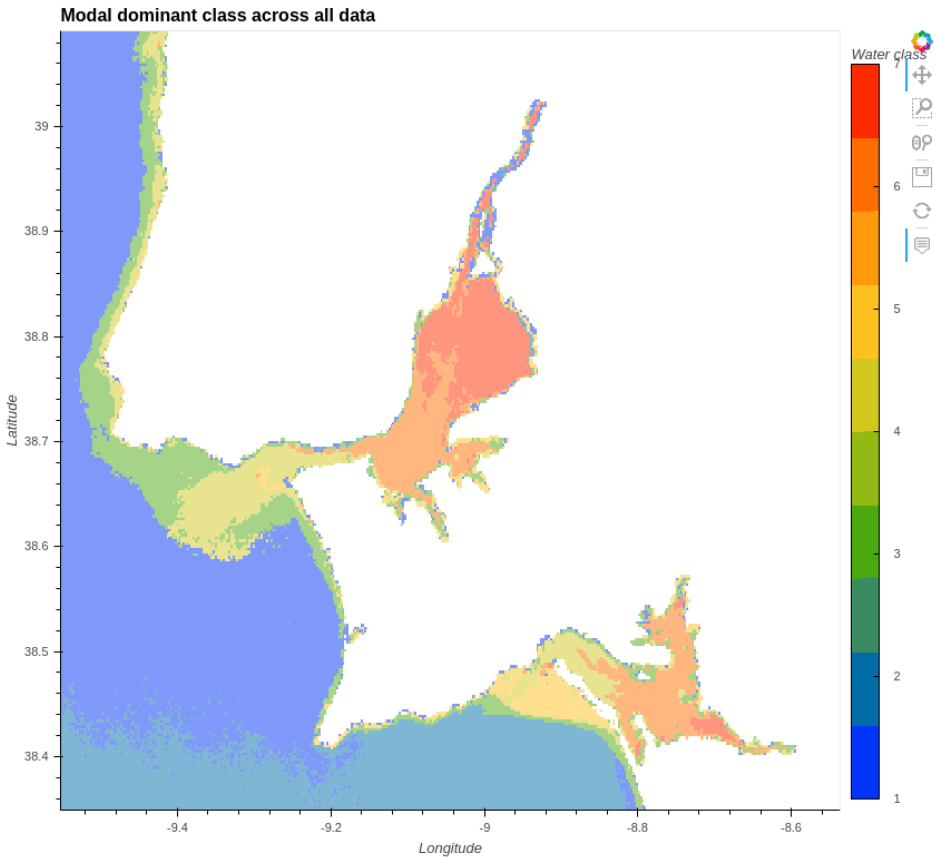

Figure 5.7: Dominant optical water class across all data for the Tagus using Sentinel 3.

5.2.5 Sentinel 3 OWT temporal analysis

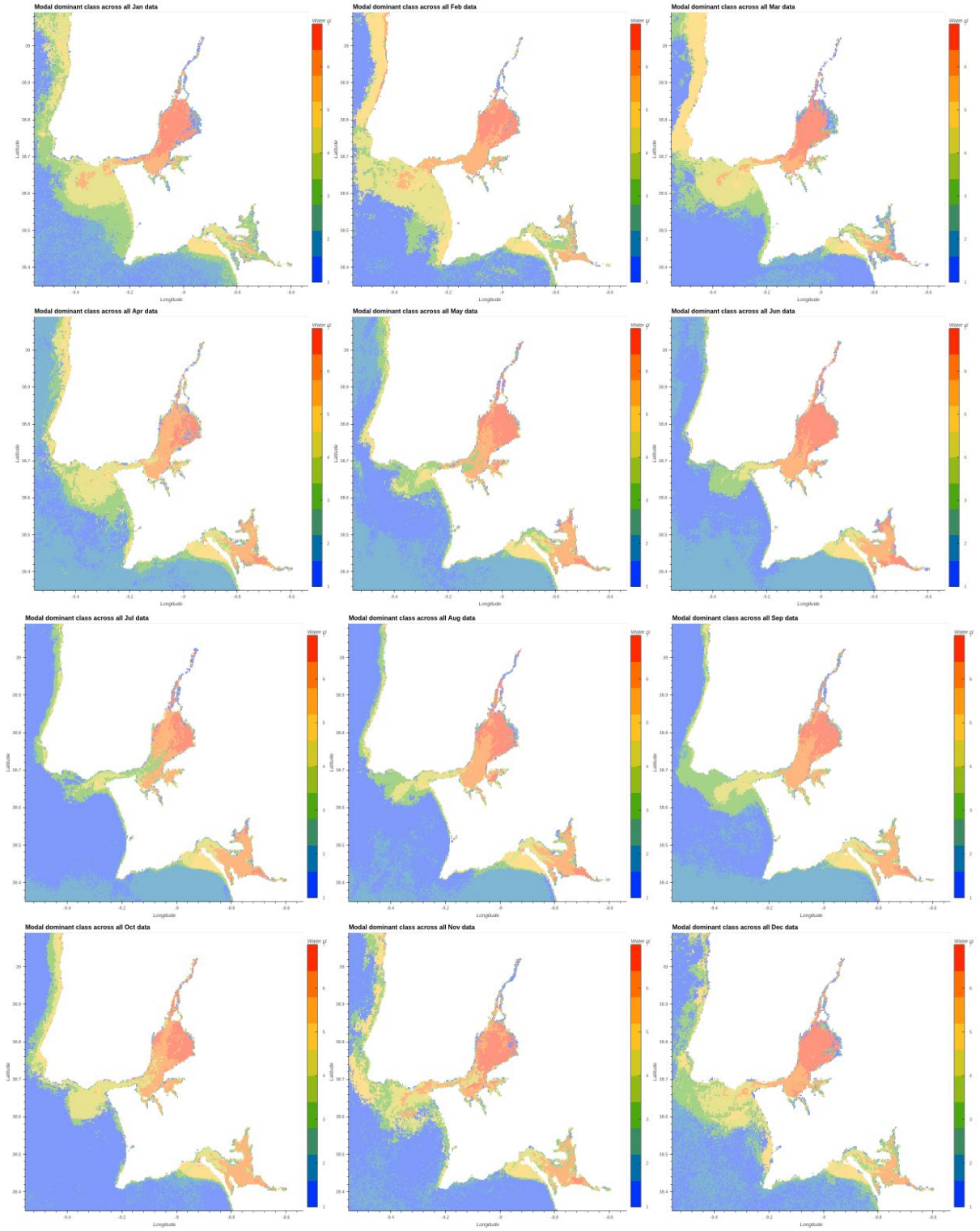

Figure 5.8: (rows, left to right) Temporal analysis of OWT in the Tagus estuary from January to December.

5.2.6 Revised Sentinel 3 OWT Analysis

The OLCI dataset has been updated to cover a longer time period that better matches that of the Sentinel 2 MSI dataset, thus cluster analyses for the OLCI dataset is being updated as follows:

- OLCI 300m data processed with the POLYMER processor: 2016-04-27 to 2021-03-08
- Training dataset built using regular subsampling along scan and cross scan directions, wavelengths used were: 400, 412, 443, 490, 510, 560, 620, 665, 674, 681, 709, 754, 779, 865 and 885 nm

- Winter month exclusion from training dataset (based on incident light level <30° calculated using NOAA solcalc): December

Analysis on the new OLCI dataset is ongoing and will be made available to the Tagus team.

5.3 Sentinel 2 OWT Analysis

5.3.1 Sentinel 2 MSI dataset

- MSI 60m data processed with POLYMER processor: 2016-11-01 to 2020-12-31
- Training dataset built using regular subsampling along scan and cross scan directions, wavelengths used were: 443, 490, 560, 665, 705, 740, 783, 865, 1610 and 2190 nm
- Winter month exclusion from training dataset (based on incident light level <30° calculated using NOAA solcalc): November-January
- Prior to clustering, spectra were standardised using a standard scalar and then principal component analysis (PCA)
- Clusters created using Euclidian distance in principle-component-space

5.3.2 Sentinel 2 OWT classes

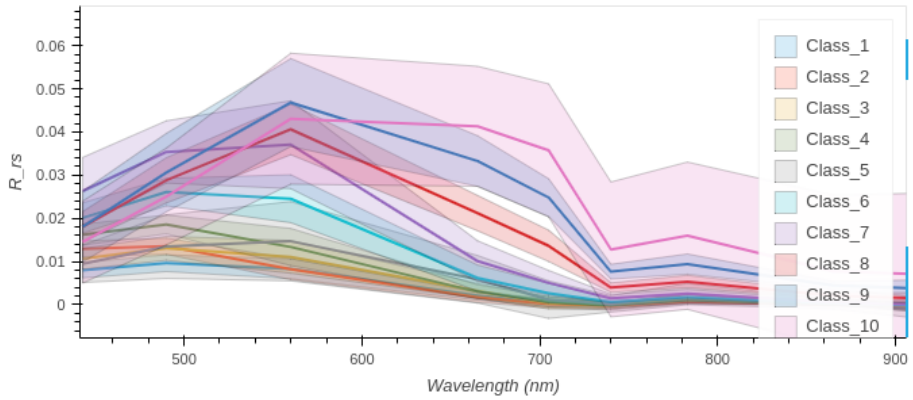

Figure 5.9: Optical Water Classes obtained in the Tagus using Sentinel 2

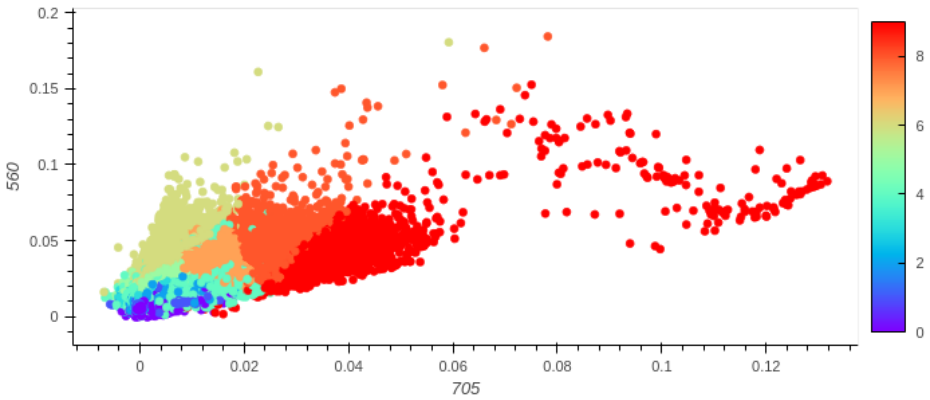

Figure 5.10: Optical Water Classes in 2 dimensional space in the Tagus using Sentinel 2. Add one to the colourbar values for the OWT (colourbar is 0 indexed).

5.3.3 Sentinel 2 OWT Spatial analysis

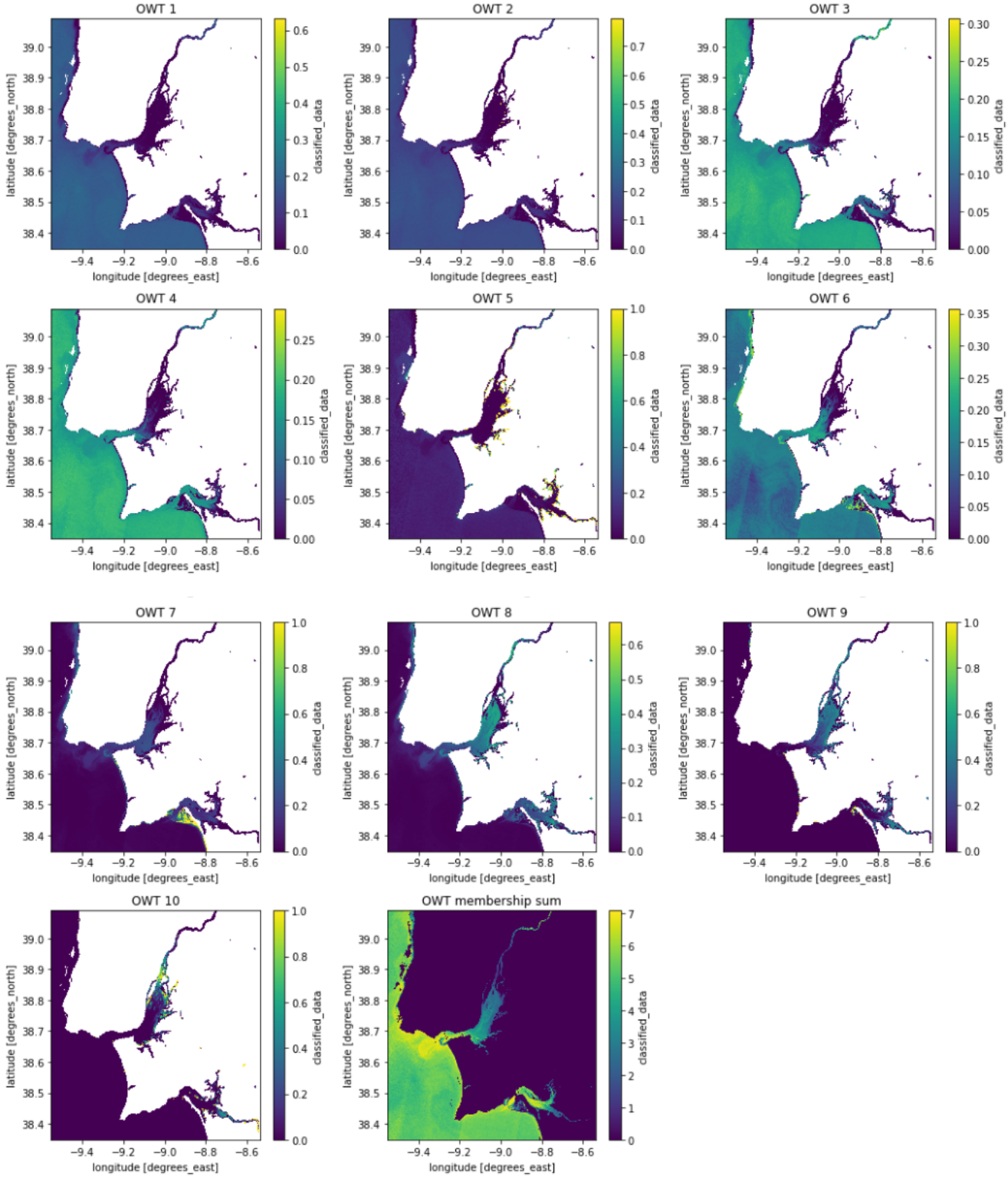

Figure 5.11: Spatial distribution of OWT classes for 2020-09-06 using Sentinel 2

5.4 Influence of local processes

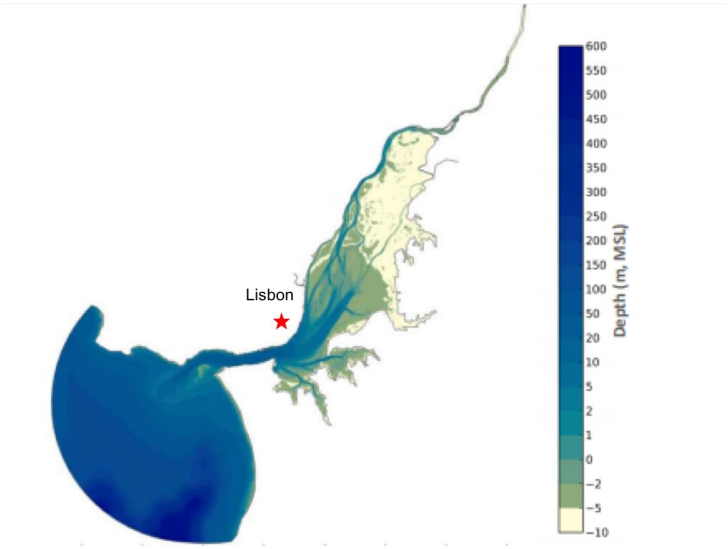

Figure 5.12. Tagus estuary bathymetry (MSL - Mean Sea Level), courtesy of Rodrigues et al. (2017).

Tidal influence

The drainage in the Tagus estuary is primarily forced by the tides (semidiurnal, as in the whole Portuguese coast). However, the circulation is also influenced by the river flow, wind, and atmospheric pressure. The maximum tidal speeds are registered at the mouth of the estuary with values around 2 m/s, where also the maximum depths are registered (Figure 5.12), decreasing towards the interior of the estuary (APA, 2016), characterised by smaller water column depths. The tidal range varies from 0.8 m (neap tide) to 4.0 m (spring tide) (Fortunato et al., 1997) and increases towards the estuary's interior as a result of a small resonance effect. During spring tides the high water can be delayed by as much as two hours between Lisbon and Vila Franca de Xira.

River discharge

River discharge may significantly influence water levels, but only further than 40 km upstream of the mouth of the Tagus estuary (Vargas et al., 2008). Downstream, the water levels are mainly controlled by the tides and storm surges. The Tagus river is the main tributary of the Tagus estuary and the principal source of freshwater. The mean river discharge is 336 $m^3 s^{-1}$ (APA, 2012). Other characteristic discharge values are: maximum (10 days/year), 828 $m^3 s^{-1}$; median (180 days/year), 239 $m^3 s^{-1}$; minimum (355 days/year), 102 $m^3 s^{-1}$. Two other rivers contribute significantly to the water inflow to the estuary: The Sorraia and Trancão rivers. The temporal variation of the river discharge into the estuary is shown in Figure 5.13. Seasonally, the highest river discharge rates are found from October/November to March/April.

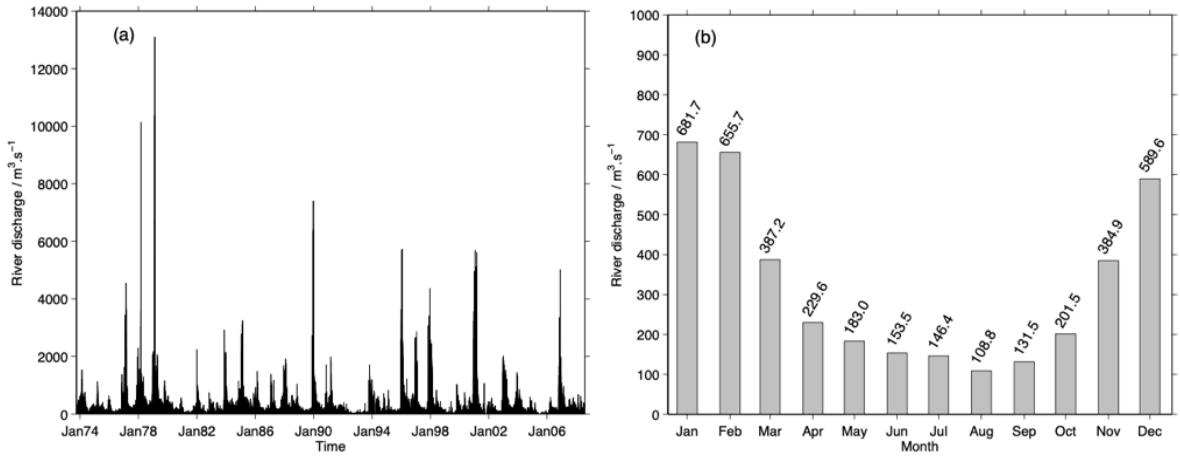

Figure 5.13. River discharge ($m^3 s^{-1}$) at Almourol (located about 80 km upstream from the Tagus estuary) as (a) daily mean values for the period 10/1973 - 07/2008 and (b) monthly means weighted by the number of months with observations (Data source: Sistema Nacional de Informação de Recursos Hidricos).

Wind regimes

The wind regime is mainly characterised by northerly winds (responsible for the locally generated waves in the inner bay which resuspend, move and accumulate sand in the southern margin of the inner Tagus estuary) predominant during summer, and by southwesterly winds mainly occurring during winter.

Sun-glint events

The strong northerly wind regimes and the high sunlight angle observed during summer months lead to higher probability of sun-glint effects between April and end of August (Figure 5.14). The sun-glint events that occur in Summer on the Tagus estuary may vary from low to strong intensities (Figure 5.15).

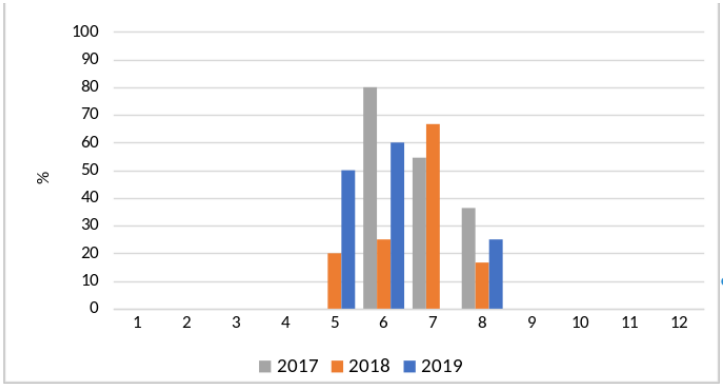

Figure 5.14. Percentage of sunglint contaminated images over the Tagus estuary. Both Sentinel-2A and Sentinel-2B have been considered.

Figure 5.15: Example of RGB S2-B image contaminated by a strong sun-glint. On the right, the Tagus estuary is completely covered by the reflection of the sun which masks the water features. RGB image captured by S2-B satellite on the 28-05-2019.

Bottom reflectance

The inlet of the estuary presents an area characterised by a small water column and white sand banks that cause bottom reflection even with high water conditions. The submerged sand bars near the mouth of the estuary (Figure 5.16) and the clear waters that characterise the area, designate the region as optically shallow (bottom reflection). These sand bars prevent small frequency waves entering the inlet channel due to the sheltering effect. Furthermore, the intertidal zone that characterises the most inner regions of the estuary may also suffer from bottom reflectance. These regions are composed of mudflats.

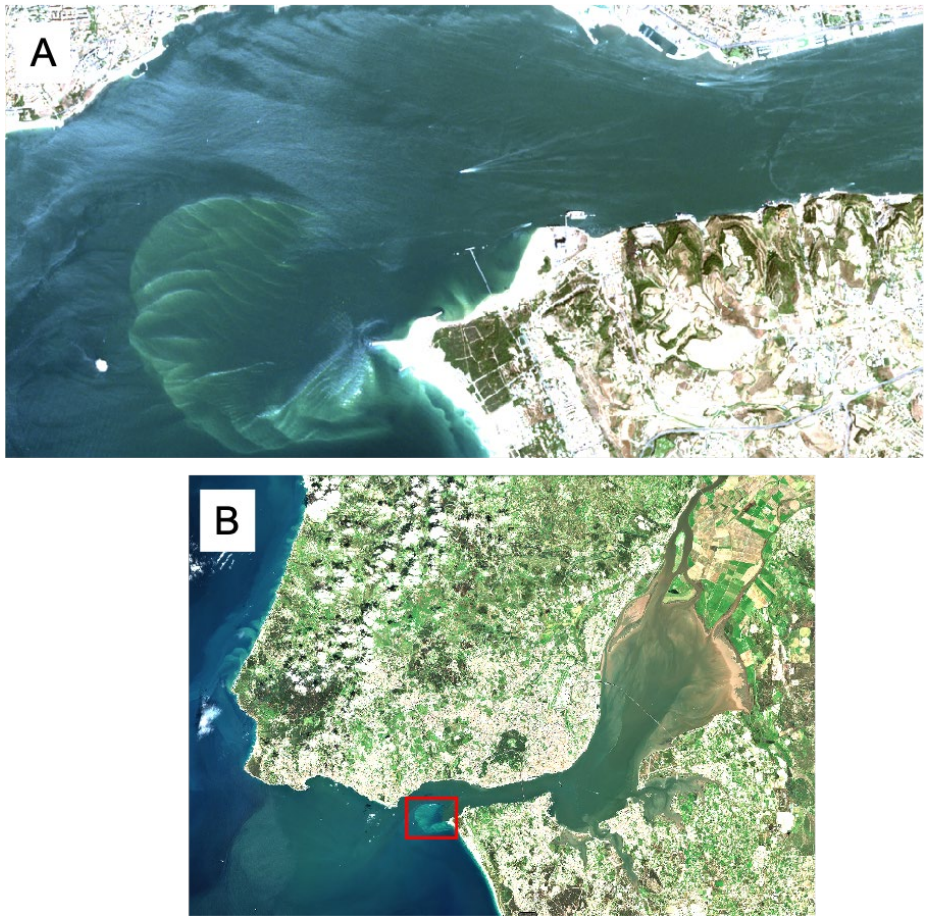

Figure 5.16. (A) bottom reflection caused by white sandbanks present at the mouth of the estuary. (B) Location of the submerged sandbanks on the Tagus estuary.

5.5 Identification of under sampled regions

5.5.1 Satellite (Sentinel 2) and in situ match up analysis

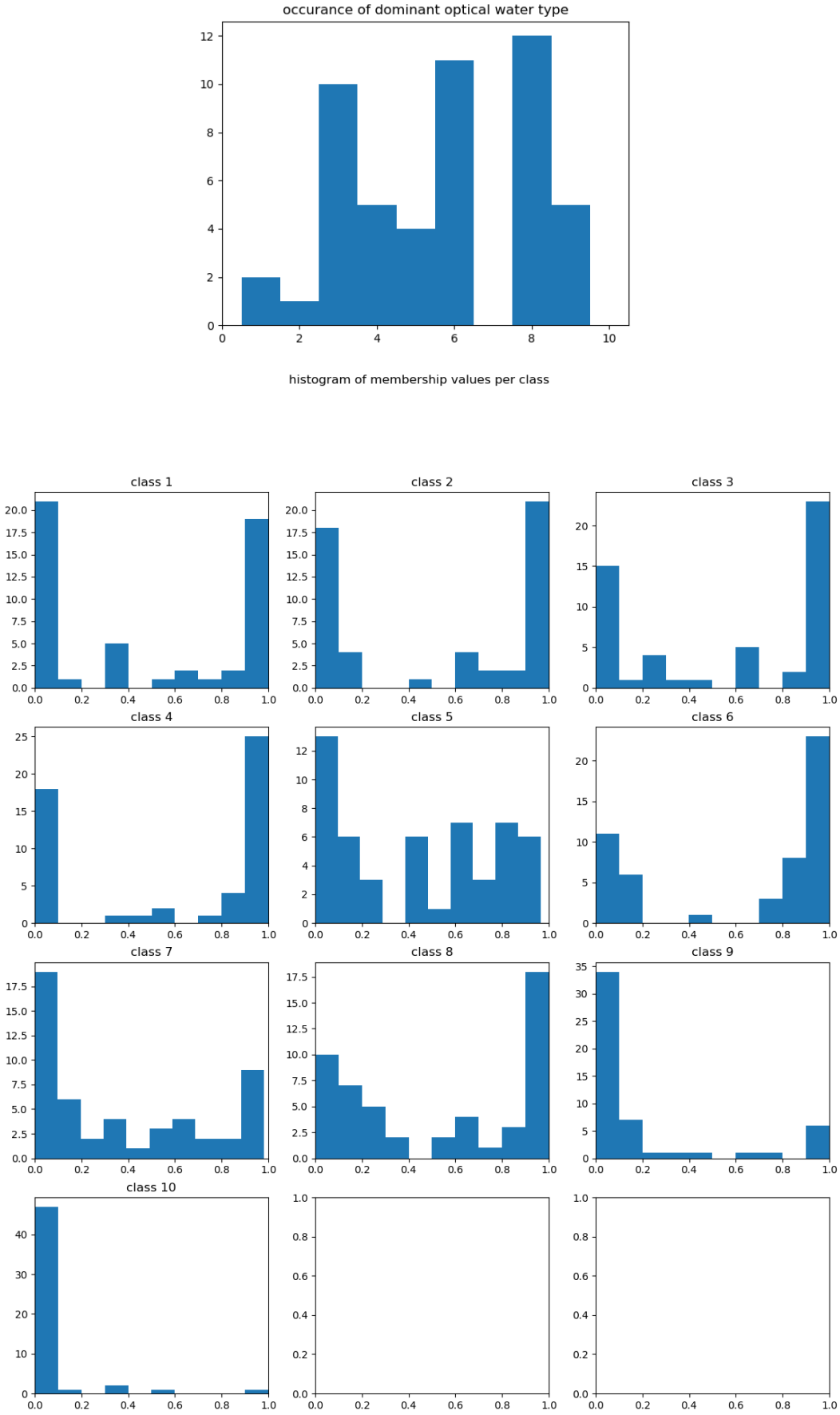

Figure 5.17: (top) Dominant optical water type and (bottom) histogram of membership values per class for the Tagus using Sentinel 2.

5.6 Proposed ideal sampling time for year 2 (2021) in the Tagus Estuary

For aiding the validation and interpretation of satellite data, the ideal sampling time would be at the same moment as the satellite overpass. This is not possible in most cases so we propose that the in situ measurements should be taken within a 3-hour window either side of the satellite overpass so that the influence of tides and weather changes are reduced.

- Time of sampling – September/October, 2021
- Sampling duration - 2 weeks
- Sampling platform availability – logistics required
- Campaign participants – FC.ID, USTIR*

Table 5.2: Sentinel 3 passes over Tagus in September-October 2021

	September (date)	September (time) UTC	October (date)	October (time) UTC
SENTINEL 3	daily	10:15-11:15	daily	10:15-11:15

Table 5.3: Sentinel 2 passes over Tagus in September-October 2021

Satellite platform	Orbit	Date	Time (UTC)
SENTINEL2A	32352	2021/09/01	11:30
SENTINEL2A	32395	2021/09/04	11:40
SENTINEL2A	32495	2021/09/11	11:30
SENTINEL2A	32538	2021/09/14	11:40
SENTINEL2A	32638	2021/09/21	11:30
SENTINEL2A	32681	2021/09/24	11:40
SENTINEL2A	32781	2021/10/01	11:30
SENTINEL2A	32824	2021/10/04	11:40
SENTINEL2A	32924	2021/10/11	11:30
SENTINEL2A	32967	2021/10/14	11:40
SENTINEL2A	33067	2021/10/21	11:30
SENTINEL2A	33110	2021/10/24	11:40
SENTINEL2A	33210	2021/10/31	11:30
SENTINEL2B	23515	2021/09/06	11:30
SENTINEL2B	23558	2021/09/09	11:40
SENTINEL2B	23658	2021/09/16	11:30
SENTINEL2B	23701	2021/09/19	11:40
SENTINEL2B	23801	2021/09/26	11:30
SENTINEL2B	23844	2021/09/29	11:40
SENTINEL2B	23944	2021/10/06	11:30
SENTINEL2B	23987	2021/10/09	11:40
SENTINEL2B	24087	2021/10/16	11:30
SENTINEL2B	24130	2021/10/19	11:40
SENTINEL2B	24230	2021/10/26	11:30
SENTINEL2B	24273	2021/10/29	11:40

5.7 Covid19 Mitigation: proposed essential measurements and USTIR support

University of Stirling will provide support in terms of instrumentation and post-sampling analysis (for sites that need support). In year 2 (2021) participation by USTIR in the sampling campaigns will be subjected to Covid19 travel restrictions. However, the plan is to replicate a small percentage of samples for Chl-a, TSM, PC and particulate absorption from all sites. Shipping of the samples to USTIR will be arranged accordingly. USTIR will arrange a shipment and a rota of required instrumentation, in association with FC.ID, across the different sites in Europe. Intercomparison experiments therefore are planned in year 3 (2022) with a possibility to participate onboard with a suite of USTIR instrumentation across the sites in the UK and Europe.

The following table represents FC.ID instrumentation capabilities available for CERTO-specific fieldwork campaigns only. This does not include the possibility of additional data gathering efforts using the So-Rad equipment as ferry boxes (i.e. Lisboat).

Table 5.4: Proposed essential measurements and USTIR support.

	Parameters to be measured (essentials in bold)	**Instrumentation/ Sample Analysis 2021**	**Instrumentation/ Sample Analysis 2022**
Biogeochemistry	Chlorophyll a, Chl-a	FC.ID	FC.ID
	Phycocyanin, PC	FC.ID	FC.ID
	Total Suspended Matter, TSM	FC.ID	FC.ID
AOPs	**Remote sensing reflectance, R_{rs}**	FC.ID (TriOS) USTIR (TriOS)	FC.ID (TriOS) USTIR (TriOS)
	Diffuse attenuation coefficient, K_d	FC.ID (PAR) USTIR (USSIMO)	FC.ID (PAR) USTIR (USSIMO)
	Secchi disk depth, Z_{SD}	FC.ID	FC.ID
IOPs	**Total absorption coefficient, a**	USTIR*(ac-s)	USTIR (ac-s)
	Absorption coefficient of phytoplankton, a_{ph}	FC.ID	FC.ID
	Absorption coefficient of non-algal particles, a_{nap}	FC.ID	FC.ID
	Coloured dissolved organic matter, CDOM	FC.ID	FC.ID
	Backscattering coefficient, b_b	USTIR (sc-6)	USTIR (sc-6)
	Beam attenuation coefficient, c	USTIR*(ac-s)	USTIR (ac-s)
Physical Parameters	Water temperature	FC.ID	FC.ID
	Salinity	FC.ID	FC.ID
	Turbidity	FC.ID	FC.ID

	Water depth	FC.ID	FC.ID
Atmospheric parameters	Wind speed	FC.ID	FC.ID
	AOT	USTIR (Microtops)	USTIR (Microtops)

5.8 References

APA (2016) "Parte 6 - Região hidrográfica do Tejo e ribeiras do oeste (rh5)". doi: 10.1179/1743132814Y.0000000460.

Bettencourt, A. et al. (2003) "Typology and reference conditions for portuguese Transitional and Coastal waters. Development of guidelines for the application of the European Union Water Framework Directive." INAG, IMAR.

Brito, A. C. et al. (2015) "Effect of phytoplankton size classes on bio-optical properties of phytoplankton in the Western Iberian coast: Application of Models", *Remote Sensing of Environment.* doi: 10.016/j.rse.2014.10.020.

A. B. Fortunato, A. M. Baptista, and R. A. Luettich, "A three-dimensional model of tidal currents in the mouth of the Tagus estuary," *Cont. Shelf Res.*, 1997, doi: 10.1016/S0278-4343(97)00047-2.

Vargas, C. I. C. et al. (2008) "Analise da vulnerabilidade de uma praia estuarina à inundação: applicação à restinga do Alfeite (estuário do Tejo)", *Revista da gestão Costeira Integrada,* 8, p. 25:43. doi: 10.5894/rgci26.

6 Case Study Area 4: Plymouth Sound

Plymouth Sound (English Channel)

Plymouth Sound is part of the Western Channel Observatory (WCO) situated on the north-west European Shelf that straddles several biogeographical provinces. The marine laboratories in Plymouth have sampled at several sites within the western English Channel for over a century in open shelf (e.g. station E1) and coastal (e.g. station L4) waters (Figure 6.1).

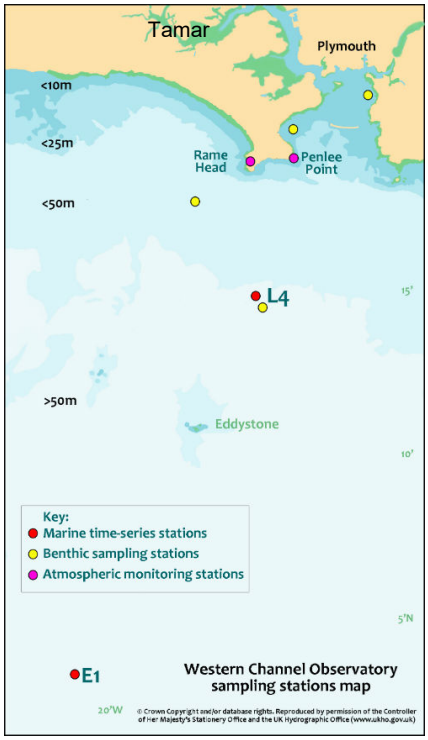

Figure 6.1: Bathymetry and location of the station L4 (coastal) and the station E1 ("oceanic"), part of the Western Channel Observatory (WCO). From http://www.westernchannelobservatory.org.uk

6.1 Current sampling locations and bio-optical monitoring

Both stations are seasonally stratified generally from mid-April until September and the biological response changes from year to year being regulated by subtle variations in temperature, light, sea-water chemistry and meteorology (Smyth et al., 2009). Station L4 is characterised by summer nutrient depletion, although intense summer precipitation increasing riverine input to the system, mainly from the river Tamar, results in pulses of increased nitrate concentration and surface freshening. Both stations have both a spring and autumn bloom, although at station E1 the autumn bloom tends to dominate in terms of chlorophyll concentration.

Historically, the sampling at L4 and E1 included sampling of the water column for general physical (temperature and salinity), chemical parameters (nutrients), and biological (pigment composition, pico and microphytoplankton counts and zooplankton counts). Intermittently, bio-optical relevant datasets have also been collected at a weekly frequency in the past. These included water sample collection for discrete optically active components characterisation (i.e. CDOM, SPM and particulate absorption) as well as in situ flow through an optics-dedicated package (including absorption-attenuation meters and backscatter meters) (Figure 6.2).

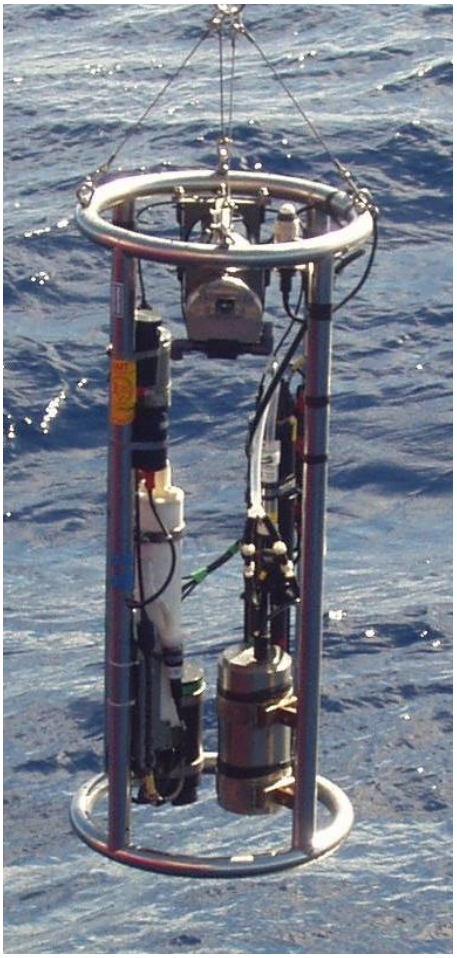

Figure 6.2: Bio-optical profiler at L4/E1, including WetLabs ac-9; Absorption & attenuation, Seabird 19 CTD; Temperature & salinity and a Wetlabs backscatter meter.

Data from past optical studies at L4 have helped to conclude that the combination of seasonal dynamics with precipitation/river outflows, wind mixing and tidal mixing, control the changes of optical properties between case I (waters whose optical properties are determined primarily by phytoplankton and related colored dissolved organic matter (CDOM) and detritus degradation products) and case II (everything else, namely waters whose optical properties are significantly influenced by other constituents such as mineral particles, CDOM, or microbubbles, whose concentrations do not covary with the phytoplankton concentration), observed at station L4 (Groom et al., 2009).

6.1.1 Underway sampling routes

An above water hyperspectral radiometer (Satlantic HyperSAS) is currently installed on the bow of PML's regular sampling vessel (RV Quest, Figure 6.3). Data are collected underway during the outings of the regular sampling for the weekly monitoring of L4 (or fortnightly for E1) and also opportunistically, when the vessel is deployed for other sampling targets.

Figure 6.3: Satlantic HyperSAS radiometers mounted on the rotating platform on the bow of RV Plymouth Quest.

The transects towards L4/E1 depart normally at 8.30am local time and return to the Plymouth harbour is around 11.00am -12.00 pm local time. The position and timing of the regular transect favours an orientation able to minimise sunglint (Mobley,1999). Sampling takes place continuously and data are stored in 1 to 3 min records (Figure 6.4).

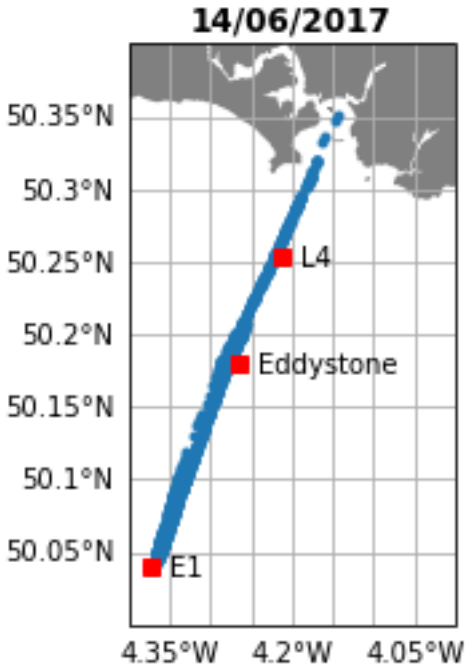

Figure 6.4: Example of location of HyperSAS samples collected on the 14/June/2017 on a transect to E1 (Figure provided by G. Gleratti).

Data from HyperSAS have been used to provide preliminary evidence about the role of the adjacency effects on the remote sensing reflectance from MODIS and VIIRS (Martinez-Vicente et al., 2013) and also to compare atmospheric correction algorithms for Sentinel-2 MSI (Warren et al., 2019).

6.1.2 L4 station

The seasonal changes on the optics at L4 have been correlated to changes in optical backscattering coefficient (b_{bp}), which in turn are dominated by changes in suspended particulate matter concentration (SPM) and proportion of mineral content. It has been shown that, for L4, SPM during winter is dominated by the mineral fraction (or particulate inorganic matter, PIM) (Martinez-Vicente et al., 2010). From a long term study (8 years, N=301) the mean±Std.dev. SPM was 1.00±0.88 mg l^{-1}. Seasonal variations in SPM coarsely follow the two modes for mixed layer depth (MLD) in the L4 station (Figure 6.5). The SPM concentrations change from spring-summer stratified conditions (around 0.80 mg l^{-1}) to autumn-winter conditions (around 1.5 mg l^{-1}). Seasonal variations are superimposed by variability in the mixing (due to wind) and riverine outflow, which are more common during the autumn-winter months.

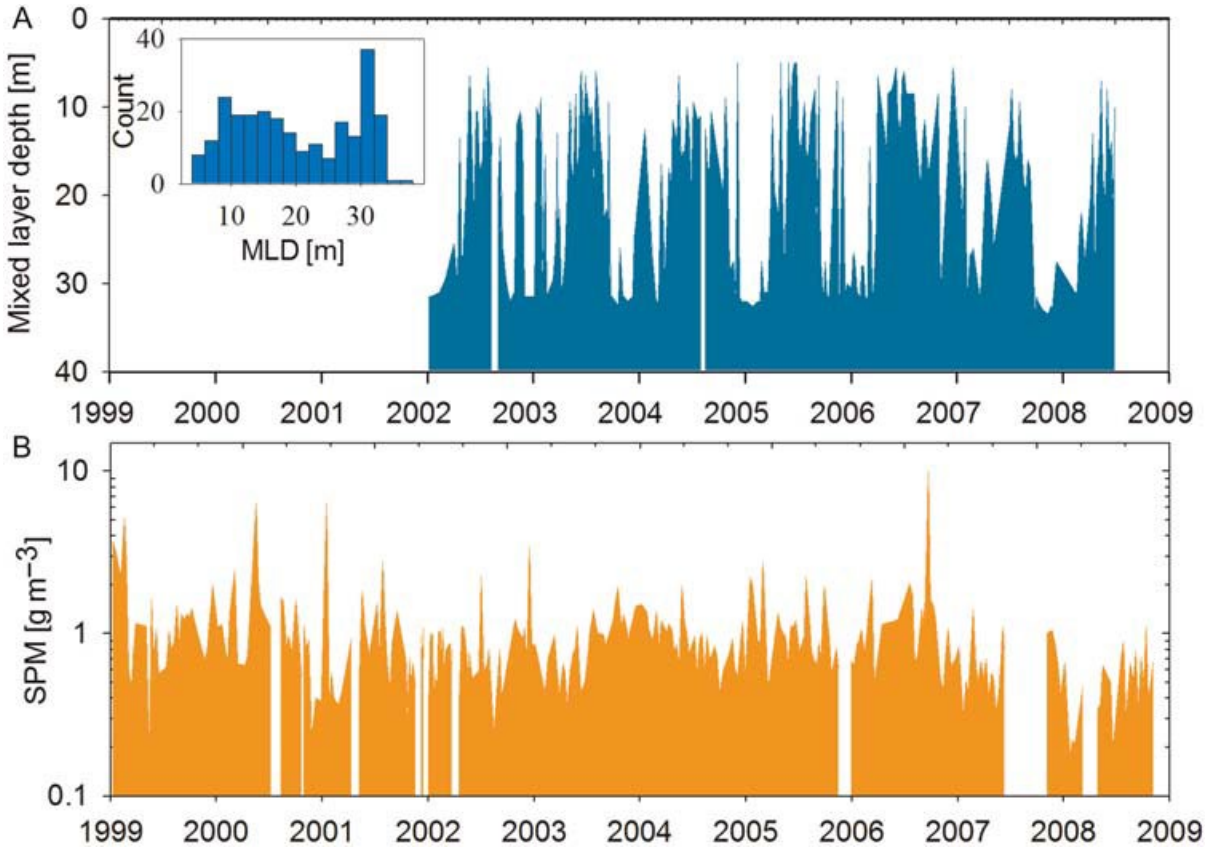

Figure 6.5. Seasonal variations at L4: A) Mixed layer depth computed from density profiles and b) SPM at the surface. Seasonality is superimposed by episodic mixing due to wind and river influx of suspended matter. From Martinez-Vicente et al. (2010)

Current weekly sampling at L4 includes vertical profiling of physical water parameters using a standard CTD package attached to the water sampling rosette (including Temperature, Salinity, chlorophyll fluorescence and optical transmissometer). In addition, discrete water samples are collected at the surface for chlorophyll concentration determination in the laboratory using fluorimetry. Discrete suspended particulate matter concentrations are not currently measured but could be added if required. Discrete particulate absorption and coloured dissolved organic matter are also not routinely sampled at the moment but could be added. The optics rig has been dismantled, but sampling in collaboration with Stirling University could deliver in situ optical data for absorption and backscattering coefficients.

6.2 Sentinel 3 OWT Analysis

6.2.1 Sentinel 3 OLCI dataset

- OLCI 300m data (2019-2021) processed with the POLYMER processor and selected pixels as the training dataset
- These were selected using a regular subsampling of the 300m data in the along scan and cross scan directions
- All visible wavelengths were used (400, 412, 443, 490, 510, 560, 620, 665, 674, 681 and 709nm)
- Prior to clustering the data, the spectra were standardised using a standard scalar and then applied a principal component analysis (PCA) to reproject the spectra
- Clusters are created using Euclidian distance in principle-component-space

6.2.2 Sentinel 3 OWT classes

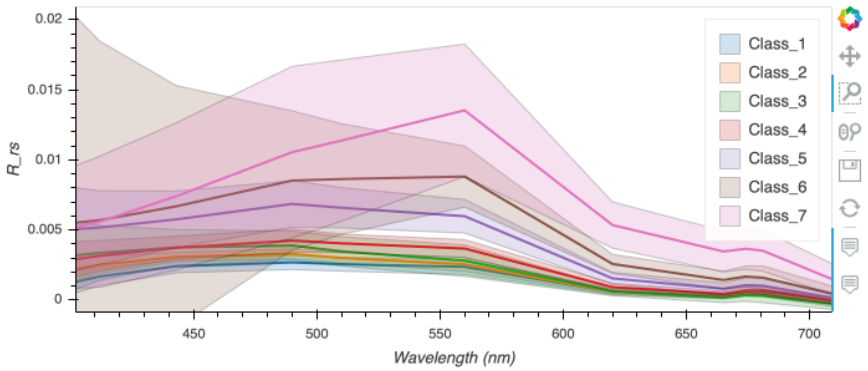

Figure 6.6: Derived optical water classes for Plymouth Sound using Sentinel 3

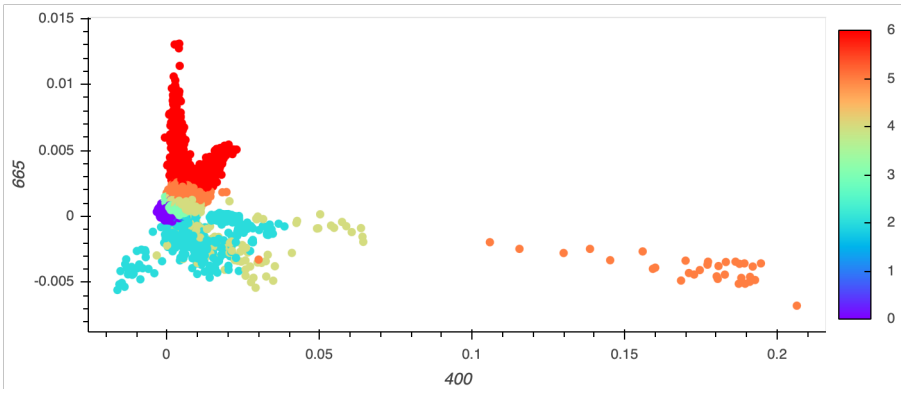

Figure 6.7: Dominant optical water class for each training data point in 2-band Rrs space for Plymouth Sound using Sentinel 3. Add one to the colourbar values for the OWT (colourbar is 0 indexed).

6.2.3 Sentinel 3 OWT Spatial Analysis

This class set was then applied to OLCI data from 2017 to 2021 (though most of the data available is from mid-2018 onwards).

The resulting memberships (daily products) were then used for a number of different types of analysis.

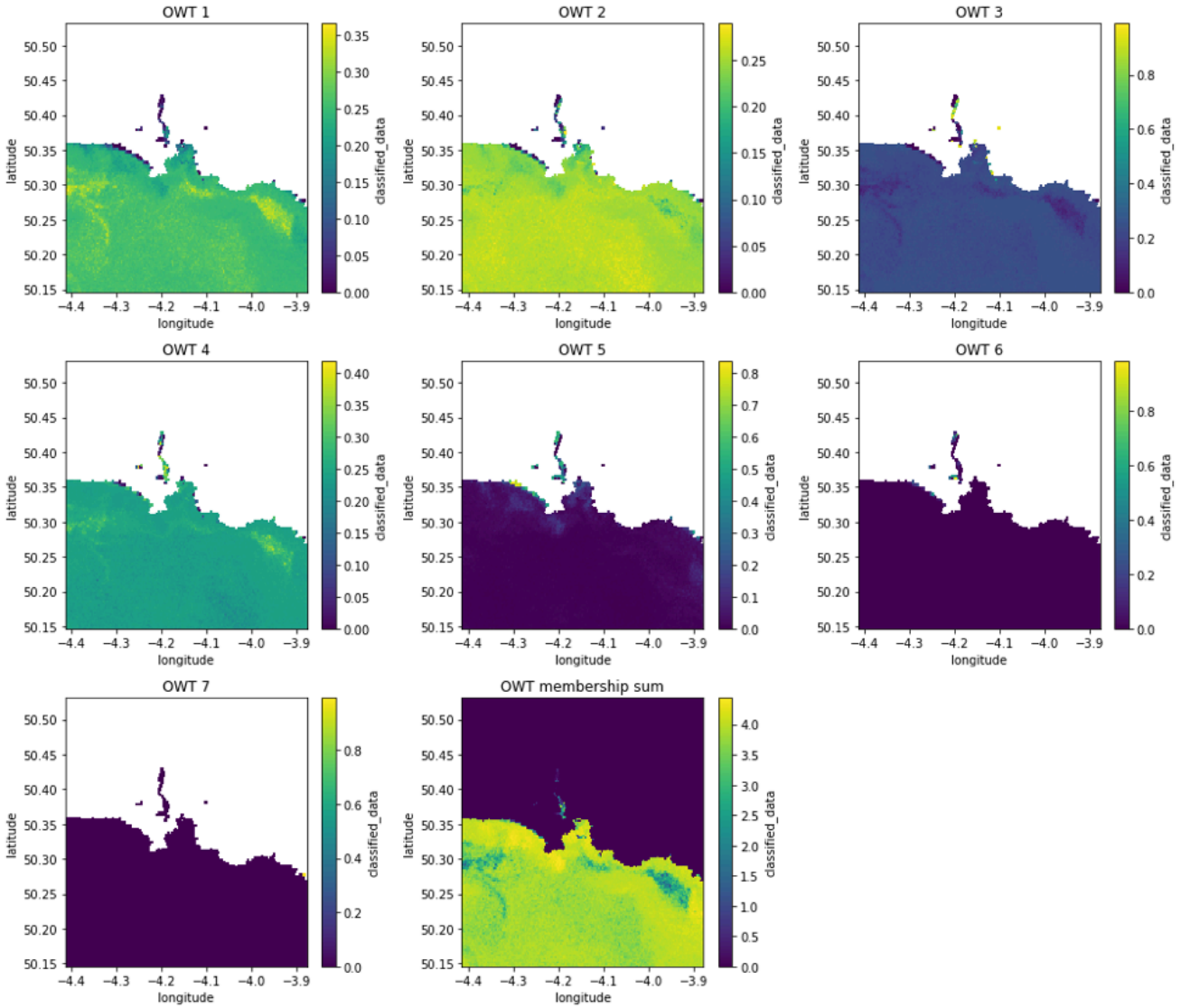

Figure 6.8: Example of clusters applied to data from 2018-08-31 for Plymouth Sound using Sentinel 3. Membership values to each class are shown normalised to the total pixel membership (which is also shown in the last plot).

6.2.4 Sentinel 3 entropy filter and edge detection

The first analysis combines entropy filter and edge detection to try to locate the boundaries between regions of change in the optical water type structure. Where boundaries occur for more than one waterclass we consider this to be a 'strong edge' that is then stored as a variable. An example of this for a single image is shown in figure 6.9.

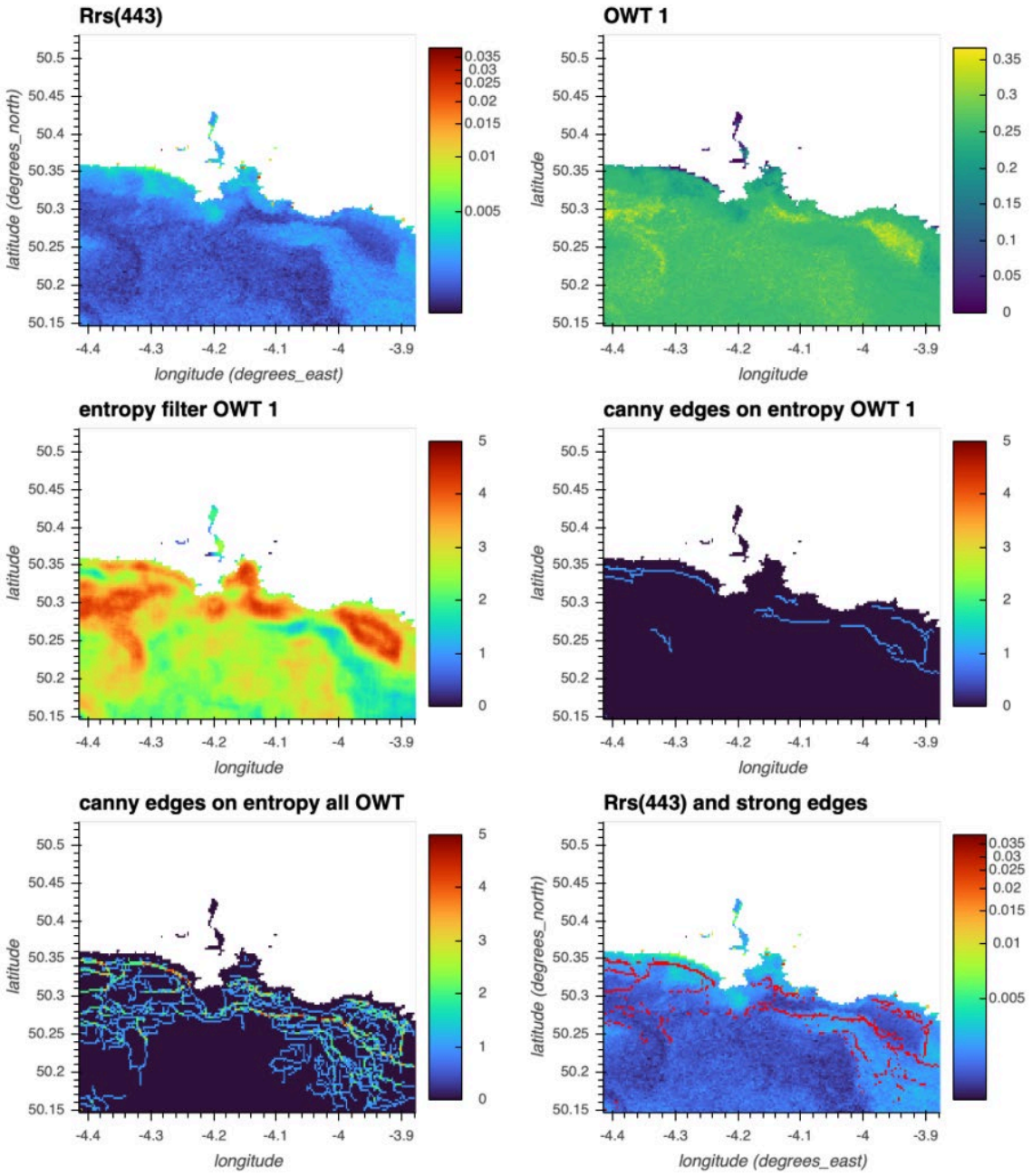

Figure 6.9: Example of entropy filter and edge detection application to data from 2018-08-31 for Plymouth Sound using Sentinel 3.

Stacking these results across all data available for each month we can look for persistent regions of change in optical water type membership structure (Figure 6.10).

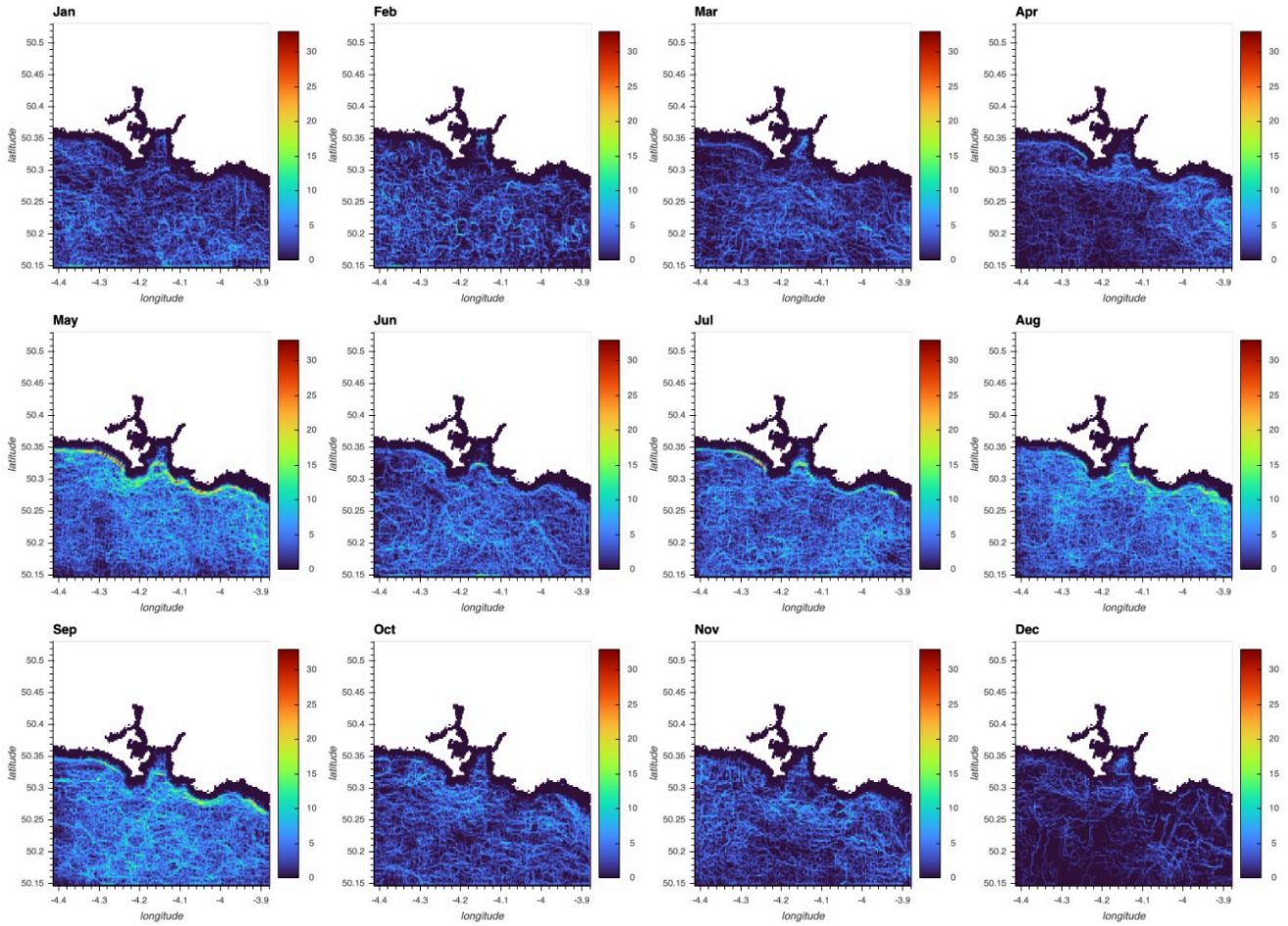

Figure 6.10: Stacked strong front incidence across all data available for a given month (across all years) for Plymouth Sound using Sentinel 3

The strongest front incidence (could have some sampling bias due to clearer skies) appears to be in May, July, August and September. There are regions of interest highlighted around the headlands to either side of the sound and also within the sound itself.

We can then stack this information across all available times (Figure 6.11) and by month (Figure 6.12) and visualise as maps. The colour bar does not line up properly (to be fixed) but for now it is interesting to see the regions of change /dominance.

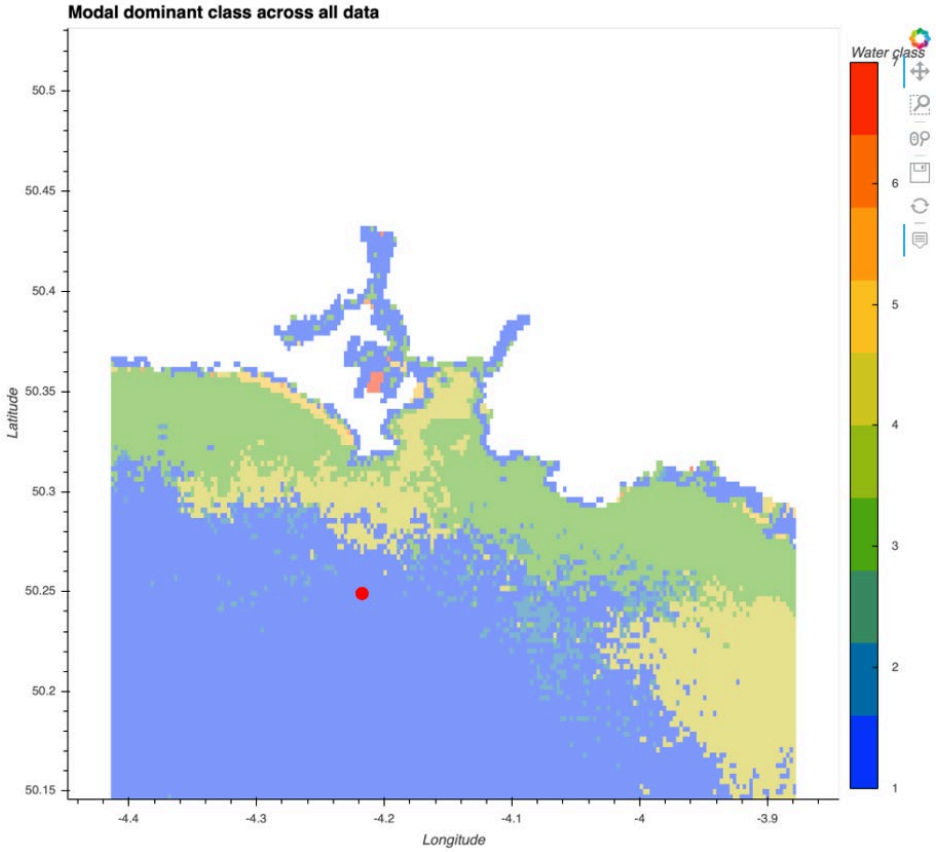

Figure 6.11: Dominant optical water class across all data for Plymouth Sound using Sentinel 3. Red Dot is approximate location of L4 station

6.2.5 Sentinel 3 OWT temporal analysis

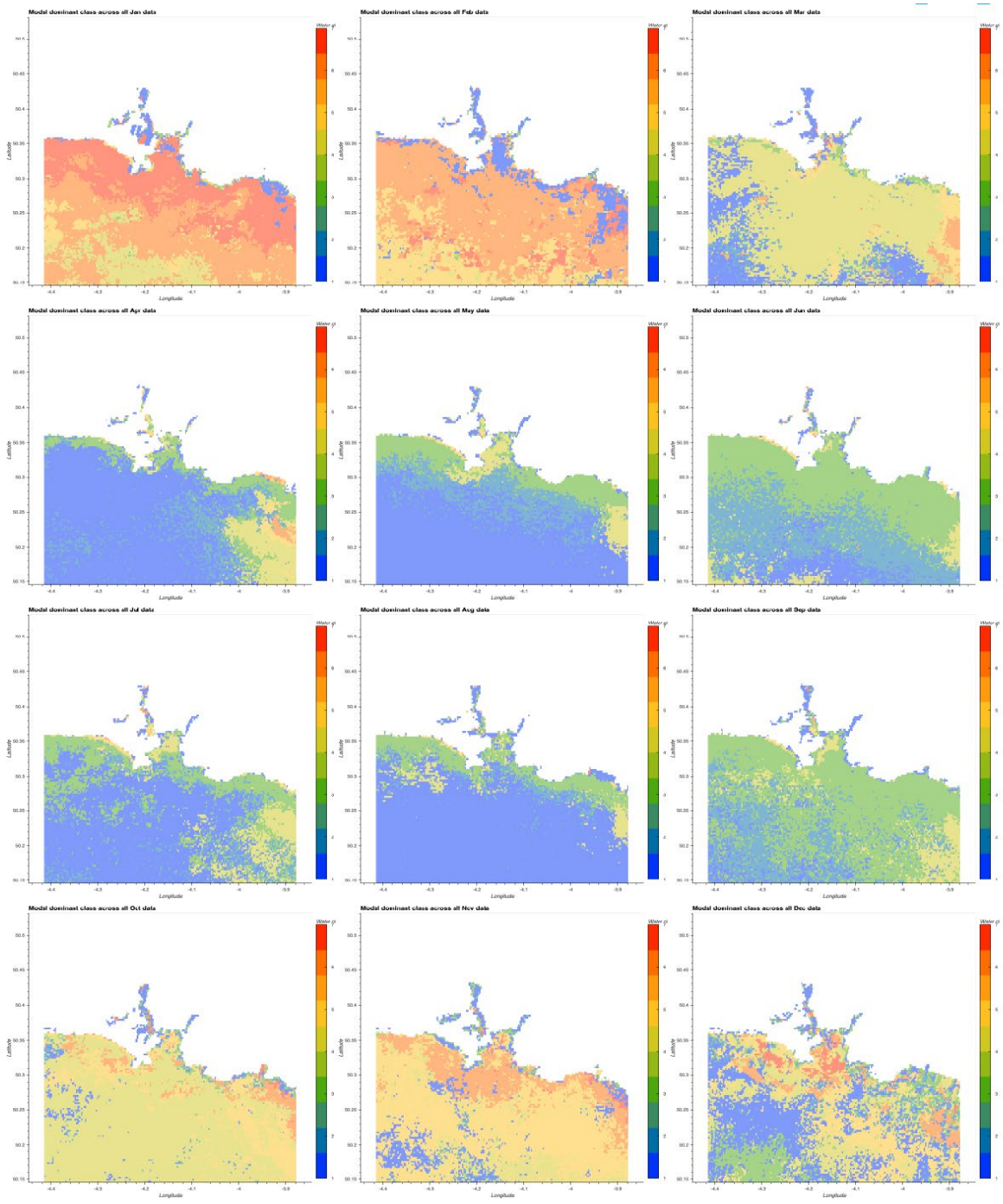

Figure 6.12: (rows, left to right) Temporal analysis of OWT in the Plymouth Sound using sentinel 3 from January to December

6.2.6 Revised Sentinel 3 OWT Analysis

The OLCI dataset has been updated to cover a longer time period that better matches that of the Sentinel 2 MSI dataset, thus cluster analyses for the OLCI dataset is being updated as follows:

- OLCI 300m data processed with the POLYMER processor: 2016-04-27 to 2021-03-08
- Training dataset built using regular subsampling along scan and cross scan directions, wavelengths used were: 400, 412, 443, 490, 510, 560, 620, 665, 674, 681, 709, 754, 779, 865 and 885 nm

- Winter month exclusion from training dataset (based on incident light level <30° calculated using NOAA solcalc): November-February

Analysis on the new OLCI dataset is ongoing and will be made available to the PML teams.

6.3 Sentinel 2 OWT Analysis

6.3.1 Sentinel 2 MSI dataset

- MSI 60m data processed with POLYMER processor: 2016-11-02 to 2020-12-29
- Training dataset built using regular subsampling along scan and cross scan directions, wavelengths used were: 443, 490, 560, 665, 705, 740, 783, 865, 1610 and 2190 nm
- Winter month exclusion from training dataset (based on incident light level <30° calculated using NOAA solcalc): November - January
- Prior to clustering, spectra were standardised using a standard scalar and then principal component analysis (PCA)
- Clusters created using Euclidian distance in principle-component-space

6.3.2 Sentinel 2 OWT classes

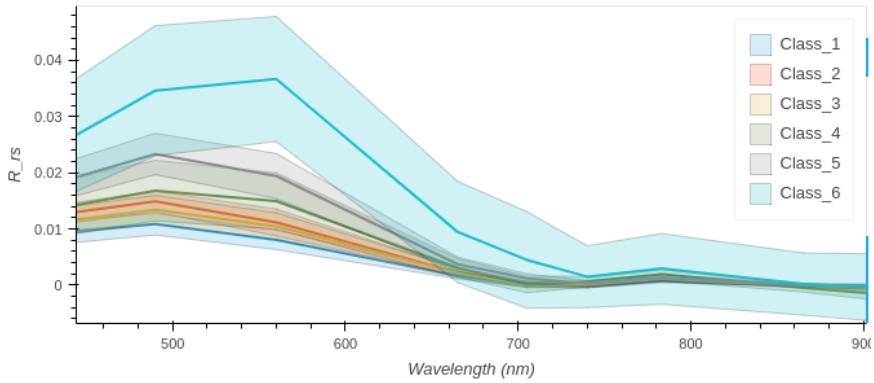

Figure 6.13: Optical Water Classes obtained in the Plymouth Sound using Sentinel 2

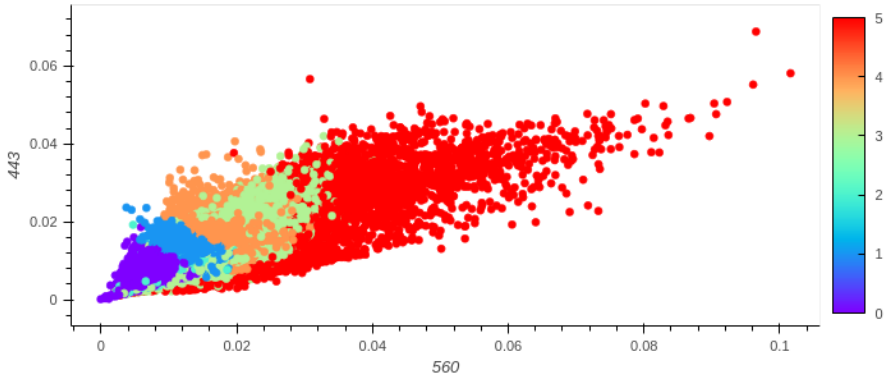

Figure 6.14: Optical Water Classes in 2 dimensional space for the Plymouth Sound using Sentinel 2. Add one to the colourbar values for the OWT (colourbar is 0 indexed).

6.3.3 Sentinel 2 OWT Spatial Analysis

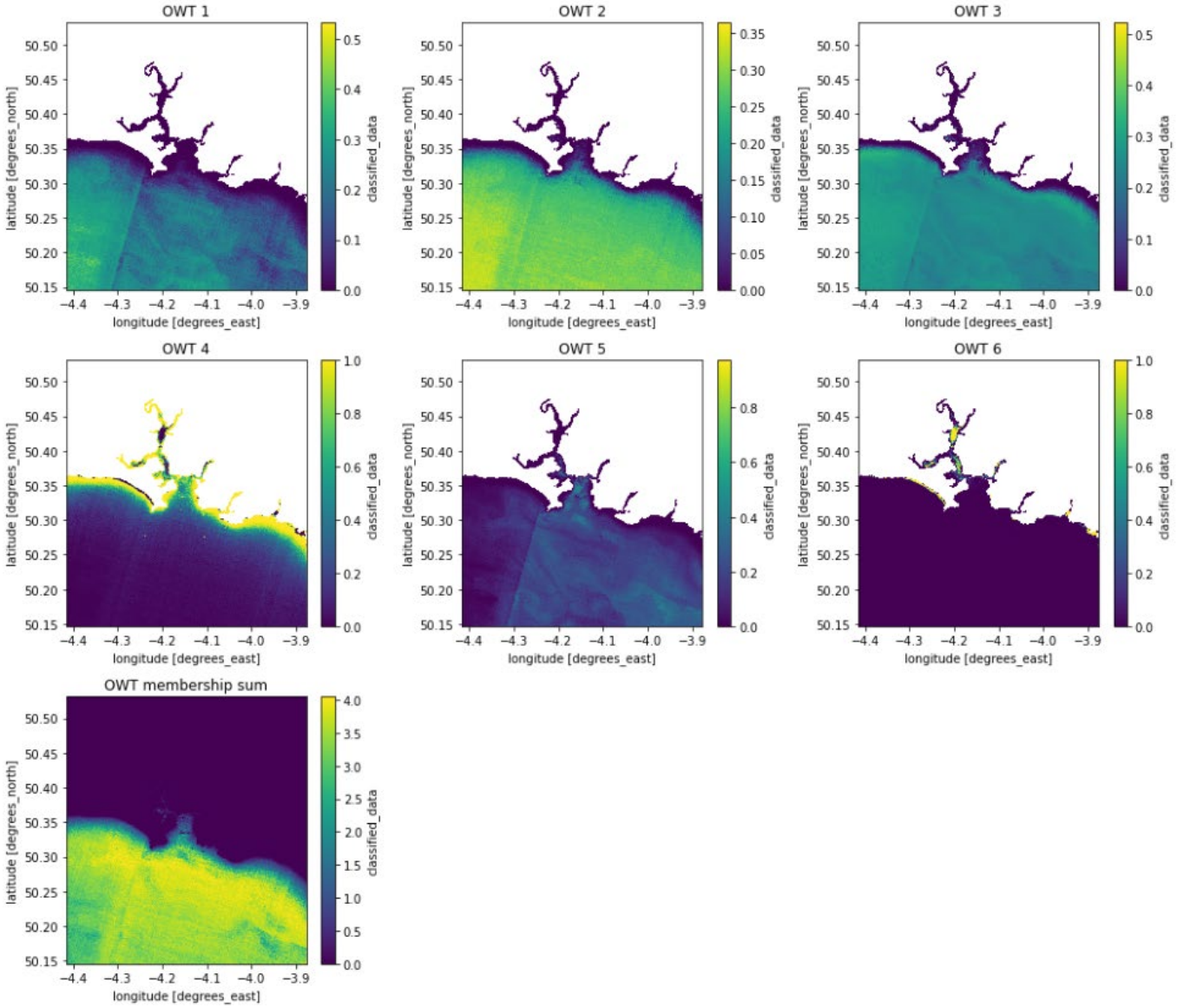

Figure 6.15: Spatial distribution of OWT classes for 2020-09-21 for the Plymouth using Sentinel 2

6.4 Influence of local processes

In addition to seasonal variations, the combination of wind, bathymetry, tidal mixing and river flows affect the dispersion of the riverine water in the area. Wind speed varies between 0 and 10 m/s (median ~3.0 m/s), with the dominant direction and strongest winds coming from the south-west, and the least frequent winds from the north-east (Smyth et al., 2010). Figure 6.16 provides a detailed bathymetry of the area.

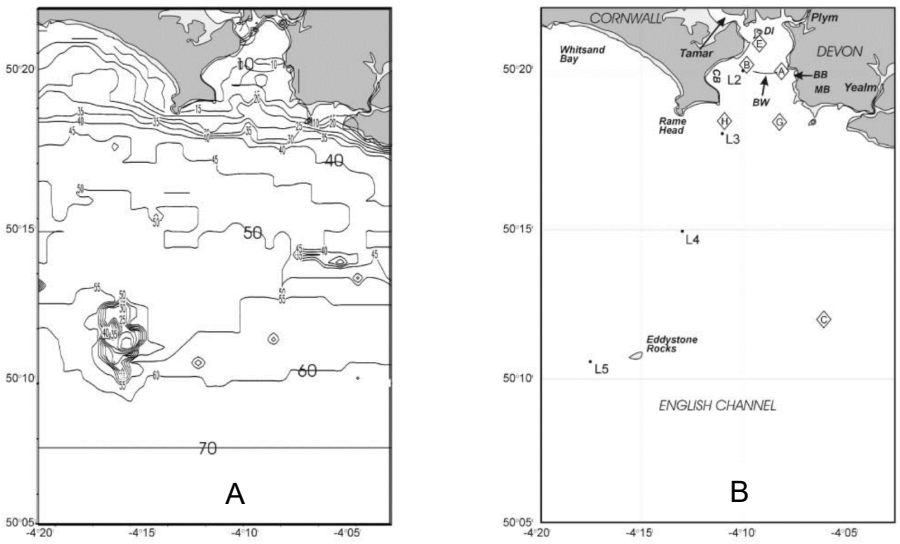

Figure 6.16: A) Bathymetry at 500m x 500m resolution for the area of the Plymouth Sound and Western Channel Observatory obtained from Admiralty charts. B) Position of the stations L4 and Admiralty tidal points (diamonds). From Siddorn et al. (2003).

Bathymetry of the area has three salient features: 1) a shallower (~10 m depth average) area at the mouth of the river Tamar and within the Plymouth Sound; 2) a steep slope off the Rame peninsula that goes down to 40 m depth in ~100 m; 3) a flat sandy bottom sloping from 40 to 70 m towards the centre of the English Channel. There is a wide tidal range (maximum amplitude of ~ 5 m) that superimposes to the bathymetry and riverine runoff (Figure 6.17).

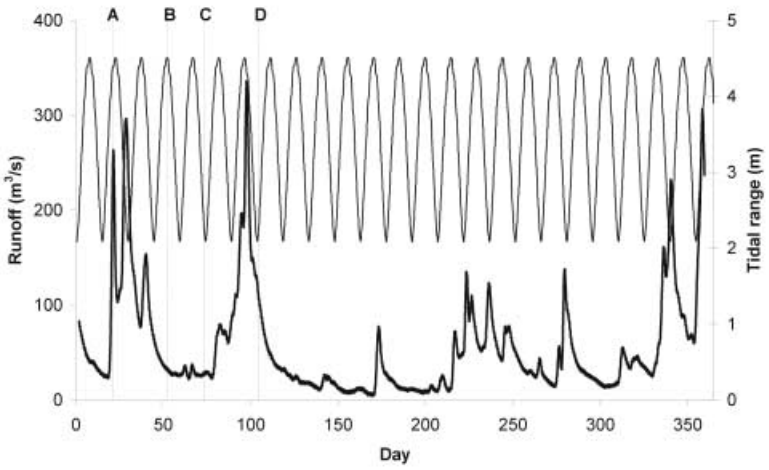

Figure 6.17: Measured runoff and modelled tidal amplitude for the River Tamar and the study area for 1985. The letters A, B, C and D are scenarios of combination of run-off with tidal amplitudes (Siddorn et al., 2003).

6.4.1 Tidal influence/bathymetry maps

Modelling studies provide background information on the influence of local processes on the transitional area of the river Tamar and the Plymouth Sound within the Western Channel Observatory (Siddorn et al., 2003).

The modelled plume coming from a hypothetical release of a passive tracer on the mouth of the river Tamar is shown in Figure 6.18. The distribution follows the tidal currents following release in the scenario where there is high runoff and spring tides (Point A in Figure 6.17). The tracer released under those conditions is predicted to flow out of the Plymouth Sound towards the West.

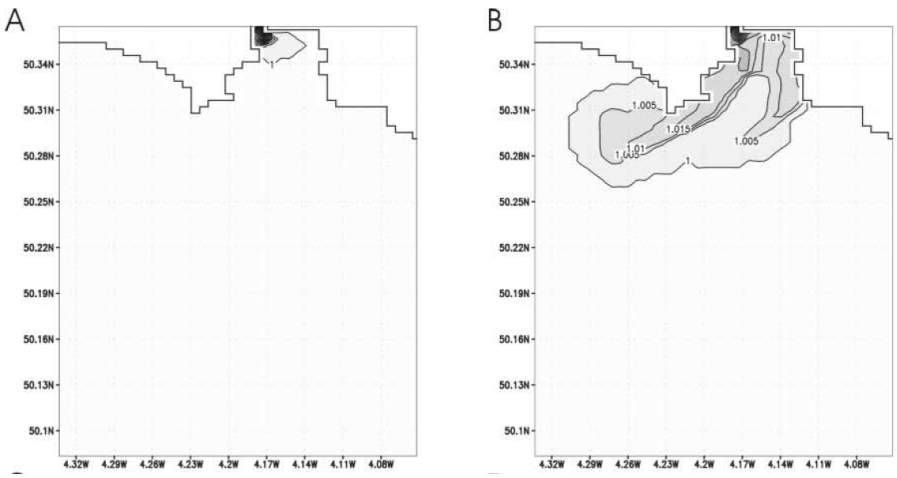

Figure 6.18: Surface tracer distribution for a release at the mouth of the river Tamar: A) high water, 6 hours after the release of the tracer; B) low water, 12 h after the release of the tracer. From Siddorn et al. (2003)

Towards the land, the Tamar estuary (31 km long) is influenced by the tide, which at high tide reaches close to Gunnislake, inland. At low water extensive inter-tidal mudflats are exposed in the central and upper parts of the estuary. At high water and summer spring tides with low run off, the salinity and temperature are vertically homogeneous and density is best explained by the salinity distribution (Figure 6.19). The estuarine turbidity maximum is located at the very low salinity location with SPM of 280 mg l^{-1} at the surface and 880 mg l^{-1} close to the estuary bed (Uncles et al., 2015).

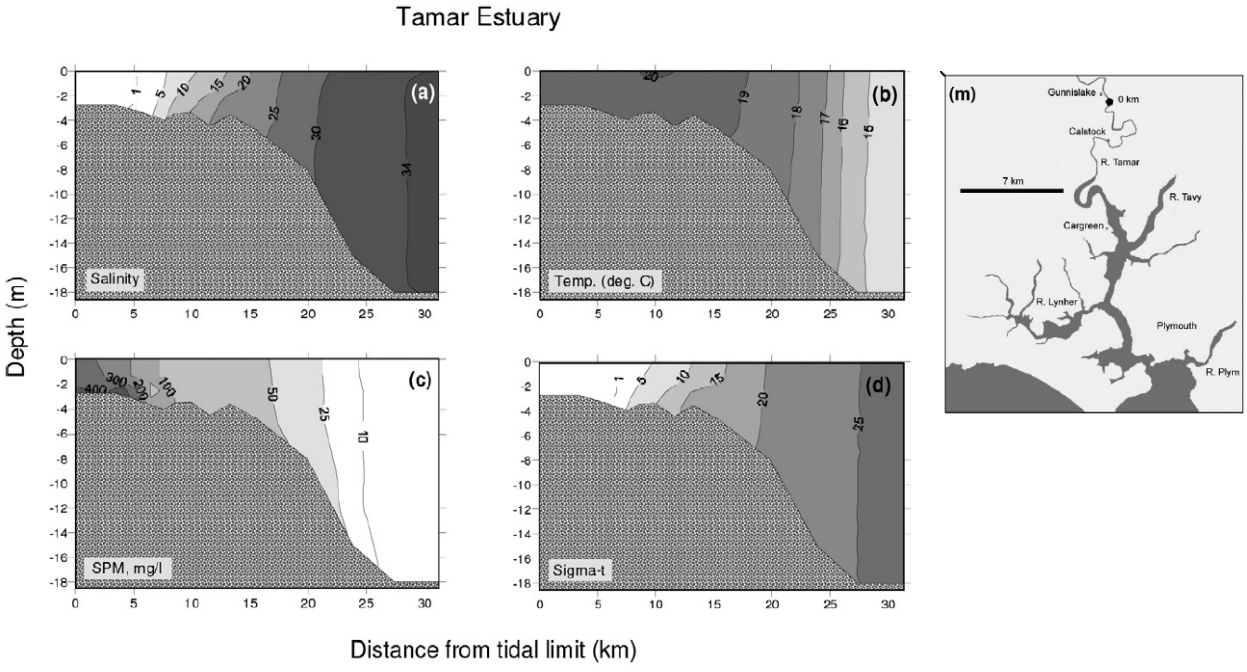

Figure 6.19: Longitudinal transect along the Tamar from the 0 km point (insert), showing a) Salinity b)Temperature c) SPM d) Sigma-t. From Uncles et al., (2015).

6.5 Identification of under sampled regions

6.5.1 Satellite (Sentinel 2) and in situ match up analysis

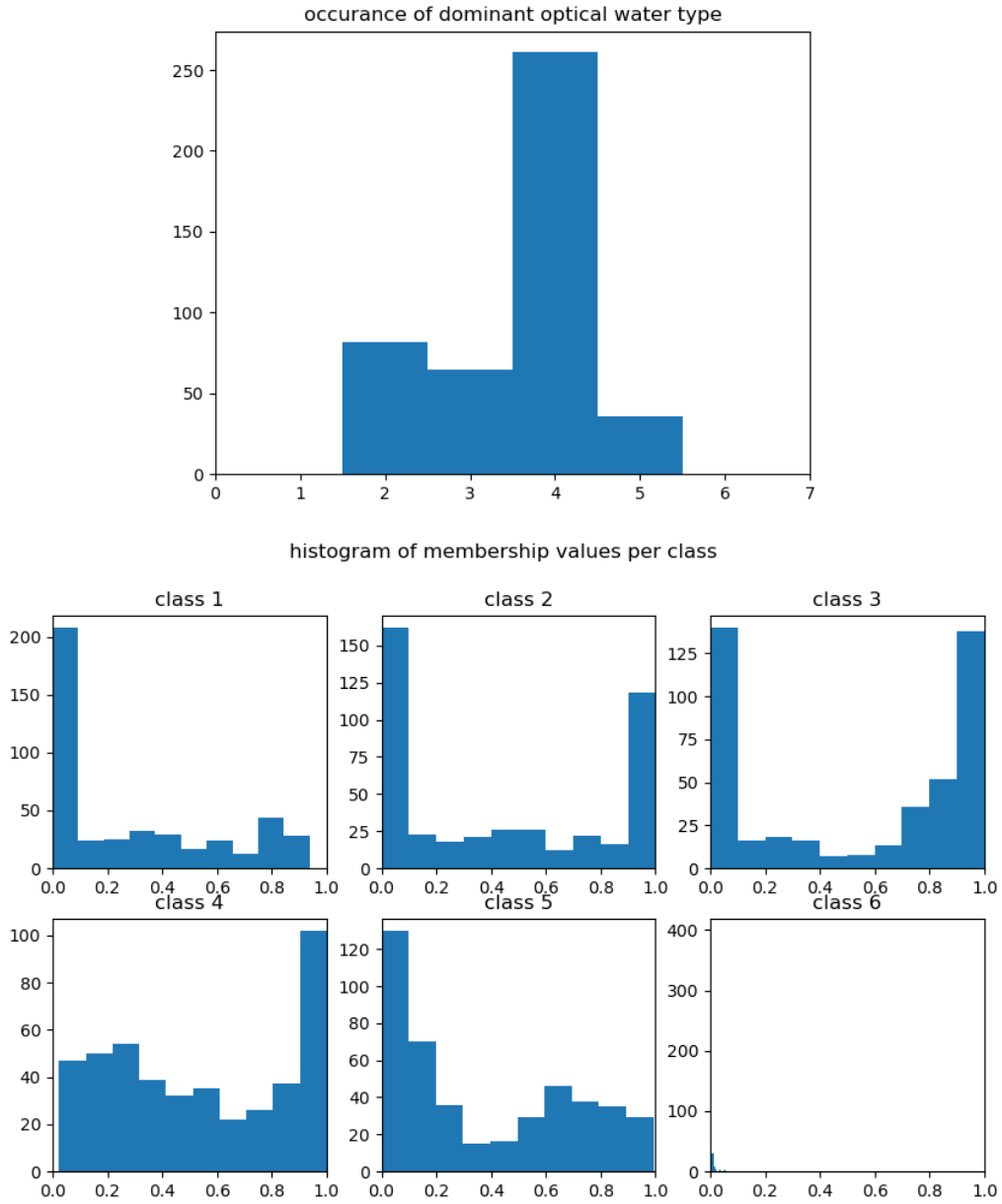

Figure 6.20: (top) Dominant optical water type and (bottom) histogram of membership values per class in the Plymouth Sound using Sentinel 2.

6.6 Proposed ideal sampling time for year 2 (2021) in Plymouth Sound

For aiding the validation and interpretation of satellite data, the ideal sampling time would be at the same moment as the satellite overpass. This is not possible in most cases so we propose that the in situ measurements should be taken within a 3-hour window either side of the satellite overpass so that the influence of tides and weather changes are reduced.

- Time of sampling – September/October 2021
- Sampling duration - 1 week
- Sampling platform availability – logistics arranged, PML Explorer
- Campaign participants – PML, USTIR

Table 6.1: Sentinel 3 passes over Plymouth Sound in September-October 2021

	September (date)	**September (time) UTC**	**October (date)**	**October (time) UTC**
SENTINEL 3	daily	10:00 - 11:10	daily	10:00 -11:00

Table 6.2: Sentinel 2 passes over Plymouth Sound in September-October 2021

Satellite platform	Orbit	Date	Time (UTC)
SENTINEL2A	32352	2021/09/01	11:27
SENTINEL2A	32395	2021/09/04	11:37
SENTINEL2A	32495	2021/09/11	11:27
SENTINEL2A	32538	2021/09/14	11:37
SENTINEL2A	32638	2021/09/21	11:27
SENTINEL2A	32681	2021/09/24	11:37
SENTINEL2A	32781	2021/10/01	11:27
SENTINEL2A	32824	2021/10/04	11:37
SENTINEL2A	32924	2021/10/11	11:27
SENTINEL2A	32967	2021/10/14	11:37
SENTINEL2A	33067	2021/10/21	11:27
SENTINEL2A	33110	2021/10/24	11:37
SENTINEL2A	33210	2021/10/31	11:27
SENTINEL2B	23515	2021/09/06	11:27
SENTINEL2B	23558	2021/09/09	11:37
SENTINEL2B	23658	2021/09/16	11:27
SENTINEL2B	23701	2021/09/19	11:37
SENTINEL2B	23801	2021/09/26	11:27
SENTINEL2B	23844	2021/09/29	11:37
SENTINEL2B	23944	2021/10/06	11:27
SENTINEL2B	23987	2021/10/09	11:37
SENTINEL2B	24087	2021/10/16	11:27
SENTINEL2B	24130	2021/10/19	11:37
SENTINEL2B	24230	2021/10/26	11:27
SENTINEL2B	24273	2021/10/29	11:37

6.7 Covid19 Mitigation: proposed essential measurements and USTIR support

University of Stirling will provide support in terms of instrumentation and post-sampling analysis (for sites that need support). In year 2 (2021) participation by USTIR in the sampling campaigns will be subjected to Covid19 travel restrictions. However, the plan is to replicate a small percentage of samples for Chl-a, TSM, PC and particulate absorption from all sites. Shipping of the samples to USTIR will be arranged accordingly. USTIR will arrange a shipment and a rota of required instrumentation, in association with FC.ID, across the different sites in Europe. Intercomparison experiments therefore are planned in year 3 (2022) with a possibility to participate onboard with a suite of USTIR instrumentation across the sites in the UK and Europe.

Table 6.3: proposed essential measurements and USTIR support

	Parameters to be measured (essentials in bold)	Instrumentation/ Sample Analysis 2021	Instrumentation/ Sample Analysis 2022
Biogeochemistry	Chlorophyll a, Chl-a	PML	PML
	Phycocyanin, PC	---	---
	Total Suspended Matter, TSM	PML	PML
AOPs	**Remote sensing reflectance, R_{rs}**	PML	PML

	Diffuse attenuation coefficient, K_d	USTIR (USSIMO)	USTIR (USSIMO)
	Secchi disk depth, Z_{SD}	PML	PML
IOPs	**Total absorption coefficient, a**	USTIR (ac-s)	PML (ac-s) USTIR (ac-s)
	Absorption coefficient of phytoplankton, a_{ph}	PML	PML
	Absorption coefficient of non-algal particles, a_{nap}	PML	PML
	Coloured dissolved organic matter, CDOM	PML	PML
	Backscattering coefficient, b_b	PML	PML
	Beam attenuation coefficient, c	USTIR (ac-s)	PML (ac-s) USTIR (ac-s)
Physical Parameters	Water temperature	PML	PML
	Salinity	PML	PML
	Turbidity	PML	PML
	Water depth	PML	PML
Atmospheric parameters	Wind speed	PML	PML
	AOT	USTIR (Microtops)	USTIR (Microtops)

7 Case Study Area 5: Elbe Estuary

Elbe Estuary (German Bight-North Sea)

The German Bight and the river Elbe estuary are highly impacted by anthropogenic pressure and, at the same time, comprise a very sensitive ecosystem including the Unesco World heritage Wadden Sea. The Port of Hamburg is the third busiest port in Europe and 15th-largest worldwide. In 2014, 9.73 million TEUs (20-foot standard container equivalents) were handled in Hamburg, with all ships passing through the German bight and the river Elbe to reach the port located 110 km distance from the North Sea. Between the coast and the open North Sea is the Wadden Sea which is the largest unbroken system of intertidal sand and mud flats in the world.

It is a large, temperate, relatively flat coastal wetland environment, formed by the intricate interactions between physical and biological factors that have given rise to a multitude of transitional habitats with tidal channels, sandy shoals, sea-grass meadows, mussel beds, sandbars, mudflats, salt marshes, estuaries, beaches and dunes. The area is home to numerous plant and animal species, including marine mammals such as the harbour seal, grey seal and harbour porpoise. Wadden Sea is one of the last remaining large-scale, intertidal ecosystems where natural processes continue to function largely undisturbed. The German Bight at the southeast of the North Sea is bounded by the Netherlands and Germany to the south, and Denmark and Germany to the east. It is heavily used for shipping, fisheries, and recently for wind energy: 19 wind parks are already in operation, and another 10 wind parks are under construction or planned. In such a heavily used area, marine spatial planning and monitoring of environmental status is of critical importance.

7.1 Current sampling locations and bio-optical monitoring

7.1.1 HZG transects Hamburg to Helgoland

The Helmholtz-Zentrum Hereon (formerly Helmholtz-Zentrum-Geesthacht) operates several research vessels, one of which is the Ludwig Prandtl. The Prandtl is a shallow water vessel, which makes it suitable to sample along the Elbe Estuary up to the German island of Helgoland. It regularly goes along transects and overnight stays measuring, amongst others, chlorophyll concentration, turbidity, as well as CDOM absorption. Dedicated cruises are also planned every year to measure remote sensing reflectance spectra alongside Sentinel-3 OLCI overpasses. One such sampling transect can be seen in red in Figure 7.9

Figure 7.9: HZG RRS sampling transect on 2016-07-20, overlayed on the Sentinel.3 OLCI-A RGB image of that day

7.1.2 Two locations monitored by Hamburg authorities

The institute for Hygiene and Environment examines air, soil and water quality as well as other environmental media. Automated monitoring networks are in place to monitor water bodies, air and radioactivity around the clock. For water quality, the institute operates nine monitoring stations in different water bodies in Hamburg

and makes the data publicly available via https://www.hamburg.de/hu/daten/. Within CERTO, there are two stations of interest, Seemannshoeft and Bunthaus, which provide data on pH, temperature, turbidity and chlorophyll concentrations.

7.1.2.1 Seemannshöft

The Seemannshöft station was put into operation in 1967. It is located on the left (south) bank of the Elbe below the port of Hamburg. Its counterpart is the Blankenese station on the opposite (north) bank of the Elbe. The floating measuring station receives its sample water via centrifugal pumps installed on the dry pontoons. The sample water reaches the measuring stations via 4 to 6-metre-long pipes or hoses laid diagonally through the steel pontoons.

Figure 7.10: Picture of the station on the pontoon (left) and its location the Elbe (right) - image copyright of HU institute.

7.1.2.2 Bunthaus

The Bunthaus station has existed since 1975 and is located just north of the point where the Norder and Süderelbe divide (Bunthausspitze). Since 1 May 1988, the station has regularly supplied data that play an important role in water quality. The floating Bunthaus measuring station receives its sample water via centrifugal pumps installed dry on the pontoons. The sample water reaches the measuring stations via 4 to 6-metre-long pipes or hoses laid diagonally through the steel pontoons.

Figure 7.11: picture of the Station on the pontoon (left) and its location on the Elbe (right) - image copyright of HU institute.

7.2 Sentinel 3 OWT Analysis

7.2.1 Sentinel 3 OLCI dataset

- OLCI 300m data processed with the POLYMER processor and selected pixels as the training dataset
- These were selected using a regular subsampling of the 300m data in the along scan and cross scan directions
- All visible wavelengths were used (400, 412, 443, 490, 510, 560, 620, 665, 674, 681 and 709nm)
- Prior to clustering the data, the spectra were standardised using a standard scalar and then applied a principal component analysis (PCA) to reproject the spectra
- Clusters created using Euclidian distance in principle-component-space

7.2.2 Sentinel 3 OWT classes

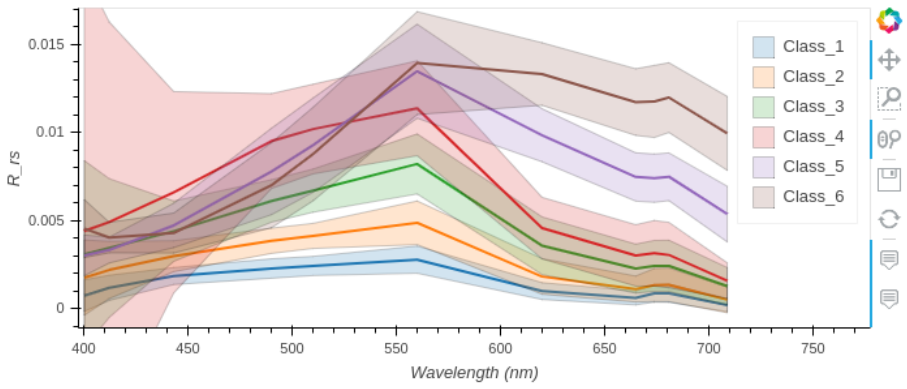

Figure 7.4: Derived optical water classes for the Elbe Estuary using Sentinel 3

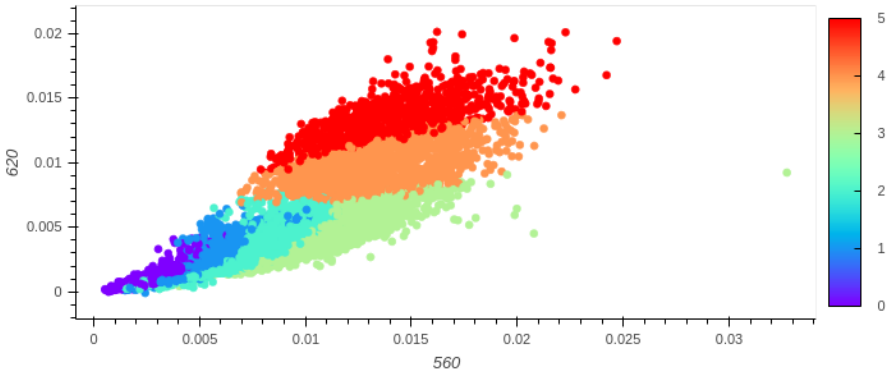

Figure 7.5: Dominant optical water class for each training data point in 2-band Rrs space for the Elbe using Sentinel 3. Add one to the colourbar values for the OWT (colourbar is 0 indexed).

7.2.3 Sentinel 3 OWT Spatial analysis

This class set was then applied to OLCI data from 2019 to 2021. The resulting memberships (daily products) were then used for a number of different types of analysis.

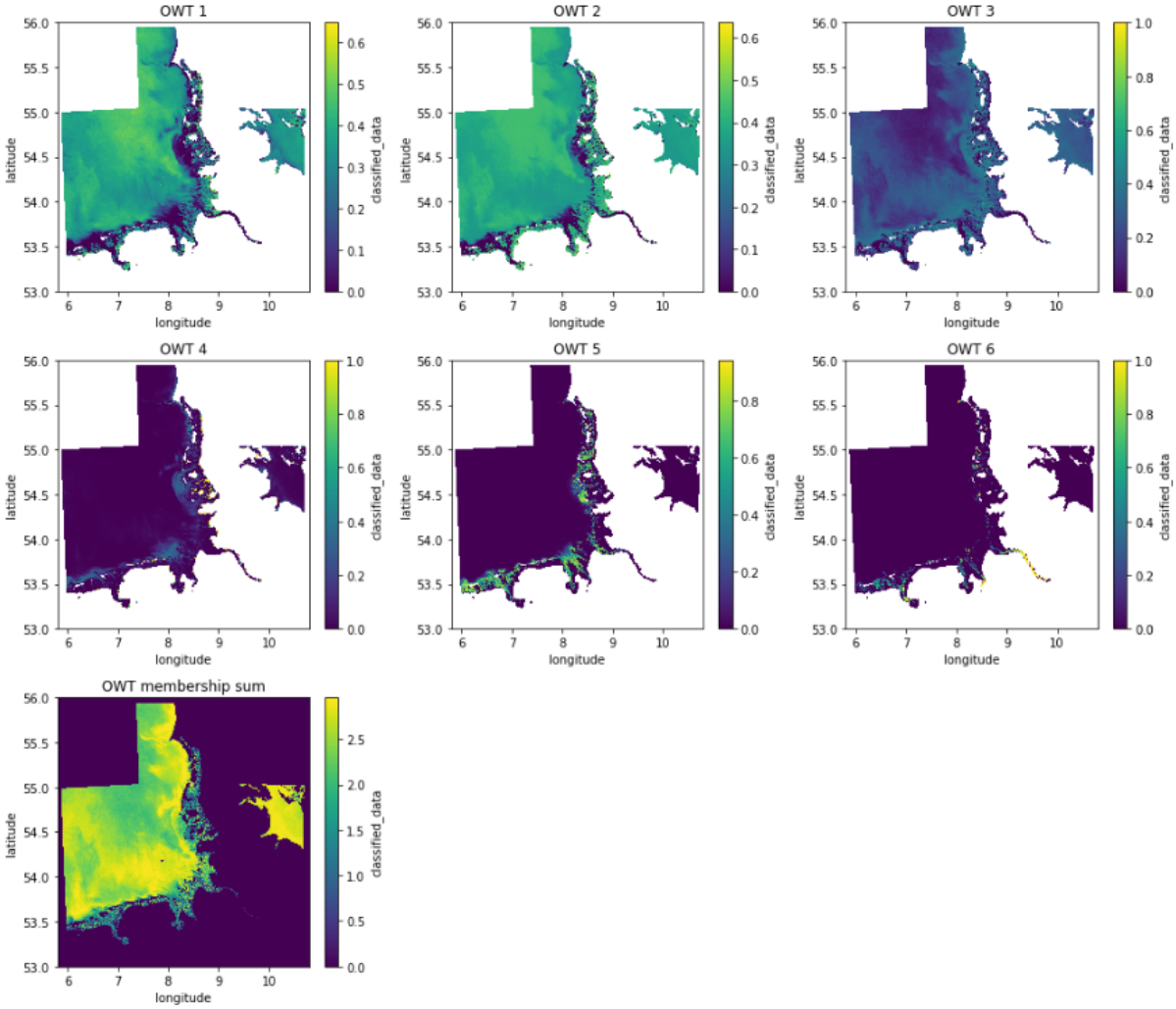

Figure 7.6: Example of clusters applied to data from 2020-08-11 for the Elbe using Sentinel 3. Membership values to each class are shown normalised to the total pixel membership (which is also shown in the last plot).

7.2.4 Sentinel 3 entropy filter and edge detection

The first analysis combines entropy filter and edge detection to try to locate the boundaries between regions of change in the optical water type structure. Where boundaries occur for more than one waterclass we consider this to be a 'strong edge' that is then stored as a variable. An example of this for a single image is shown in Figure 7.7.

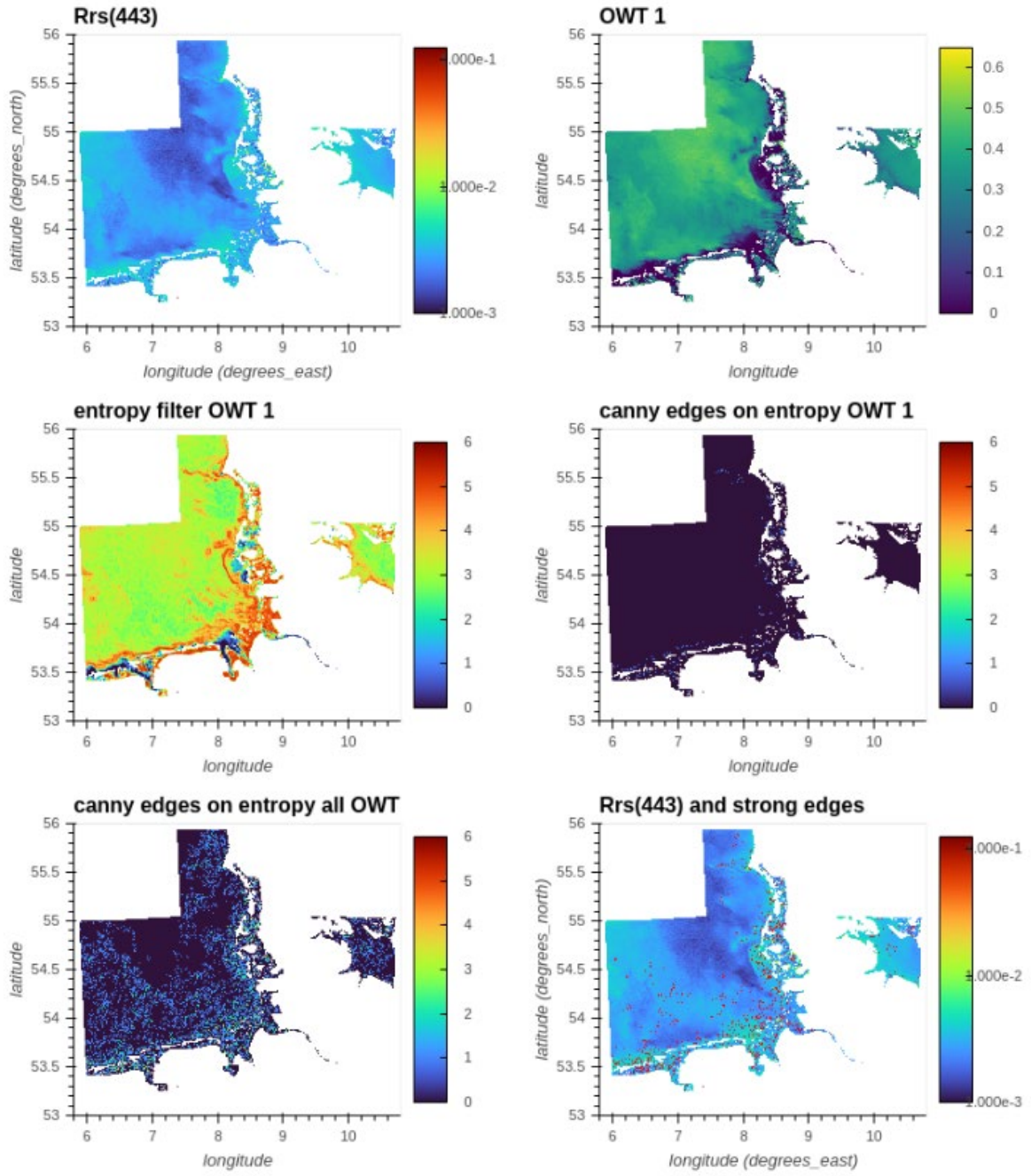

Figure 7.7: Example of entropy filter and edge detection application to data from 2020-08-11 for the Elbe using Sentinel 3

Stacking these results across all data available for each month we can look for persistent regions of change in optical water type membership structure (Figure 7.8).

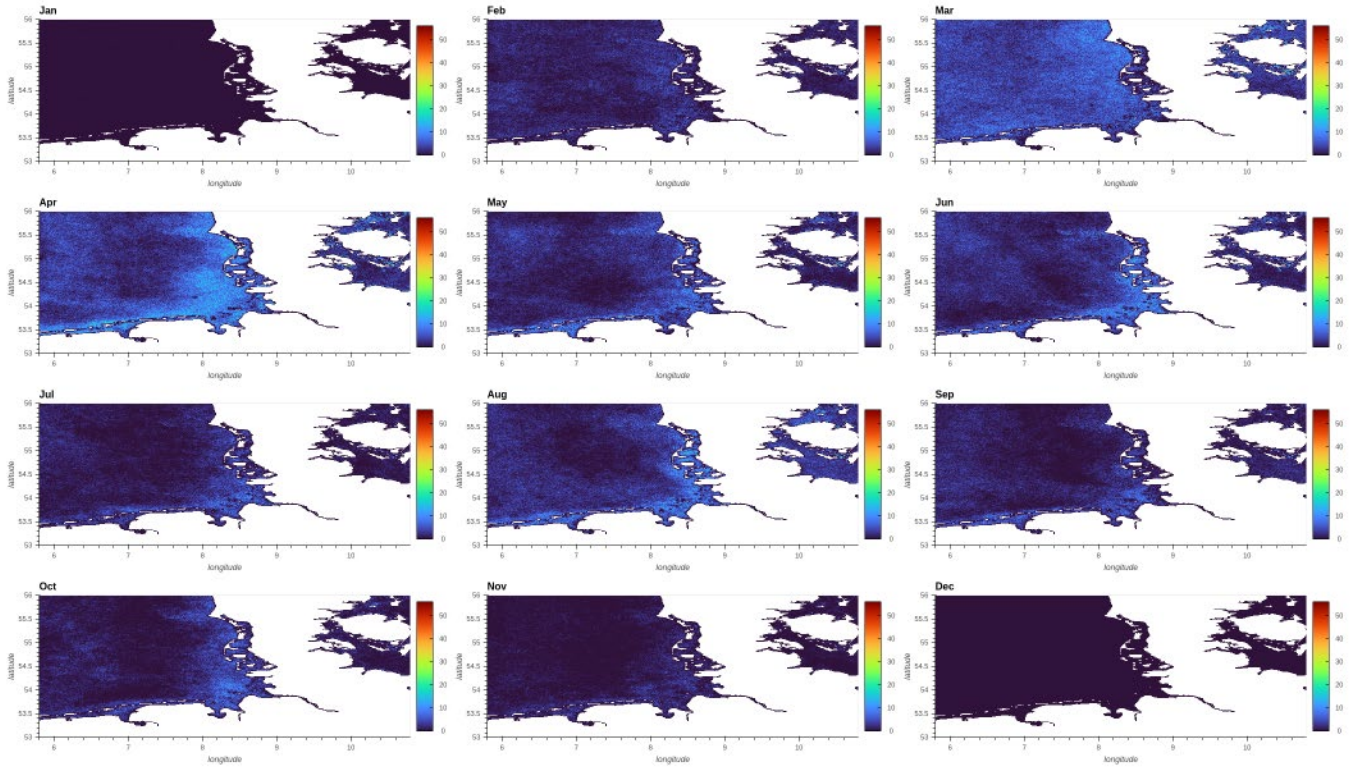

Figure 7.8: Stacked strong front incidence across all data available for a given month (across all years)

The strongest front incidence (could have some sampling bias due to clearer skies) appears to be in March, April, June and August. There are regions of interest highlighted along the Wattenmeer (Wadden Sea), as well as along the northern border off Esbjerg in Denmark.

7.2.5 Sentinel 3 OWT temporal Analysis

Processing issues came up during the temporal analysis for this region since it is the largest area study region of all six CERTO sites. Analyses are being performed in a jupyter notebook environment with the goal being to more easily share code with the project consortium, but this platform introduces a RAM-heavier processing chain. The solution will be to change the development strategy by moving to python scripts run over a shell window.

7.2.6 Revised Sentinel 3 OWT Analysis

The OLCI dataset has been updated to cover a longer time period that better matches that of the Sentinel 2 MSI dataset, thus cluster analyses for the OLCI dataset is being updated as follows:

- OLCI 300m data processed with the POLYMER processor: 2016-04-26 to 2021-03-07
- Training dataset built using regular subsampling along scan and cross scan directions, wavelengths used were: 400, 412, 443, 490, 510, 560, 620, 665, 674, 681, 709, 754, 779, 865 and 885 nm
- Winter month exclusion from training dataset (based on incident light level <30° calculated using NOAA solcalc together with request from site leads to include October and February in training data): November-January

Analysis on the new OLCI dataset is ongoing and will be made available to the Elbe team.

7.3 Sentinel 2 OWT Analysis

7.3.1 Sentinel 2 MSI dataset

- MSI 60m data processed with POLYMER processor: 2016-11-01 to 2020-12-31
- Training dataset built using regular subsampling along scan and cross scan directions, wavelengths used were: 443, 490, 560, 665, 705, 740, 783, 865, 1610 and 2190 nm
- Winter month exclusion from training dataset (based on incident light level <30° calculated using NOAA solcalc): November-January
- Prior to clustering, spectra were standardised using a standard scalar and then principal component analysis (PCA)
- Clusters created using Euclidian distance in principle-component-space

7.3.2 Sentinel 2 OWT classes

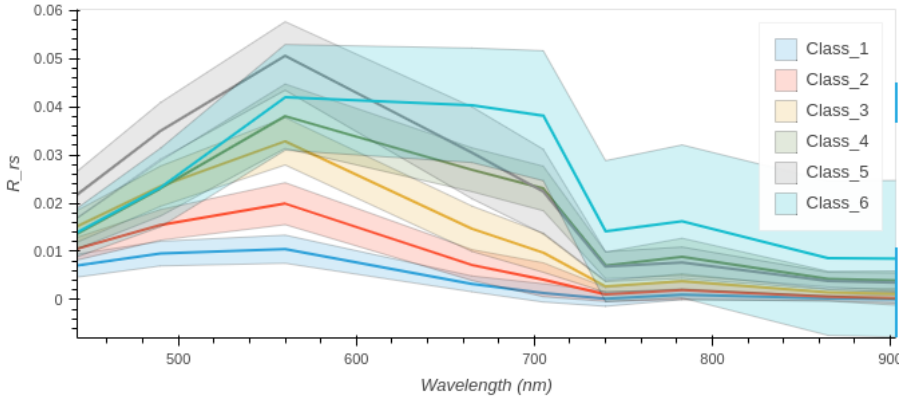

Figure 7.9: Optical Water Classes obtained in the Elbe using Sentinel 2

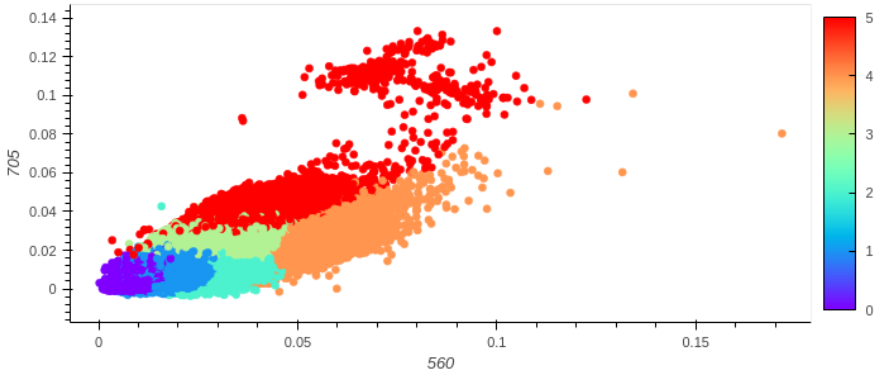

Figure 7.10: Optical Water Classes in 2-dimensional space for the Elbe using Sentinel 2. Add one to the colour bar values for the OWT (colourbar is 0 indexed).

7.3.3 Sentinel 2 OWT Spatial analysis

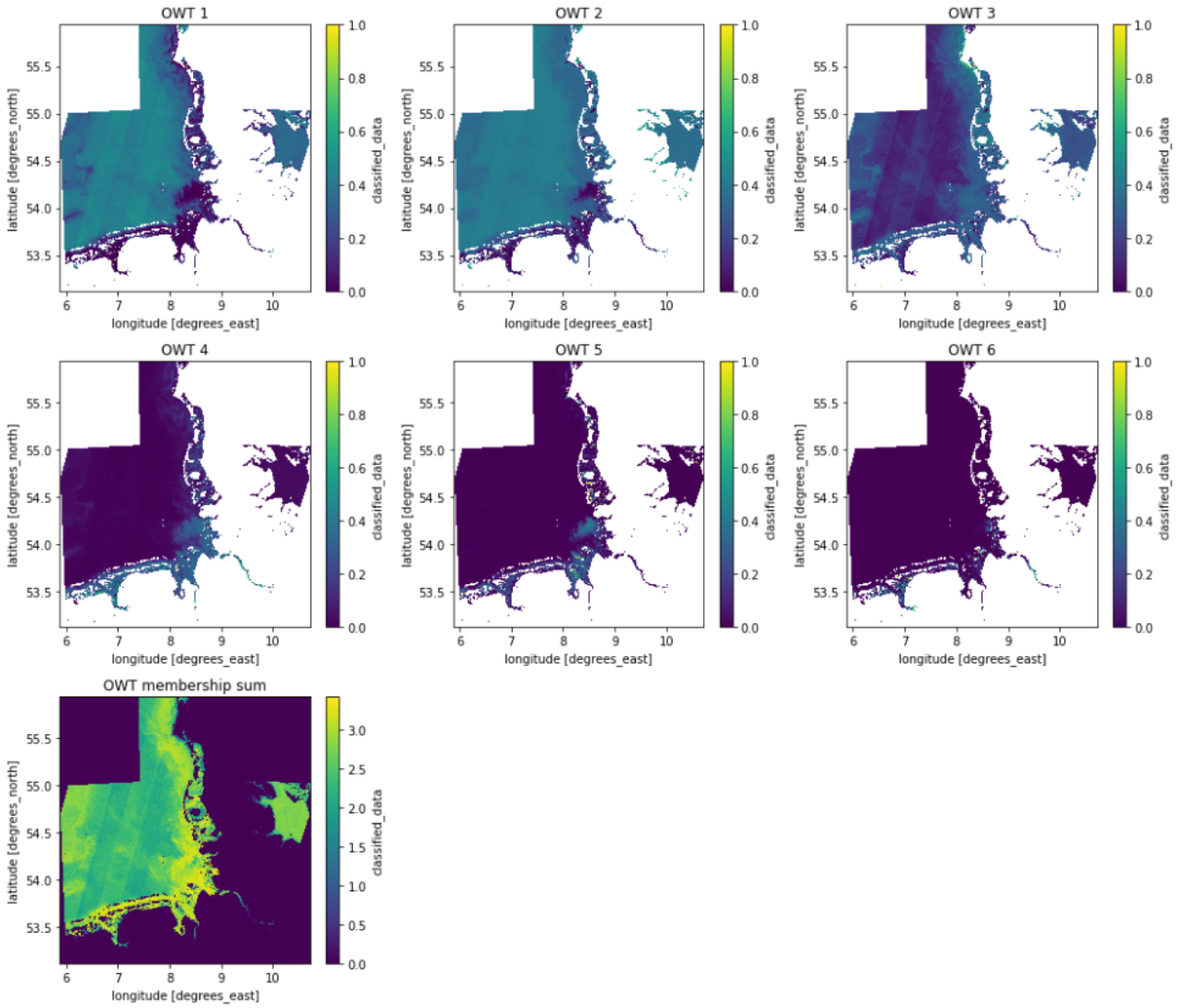

Figure 7.11: Spatial distribution of OWT classes for 2020-09-14 for the Elbe using Sentinel 2

7.4 Influence of local processes

The estuarine part of the Elbe starts 140 km upstream from the river mouth and begins at the weir in Geesthacht, where the tidal influence starts. Approximately 10 km upstream of the Port of Hamburg, the estuary divides into two branches, the Norderelbe and the Süderelbe, which unite again in the port area. The estuary is heavily impacted by anthropogenic influences, with Hamburg at around 130 km inland. Hamburg harbour is the biggest in Germany and second biggest in Europe. The river has also undergone intensive dredging activities to deal with the ever-bigger shipping containers traveling to and from Hamburg. The last deepening of the Elbe started in 2019 and ended in early 2021. The tidal influence can be measured up to the weir in Geesthacht, although brakish waters only start around Hamburg.

Gauge	River-km	mean low tide	mean high tide	mean tidal range
Hamburg-Zollenspieker	598.2	4.87	7.43	2.56
Hamburg-St. Pauli	623.1	3.50	7.07	3.57
Stadersand	654.8	3.72	6.74	3.02
Glückstadt	674.3	3.75	6.56	2.81
Cuxhaven	724.0	3.54	6.52	2.98

Figure 7.12: Longterm tidal range of the Elbe (from Hamburg to the river mouth) [m]. Copied from Hofstede J., EUROSION Case Study Elbe Estuary

The bathymetry of the estuary shows a relatively extensive flat area at the river mouth, which feeds into the Wadden Sea (north and south west of the river mouth), where tidal influences are quite marked. The river is at its deepest in the centre, where ships with drafts of up to 15 m can enter the harbour at high tide. Storm surges are also of concerns in the estuary, and areas at a high risk of flooding are mapped in blue in Figure 7.14.

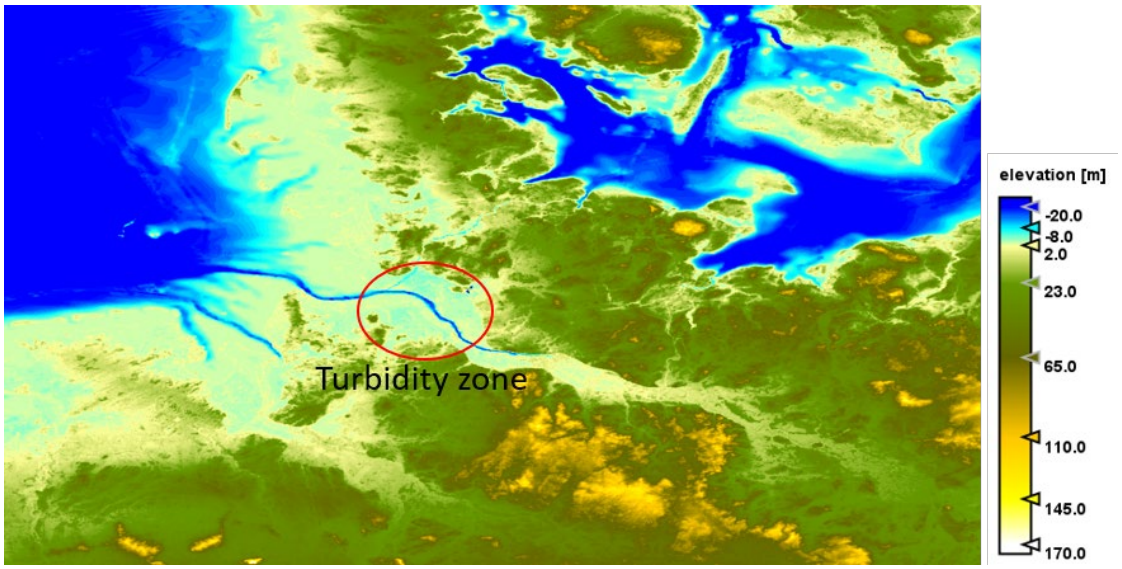

Figure 7.13: Bathymetry of the Elbe Estuary (GEBCO, 2020), with the turbidity zone circled in red.

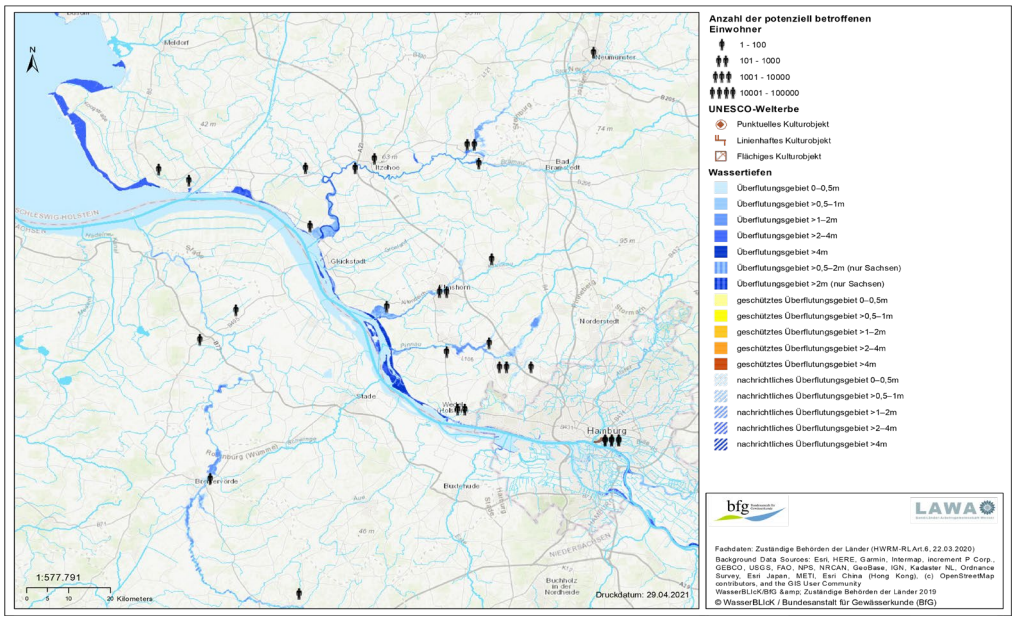

Figure 7.14: high frequency zones of flood hazard and flood risk along the Elbe estuary (status 2019)

7.5 Identification of under sampled regions

7.5.1 Satellite (Sentinel 2) and in situ match up analysis

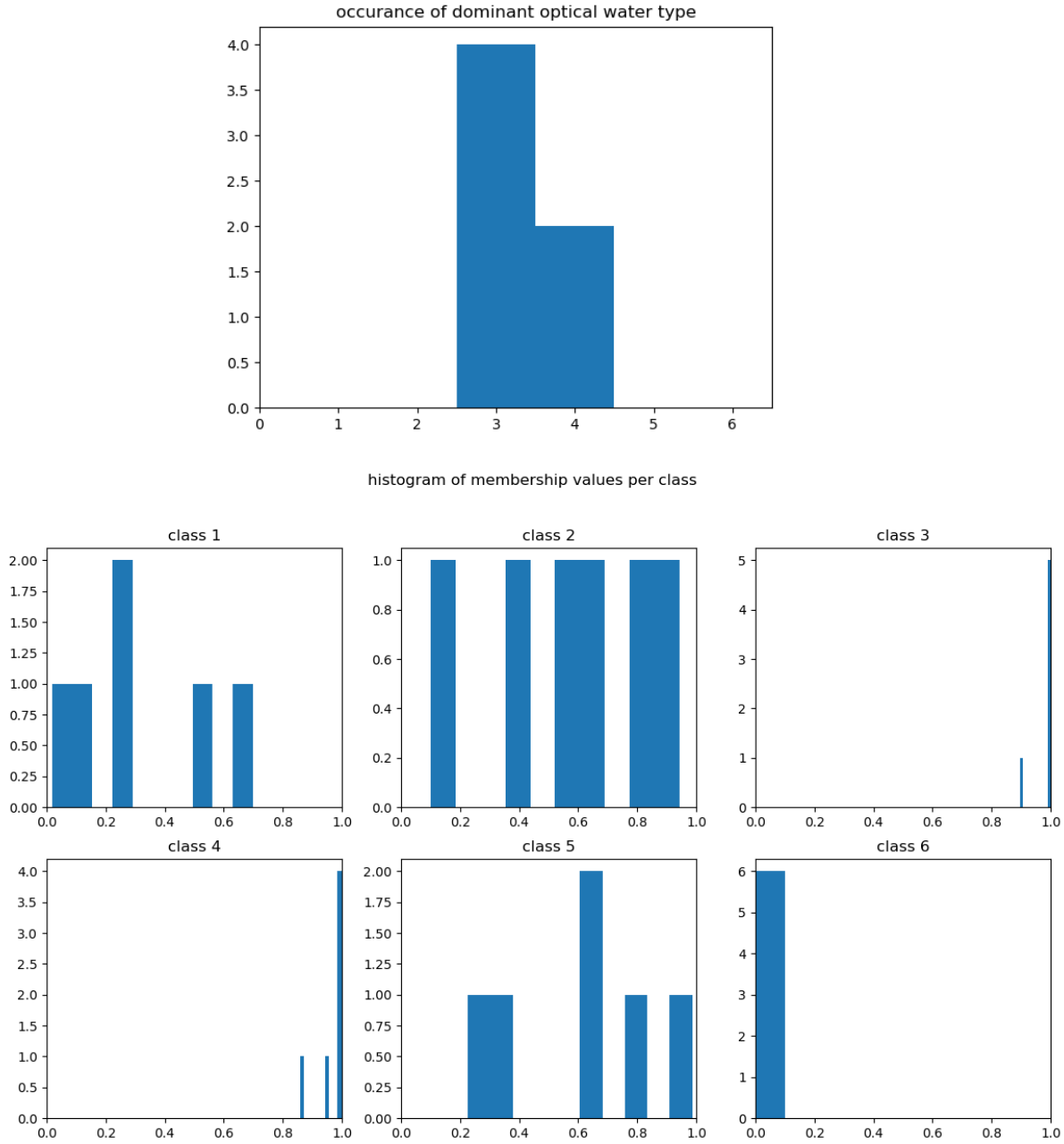

Figure 7.15: (top) Dominant optical water type and (bottom) histogram of membership values per class in the Elbe using Sentinel 2.

7.6 Proposed ideal sampling time for year 2 (2021) in the Elbe Estuary

For aiding the validation and interpretation of satellite data, the ideal sampling time would be at the same moment as the satellite overpass. This is not possible in most cases so we propose that the in situ measurements should be taken within a 3-hour window either side of the satellite overpass so that the influence of tides and weather changes are reduced.

- Time of sampling – June 28 – July 3, 2021
- Sampling platform availability – logistics arranged, Ludwig Prandtl
- Campaign participants – HZ Hereon, USTIR

Table 7.1: Sentinel 3 passes over Elbe estuary in June 28 – July 3, 2021

	June (date)	**June (time) UTC**	**July (date)**	**July (time) UTC**
SENTINEL 3	daily	09:00 - 10:10	daily	09:00 -10:10

Table 7.2: Sentinel 2 passes over Elbe estuary in June 28 – July 3, 2021

Satellite platform	Orbit	Date	Time (UTC)
SENTINEL2A	31422	2021/06/28	10:35
SENTINEL2A	31465	2021/07/01	10:45
SENTINEL2B	22585	2021/07/03	10:35

7.7 Covid19 Mitigation: proposed essential measurements and USTIR support

University of Stirling will provide support in terms of instrumentation and post-sampling analysis (for sites that need support). In year 2 (2021) participation by USTIR in the sampling campaigns will be subjected to Covid19 travel restrictions. However, the plan is to replicate a small percentage of samples for Chl-a, TSM, PC and particulate absorption from all sites. Shipping of the samples to USTIR will be arranged accordingly. USTIR will arrange a shipment and a rota of required instrumentation, in association with FC.ID, across the different sites in Europe. Intercomparison experiments therefore are planned in year 3 (2022) with a possibility to participate onboard with a suite of USTIR instrumentation across the sites in the UK and Europe.

Table 7.3 Proposed essential measurements and USTIR support

Category	Parameters to be measured (essentials in bold)	Instrumentation/ Sample Analysis 2021	Instrumentation/ Sample Analysis 2022
Biogeochemistry	Chlorophyll a, Chl-a	HZ Hereon	HZ Hereon
	Phycocyanin, PC	---	---
	Total Suspended Matter, TSM	HZ Hereon	HZ Hereon
AOPs	**Remote sensing reflectance, R_{rs}**	HZ Hereon (TriOS) USTIR (TriOS)	HZ Hereon (TriOS) USTIR (TriOS)
	Diffuse attenuation coefficient, K_d	USTIR (USSIMO)	USTIR (USSIMO)
	Secchi disk depth, Z_{SD}	HZ Hereon	HZ Hereon
IOPs	**Total absorption coefficient, a**	HZ Hereon	HZ Hereon
	Absorption coefficient of phytoplankton, a_{ph}	HZ Hereon	HZ Hereon
	Absorption coefficient of non-algal particles, a_{nap}	HZ Hereon	HZ Hereon
	Coloured dissolved organic matter, CDOM	HZ Hereon	HZ Hereon
	Backscattering coefficient, b_b	HZ Hereon	HZ Hereon
	Beam attenuation coefficient, c	HZ Hereon	HZ Hereon
Physical Parameters	Water temperature	HZ Hereon	HZ Hereon
	Salinity	HZ Hereon	HZ Hereon
	Turbidity	HZ Hereon	HZ Hereon

	Water depth	HZ Hereon	HZ Hereon
Atmospheric parameters	Wind speed	HZ Hereon	HZ Hereon
	Aerosol Optical Thickness, AOT	USTIR (Microtops)	USTIR (Microtops)

7.8 References

Boehlich, Marcus J., Strotmann Thomas. The Elbe Estuary, Die Küste; 2008; 74 ICCE:288-306

Herman PMJ, Heip CHR. Biogeochemistry of the MAximum TURbidity Zone of Estuaries (MATURE): some conclusions. Journal of Marine Systems. 1999;22(2-3):89-104. https://doi.org/10.1016/S0924-7963(99)00034-2
(this one is more of a grey publication, but has good info):

Hofstede Jacobus. Elbe Estuary (Germany). EUROSION Case Study. 2007

Jens K, Michael B, Nino O, Rolf R, Dagmar S. Variation of Hydrodynamics and Water Constituents in the Mouth of the Elbe Estuary, Germany. Civil Eng Res J. 2018; 4(4): 555643.DOI:10.19080/CERJ.2018.04.555643

Papenmeier S, Schrottke K, Bartholomä A. Over time and space changing characteristics of estuarine suspended particles in the German Weser and Elbe estuaries. Journal of Sea Research. 2014; 85:104-115. 10.1016/j.seares.2013.03.010

Weilbeer Holger. Sediment Transport and Sediment Management in the Elbe Estuary. Die Küste; 2014;81:409-426

8 Case Study Area 6: Curonian Lagoon

Curonian Lagoon (Baltic Sea)

The Curonian Lagoon is a transboundary water shared between Russia and Lithuania and separated from the Baltic Sea by the Curonian Spit. With a surface area of 1,584 km^2, it is the largest lagoon in Europe. The lagoon is a shallow (mean depth 3.8 m) and mainly a freshwater ecosystem. The main tributary is the Nemunas river that provides the main inflow, both in terms of the amount of water, nutrients and persistent pollution. Curonian Lagoon is hypereutrophic environment often dominated by cyanobacterial blooms in summer.

According to long term monitoring data (2001–2012) collected by the Marine Research Department of the Lithuanian Ministry of Environment, monthly average chlorophyll a (chl-a) concentrations reach 47 ± 14 µg L^{-1} during the spring diatom bloom and 96 ± 56 µg L^{-1} during the summer bloom. Cyanobacteria blooms appear in the summer, due to combination of favourable nutrient stoichiometry (N and Si limitation), elevated water temperature, low wind speed and low grazing pressure (Bartoli et al., 2018). Several publications have analysed the hypereutrophic condition of Curonian Lagoon (Zilius et al., 2014; Bresciani et al., 2014), the Curonian water impact on the quality of Baltic Sea (Vaiciute et al., 2012) and the higher concentration of CDOM in the Nemunas river Delta (Vaiciute et al., 2015).

Fishing and small-scale fish processing has traditionally provided an important economic basis for many small communities around the lagoon and tourism, port activities, and agriculture also play an important and continuously growing role. The water-quality management and nature conservation system in the Lithuanian part of the Curonian Lagoon is based on both national legal acts and on EU directives, particularly the WFD and the Habitat Directive (HD, 92/43/EEC). In the Russian Federation, the protection and management of water resources is regulated by the Water Code, adopted in 2006.

8.1 Current sampling locations and bio-optical monitoring

8.1.1 Recurring and occasional stations

The existing national monitoring system in the Lithuanian part of the Curonian Lagoon involves the collection of in situ measurements and water samples in the Klaipeda Strait, within the inner part of the lagoon, and in

the mouth of the Nemunas river. Sampling is conducted approximately every month. The key parameters measured include: meteorological (temperature, wind speed and direction, humidity etc.) and hydrological (water temperature, salinity, currents direction and speed, transparency (Secchi disk depth)) and colour, pH (since 1954), dissolved oxygen concentration (since 1961), nutrients (1967-1979), phytoplankton species composition, abundance and biomass (since 1980), chlorophyll a concentration (since 1983), and total suspended matter (TSM, since 1999). Samples are taken from the surface (upper 0.5 m). Since 2009, Remote Sensing Reflectances (R_{rs}) with portable spectroradiometers have been collected synchronous with water sampling. Figure 8.1 shows the recurring and occasional stations.

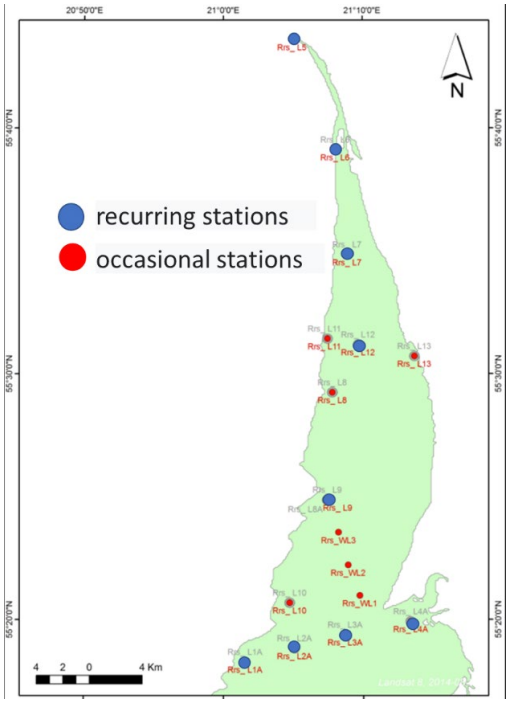

Figure 8.1. Map of the recurring (blue dots) and occasional (red dots) stations for spectroradiometric measurements and water collection in the northern portion (Lithuania) of the Curonian Lagoon.

The biogeochemical parameters of the sediments and nutrients in the water were generally collected in the stations reported in the Figure 8.2. In addition to *in situ* sampling, in the Lithuanian part of Curonian Lagoon there are 3 weather stations (stars in Figure 8.3a) and during H2020 EOMORES project a fixed spectroradiometer WISPstation was deployed in 2018 which made it possible to collect spectral signatures of the waters in a coastal area of the lagoon every 15 minutes (green triangle in the Fig.8.3a). The automated salinity and water level stations are reported in Figure 8.3b.

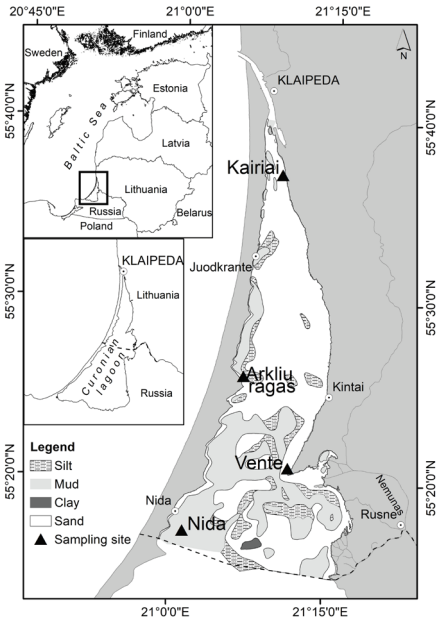

Figure 8.2. The Curonian Lagoon with the four sampling sites normally sampled for bio-geochemical parameters. The dotted line in the central map separates the southern, Russian side of the lagoon from the Lithuanian one (from Bartoli et al., 2021).

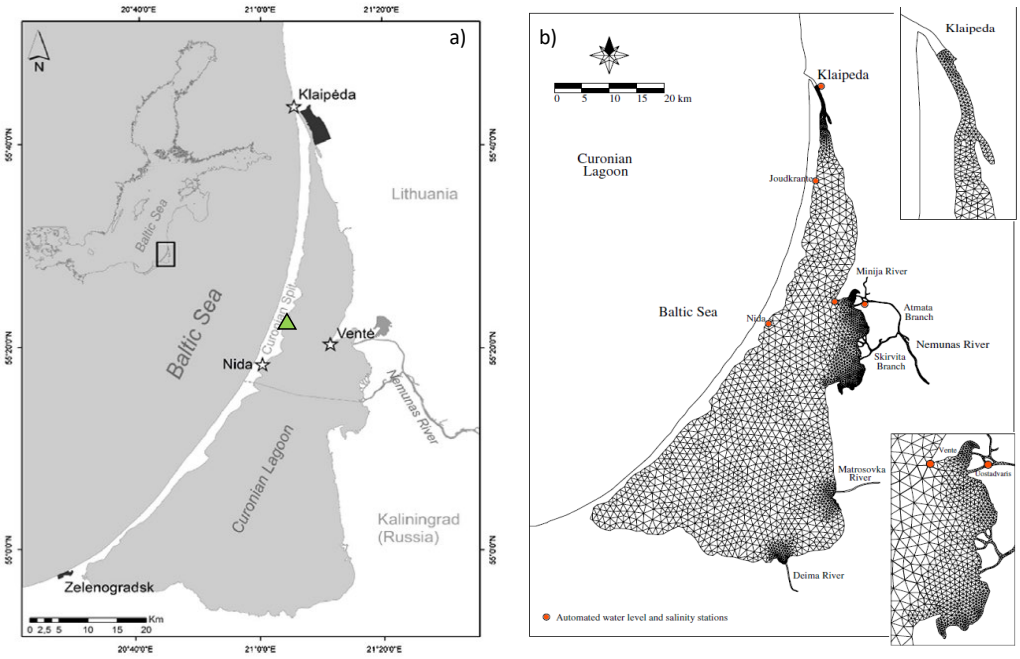

Figure 8.3. Maps of the locations (a) of the weather stations in Klaipėda, Ventė and Nida (stars) and the location of the WISP station installed for the continuous measurement of remote sensing reflectance (green triangle) and (b) automated water level and salinity stations (red dots; from Ferrarin et al., 2008).

8.2 Sentinel 3 OWT Analysis

8.2.1 Sentinel 3 OLCI dataset

We used OLCI 300m data (2019-2021) processed with the POLYMER processor and selected pixels as the training dataset. It should be noted that these data were processed following the CALIMNOS lakes database chain, thus are different from the analyses presented for the other regions (a peculiarity for the S-3 data, this will not be the case for future clustering with Sentinel-2).

Specific differences include:

- Reflectances in Rw as oppose to Rrs
- Data only available inside of the Curonian Lagoon, no open ocean pixels

- L3 data has been collected into 10-day composites

As with the other datasets:

- Training data were selected using a regular subsampling of the 300m data in the along scan and cross scan directions
- All visible wavelengths were used (400, 412, 443, 490, 510, 560, 620, 665, 674, 681 and 709nm)
- Prior to clustering the data, the spectra were standardised using a standard scalar and then applied a principal component analysis (PCA) to reproject the spectra
- We then created clusters using Euclidian distance in principle-component-space

8.2.2 Sentinel 3 OWT classes

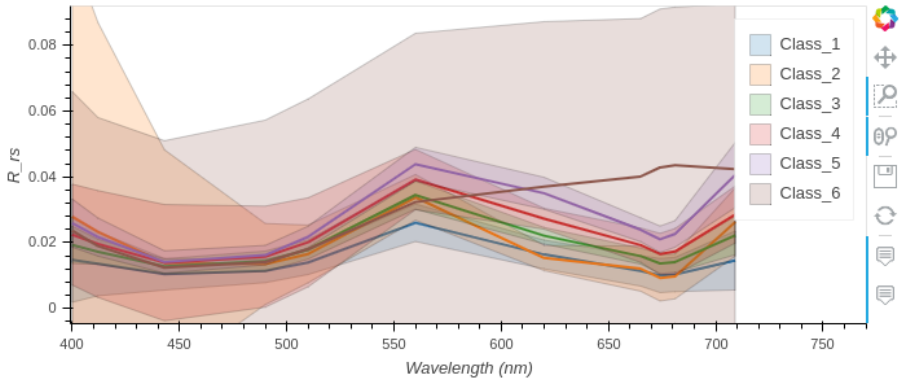

Figure 8.4: Derived optical water classes for the Curonian Lagoon using Sentinel 3

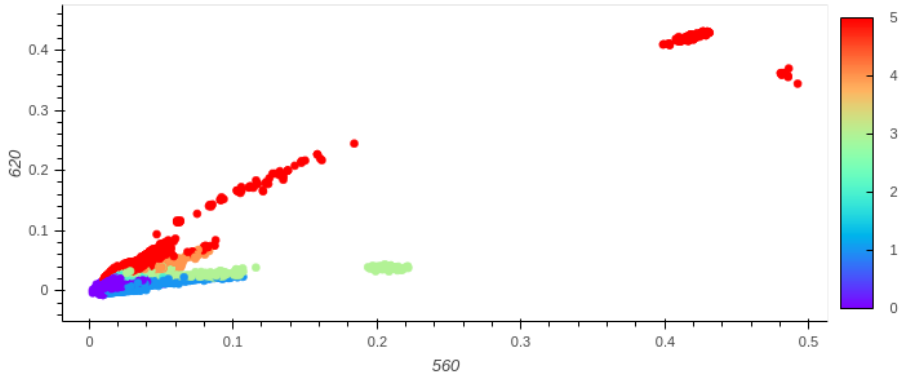

Figure 8.5: Dominant optical water class for each training data point in 2-band Rrs space for the Curonian Lagoon using Sentinel 3. Add one to the colourbar values for the OWT (colourbar is 0 indexed).

8.2.3 Sentinel 3 OWT spatial analysis

This class set was then applied to OLCI data from 2020 to 2021. The resulting memberships (daily products) were then used for a number of different types of analysis.

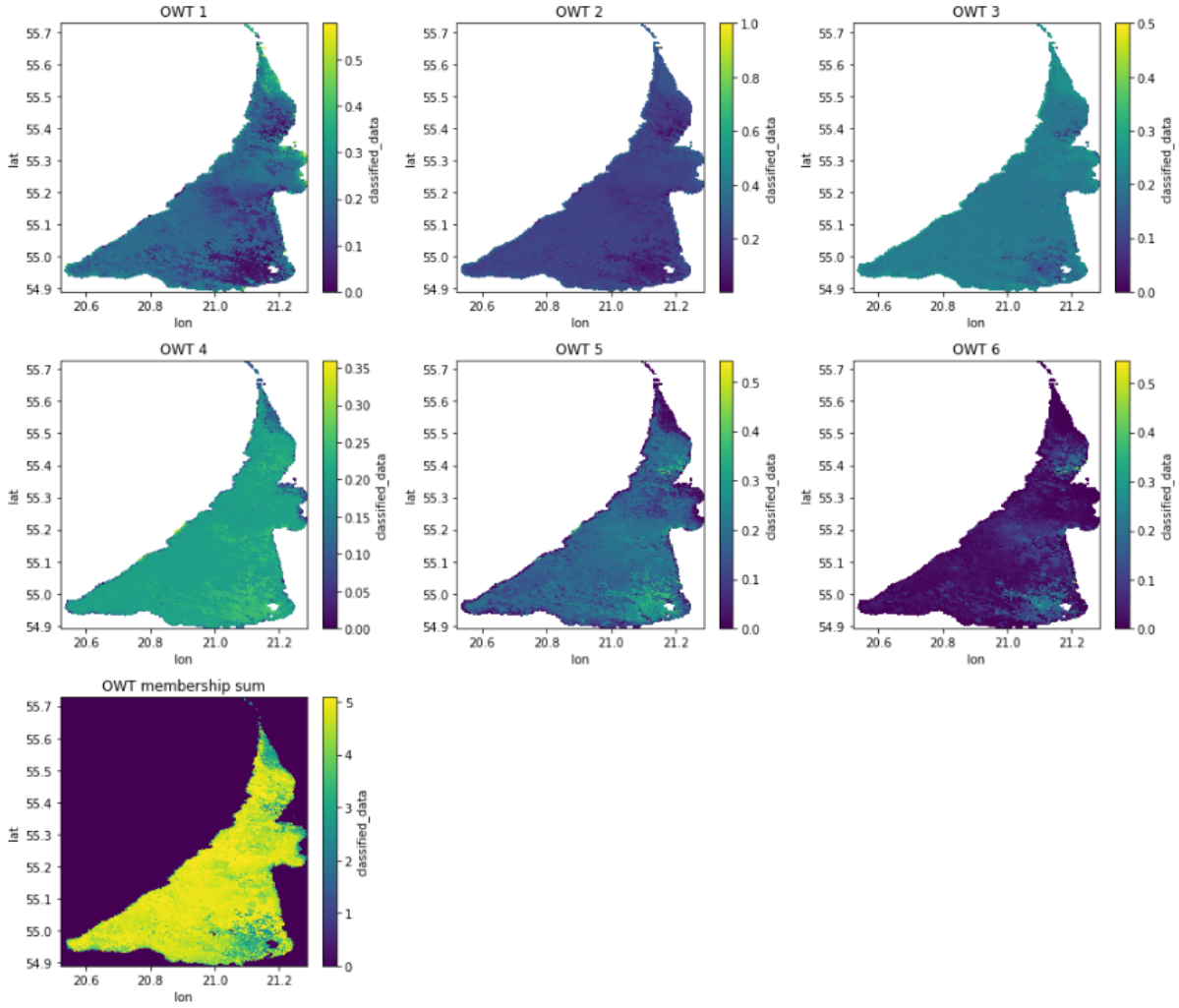

Figure 8.6: Example of clusters applied to data from 2020-07-21 (represents a 10-day composite) for the Curonian Lagoon using Sentinel 3. Membership values to each class are shown normalised to the total pixel membership (which is also shown in the last plot).

8.2.4 Sentinel 3 entropy filter and edge detection

The first analysis combines entropy filter and edge detection to try to locate the boundaries between regions of change in the optical water type structure. Where boundaries occur for more than one water class, we consider this to be a ‘strong edge’ that is then stored as a variable. An example of this for a single image is shown in figure 8.7.

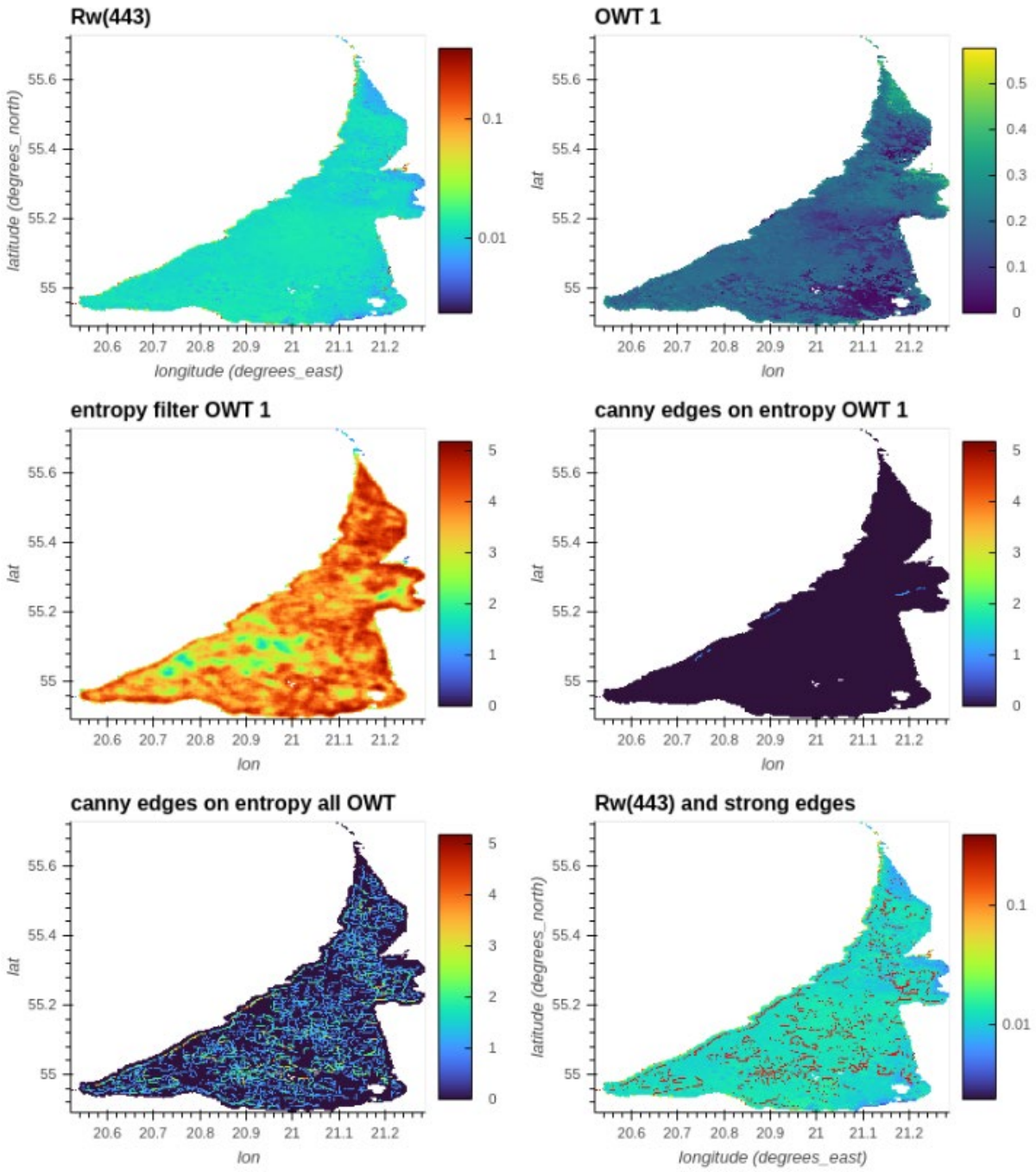

Figure 8.7: Example of entropy filter and edge detection application to data from 2020-07-21 (represents a 10-day composite) for the Curonian Lagoon using Sentinel 3.

Stacking these results across all data available for each month we can look for persistent regions of change in optical water type membership structure (Figure 8.8).

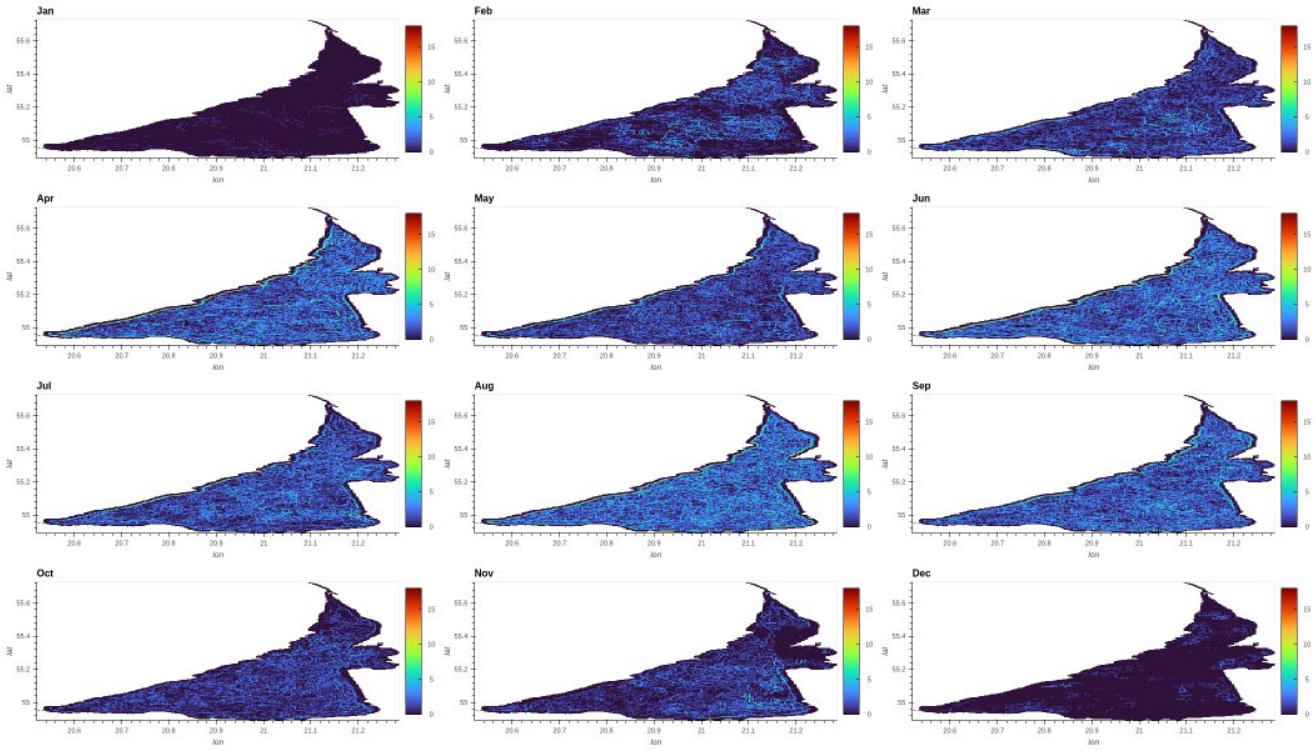

Figure 8.8: Stacked strong front incidence across all data available for a given month (across all years) for the Curonian Lagoon using Sentinel 3

The strongest front incidence (could have some sampling bias due to clearer skies) appears to be in April and June through September.

We can then stack this information across all available times (Figure 8.9) and by month (Figure 8.10) and visualise as maps. The colour bar does not line up properly (to be fixed) but for now it is interesting to see the regions of change /dominance.

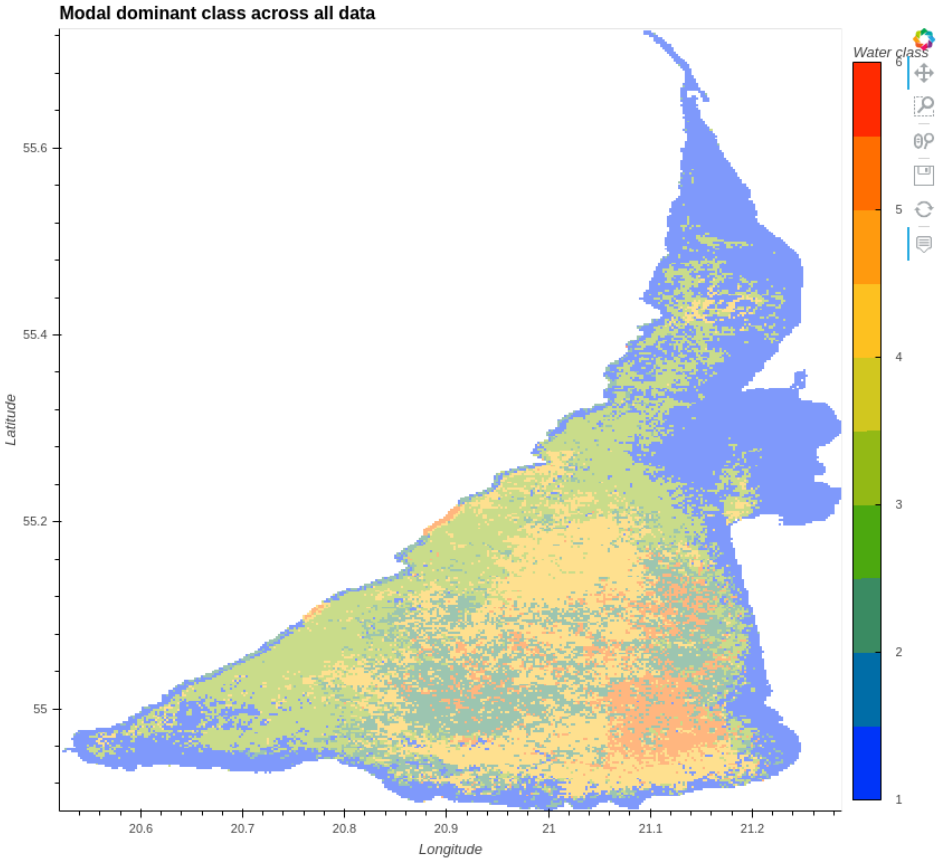

Figure 8.9: Dominant optical water class across all data for the Curonian Lagoon using Sentinel 3.

8.2.5 Sentinel 3 OWT temporal analysis

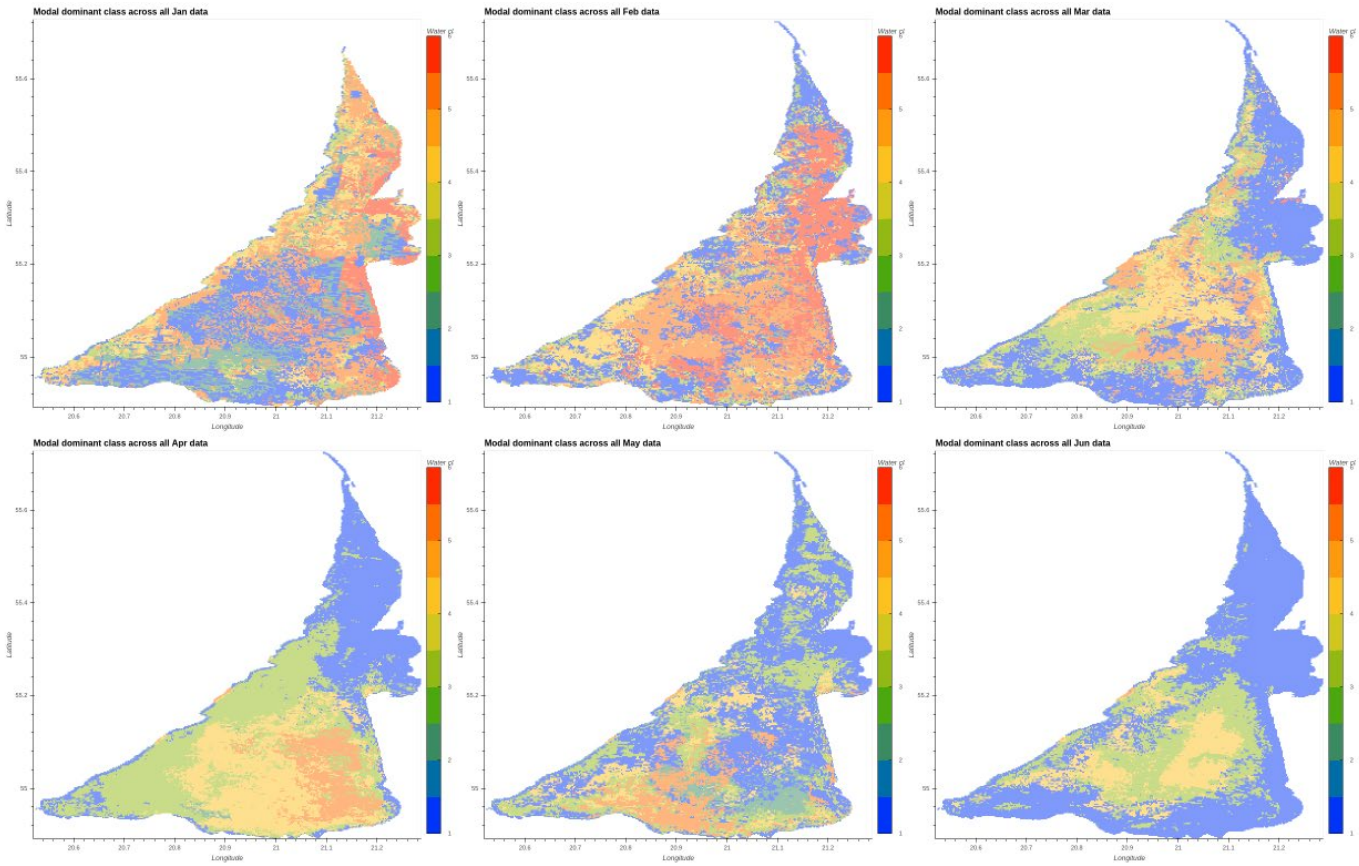

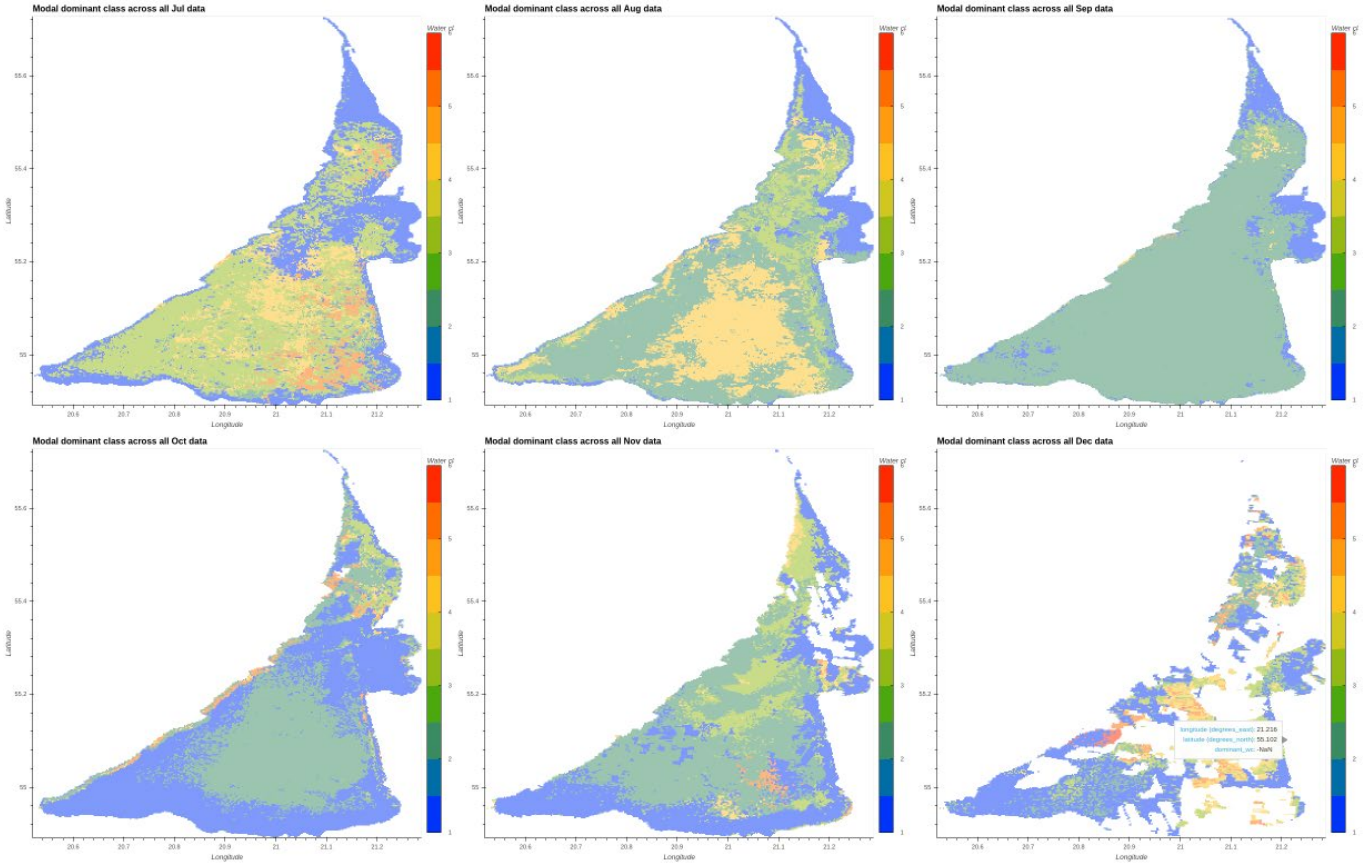

Figure 8.10: (rows, left to right) Temporal analysis of OWT in the Curonian Lagoon from January to December

8.2.6 Revised Sentinel 3 OWT Analysis

The OLCI dataset has been updated to cover a longer time period that better matches that of the Sentinel 2 MSI dataset, thus cluster analyses for the OLCI dataset is being updated as follows:

- OLCI 300m data processed with the POLYMER processor: 2016-04-26 to 2021-03-08
- Training dataset built using regular subsampling along scan and cross scan directions, wavelengths used were: 400, 412, 443, 490, 510, 560, 620, 665, 674, 681, 709, 754, 779, 865 and 885 nm
- Winter month exclusion from training dataset (based on incident light level <30° calculated using NOAA solcalc): October-February

Analysis on the new OLCI dataset is ongoing and will be made available to the Curonian team.

8.3 Sentinel 2 OWT Analysis

8.3.1 Sentinel 2 MSI dataset

- MSI 60m data processed with POLYMER processor: 2016-11-01 to 2020-12-31
- Training dataset built using regular subsampling along scan and cross scan directions, wavelengths used were: 443, 490, 560, 665, 705, 740, 783, 865, 1610 and 2190 nm
- Winter month exclusion from training dataset (based on incident light level <30° calculated using NOAA solcalc): November-January
- Prior to clustering, spectra were standardised using a standard scalar and then principal component analysis (PCA)
- Clusters created using Euclidian distance in principle-component-space

8.3.2 Sentinel 2 OWT classes

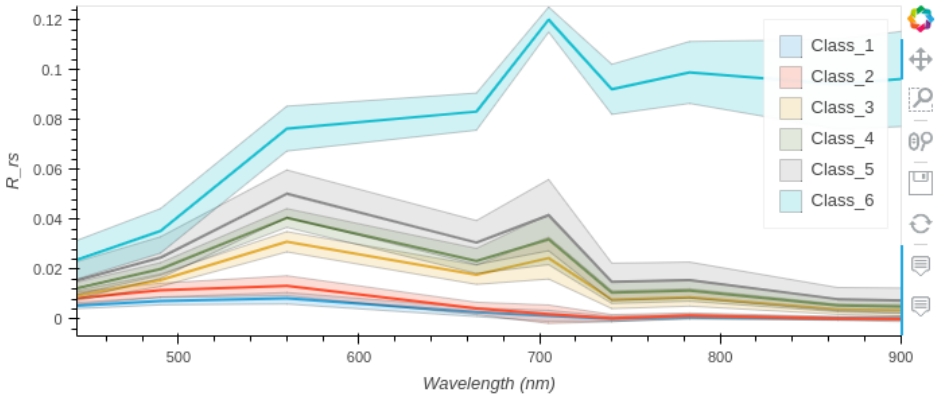

Figure 8.11: Optical Water Classes obtained in the Curonian Lagoon using Sentinel 2

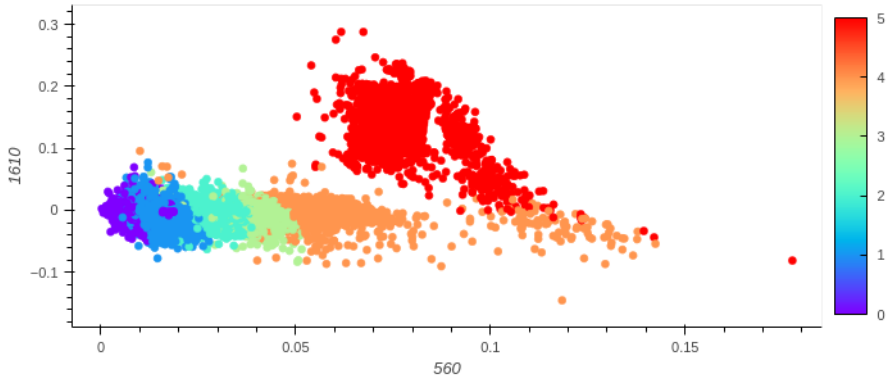

Figure 8.12: Optical Water Classes in 2-dimensional space for the Curonian Lagoon using Sentinel 2. Add one to the colourbar values for the OWT (colourbar is 0 indexed).

8.3.3 Sentinel 2 OWT Spatial analysis

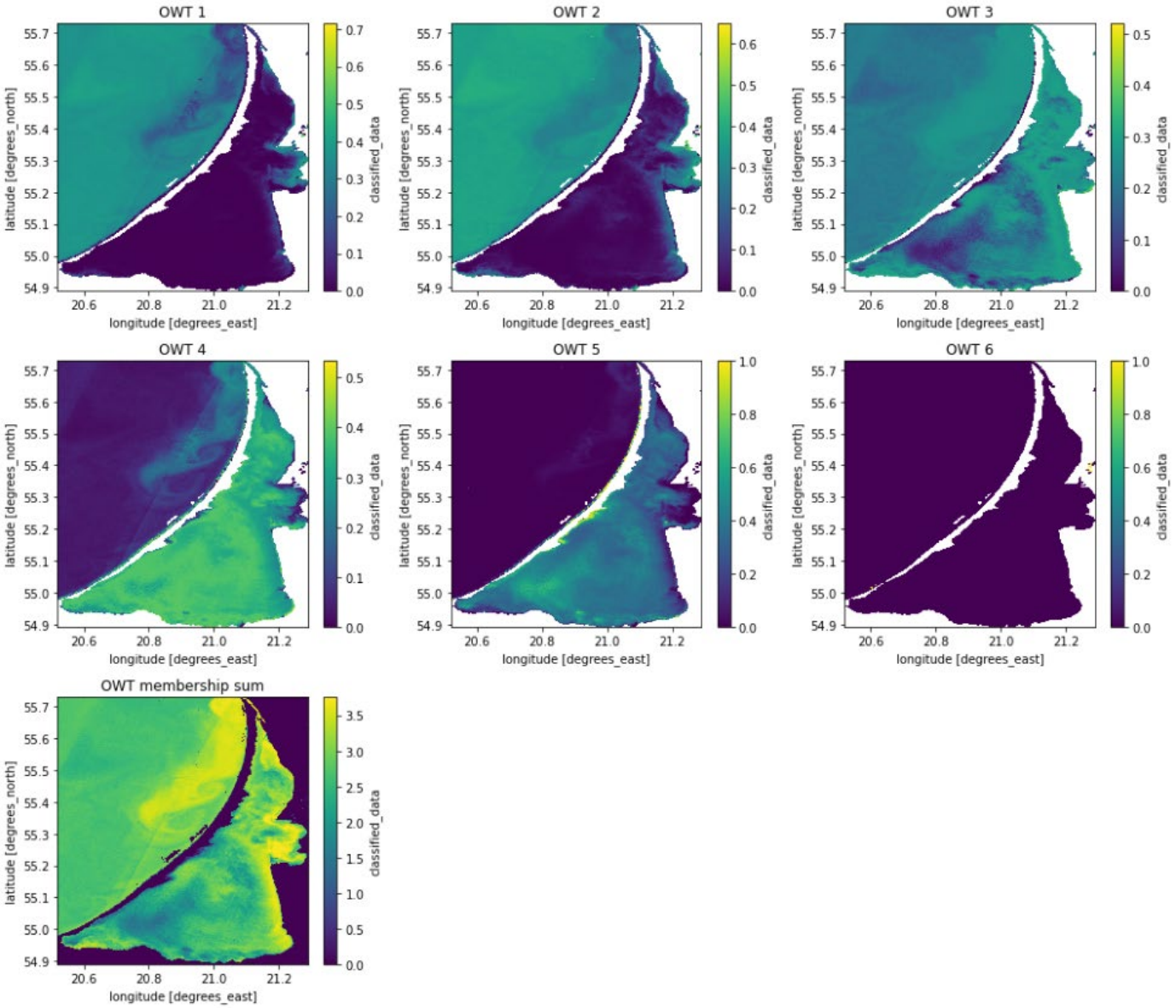

Figure 8.13 Spatial distribution of OWT classes for 2020-09-21 using Sentinel 2

8.4 Influence of local processes

Hydrology, wind, ice cover, bathymetry and sediments

The water circulation of the Curonian Lagoon is generally determined by both the freshwater flow and lagoon–sea exchange and by the wind. From the hydrological point of view, the northern part is influenced mainly by the Nemunas river flow followed by the lagoon–sea exchange and in the southern part the wind is the main driving factor (Razinkovas et al. 2005: Ferrarin et al., 2008). Annually the freshwater river runoff that enters the lagoon is about 23 km^3 (about 700m^3 s^{-1}; Jakimavičius, 2012) of which 40% outflows into the Baltic sea during the spring months (Žaromskis 1996), whereas 5 km^3 incoming seawater are mixed in the lagoon mostly in the autumn months (Pustelnikovas 1998). Every year the rivers carries fresh water about 4 times the volume of the lagoon. Therefore, the southern and central parts of the lagoon are freshwater (average salinity is 0.08‰), while the northern part has an average annual water salinity of 2.45‰ with irregular salinity fluctuations of up to 7‰ due to episodic and irregular rapid (from hours to days) sea water intrusion (up to 40 km; Gasiūnaitė 2000, Daunys 2001, Dailidienė and Davulienė, 2008). In the southern part, where the current regime is mainly driven by the wind, different wind directions and speeds create different circulation sub-systems. As shown in Figure 8.14, the system evolves a dominant gyre, with anti-clockwise (wind from west) or clockwise (wind from south-east) direction, and some smaller gyres. In a south-western wind, the circulation pattern is characterised by a two-gyre system (Razinkovas et al. 2005, Ferrarin et al., 2008).

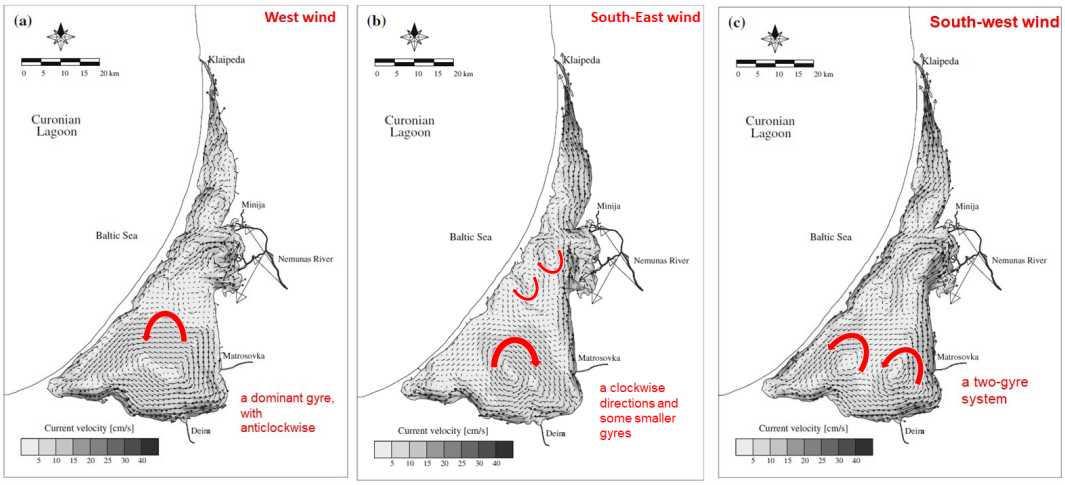

Figure 8.14. Simulated water circulation imposing idealised wind forcing: (a) West wind; (b) South-East wind; (c) South-West wind (modified by Ferrarin et al., 2008).

The average water level in the lagoon is normally higher compared to the sea level of the Baltic Sea. The tidal action is absent because tides in the eastern Baltic Sea are of negligible magnitude (Umgiesser et al., 2016). Due to Nemunas water input and water level differences between the sea and the lagoon, a south–north current moves from the river delta to the north towards the Klaipeda strait (Žaromskis 1996), which is more evident during the spring flood period (Pustelnikovas 1998).

The seasonal pattern of water temperature is typical of shallow temperate water bodies (up to 25–29°C; Žaromskis 1996), and water column stratification is weak and unstable (Pustelnikovas 1998). The Klaipeda strait is always ice free, while in the rest of the lagoon ice cover is present for 50-85 days per year on average (Figure 8.15, Idzelytė et al., 2019). Figure 8.16 shows the 10-day averaged percentage of the ice cover extent in the lagoon for the three winter categories, short, intermediate and long, as reported by Idzelytė et al. (2019).

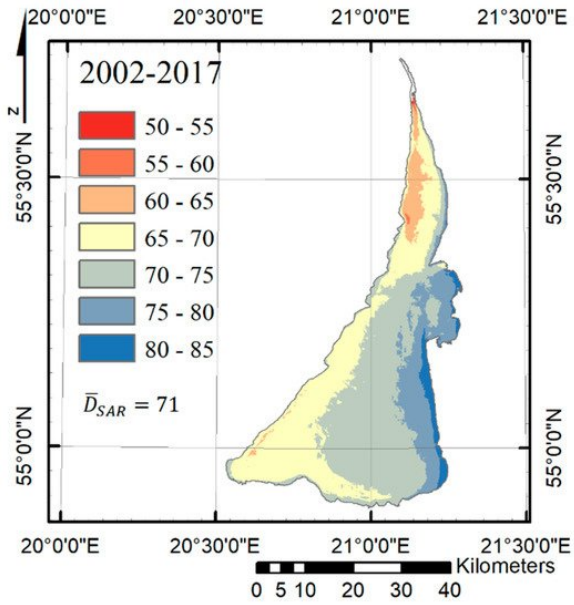

Figure 8.15. Annual mean ice season duration in the Curonian Lagoon as derived from the satellite data in 2002–2017 (from Idzelytė et al., 2019).

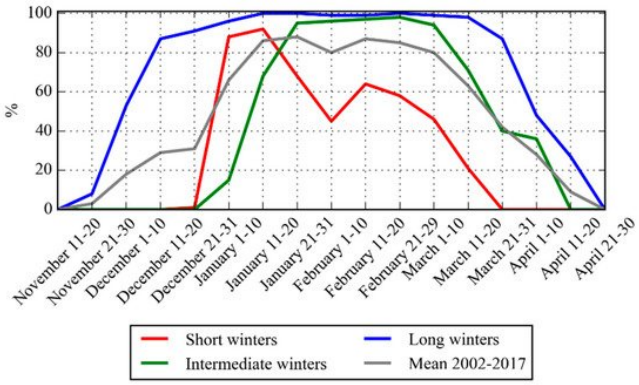

Figure 8.16. The 10-day averaged percentage of the ice cover extent in the Curonian Lagoon for the three winter categories (from Idzelytė et al., 2019).

The bathymetry map of the Curonian Lagoon is shown in Figure 8.17. Wind forcing is the main driver, and much less the river discharge, of the exchanges between the southern and the northern part of the lagoon. However, the river discharge is the most important factor for the water residence time (Figure 8.17). Other physical forcings only marginally influence the renewal time and ice cover actually strongly inhibits the exchanges between the southern and northern lagoon (Umgiesser et al., 2016). Lowest residence time value (10–40 days) was found in front of the Nemunas delta, due to river runoff, and in the Klaipeda Strait, due to the water exchange with the Baltic Sea. The southern part of the lagoon has high residence times (up to 120 days; Ferrarin et al., 2008).

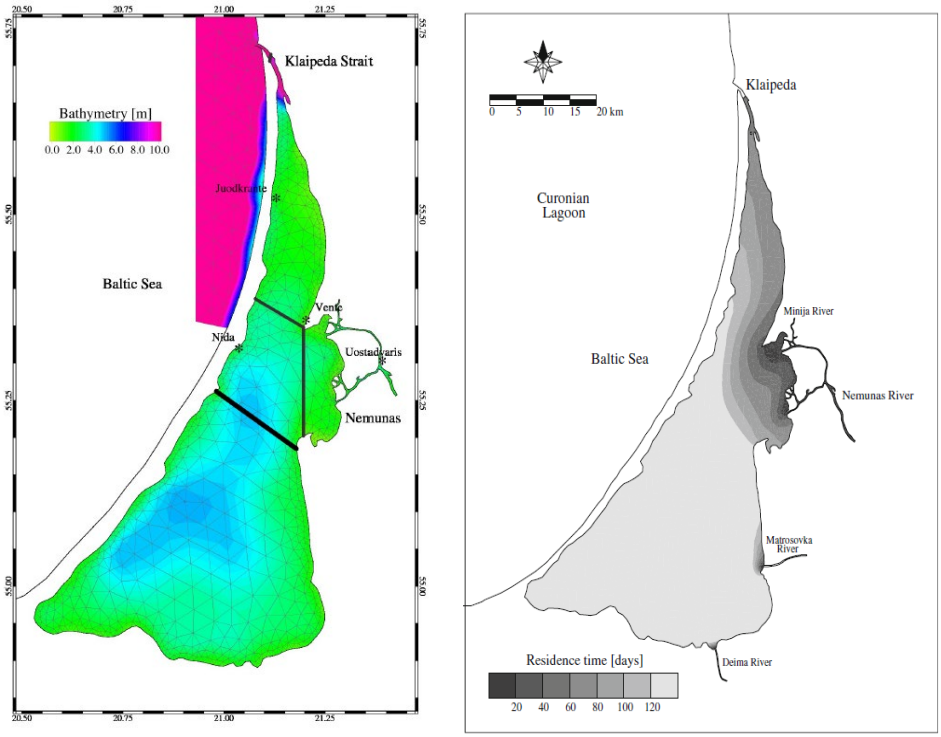

Figure 8.17. The bathymetry maps of the Curonian Lagoon (on the left; from Umgiesser et al., 2016) and the modelled average residence time distribution of the Curonian Lagoon (1999–2001) (on the right, from Ferrarin et al., 2008).

On a seasonal basis, lower water renewal time can be found close to the Nemunas outflow during spring, due to the higher discharge of the river, and highest values in summer in the southern basin (Umgiesser et al., 2016; Fig. 8.18). The northern basin shows renewal time of about 77 days, while the average for the southern basin is nearly 200 days (Umgiesser et al., 2016).

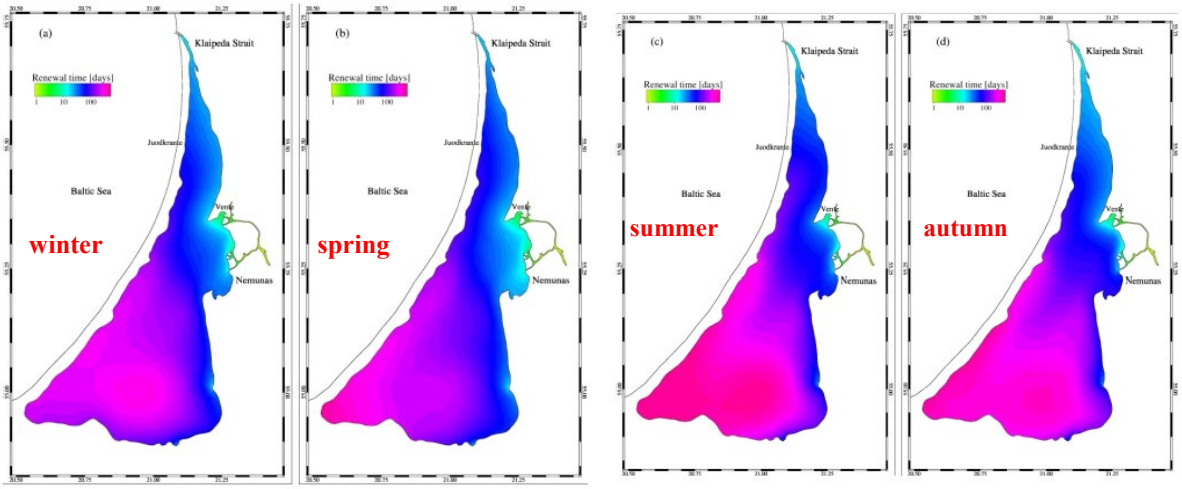

Figure 8.18. Seasonal renewal time maps averaged over the years 2004–2014 (from Umgiesser et al., 2016, Fig. 7).

The main composition of bottom sediments in the lagoon are sand and silt (Figure 8.19). Sediment transport prevails in the northern part of the lagoon, while the central portion is heterogeneous both in geomorphology and sediment type (fine sand, mixed with gravel and pebbles, peat and moraine) (Gasiūnaitė et al., 2008). In local depressions in the deeper western part of the lagoon a muddy bottom occurs (Pustelnikovas 1998).

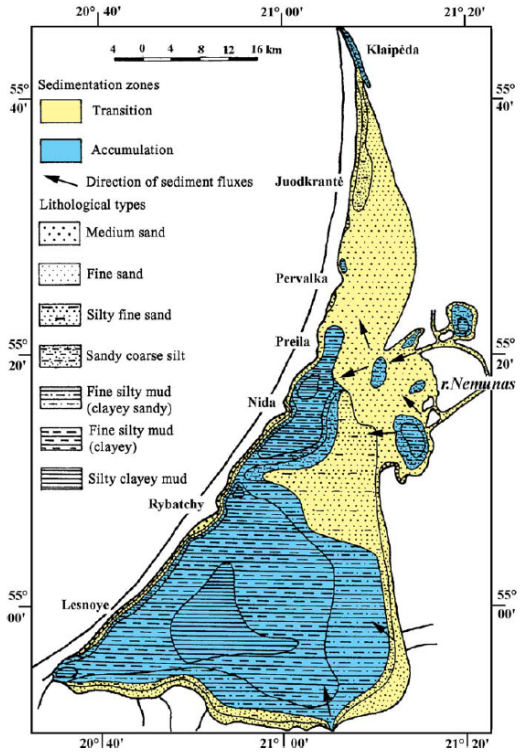

Figure 8.19. Transition-accumulation map based on in situ measured sediment characteristics and water depth for the whole Curonian Lagoon (from Ferrarin et al. 2008).

The oxygen concentration fluctuates spatially and temporally (both diurnally and seasonally) (Jurevičius, 1959): summer local anoxia may take place at night and low concentrations (<1.8 mg l^{-1}) were found during the ice cover period. The dynamics of nutrient loads are typical of temperate and boreal transitional waters with strong riverine inputs (Gasiūnaitė et al., 2008). The highest nutrients concentrations were observed in winter and early spring. The phosphate concentration decreases in April due to primary producer uptake and starts to increase in early summer due to decomposition of organic matter. The nitrogen concentration can decrease to zero in May. In particular, ammonium concentrations have no pronounced seasonal pattern, while nitrate concentration tends to increase from midsummer. The silica concentration is lowest during spring

after the diatom bloom, then remains low throughout the summer and starts to increase again in early autumn (Razinkovas and Pilkaityt 2002).

Phytoplankton and optical data

Phytoplankton blooms in the Curonian Lagoon have been tracked since the 1930s via synoptic sampling (Schmidt-Ries, 1940). Fresh-brackish species dominate the phytoplankton community of the Curonian Lagoon. Diatoms dominate the spring phytoplankton community, after which, following a short clear-water phase, cyanobacteria biomass increases (Gasiūnaite et al., 2005; Pilkaitytė and Razinkovas, 2007). *Stephanodiscus hantzschii*, *Diatoma tenuis*, *Aulacoseira islandica*, *Asterionella formosa* are the dominant diatom species during spring while the N-fixing cyanobacteria *Aphanizomenon flosaquae*, *Dolichospermum affine*, *D. flosaquae*, as well as other cyanobacteria such as *Microcystis aeruginosa*, *M. wesenbergii*, *M. viridis*, and *Planktothrix agardhii* contribute to the summer biomass peak (Pilkaitytė and Razinkovas, 2007; Gasiūnaite et al., 2008).

As reported in Vaiciute et al. (2021) and in Figure 8.20, the cyanobacteria scum events usually start in June–early July and ended in August–middle of September. The earliest start of a scum event, at the beginning of June, was observed in 1986, 2011, and 2015, while the latest scum event lasted until the beginning of November in the most recent year, i.e. 2018.

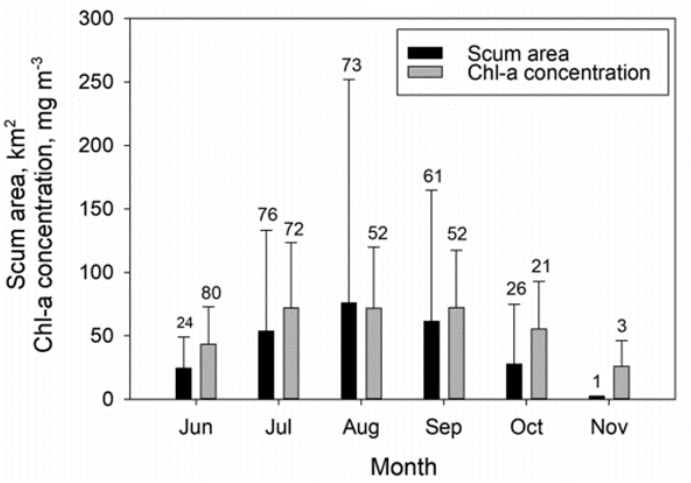

Figure 8.20. Monthly mean area covered by cyanobacteria scum (km^2) during the period from 1985 to 2018, and the monthly mean Chl-a concentration ($mg\ m^{-3}$) during the period from 2004 to 2018 in the Curonian Lagoon (from Vaiciute et al., 2021, Fig. 2D).

As reported in Vaiciute et al. (2021) and in Figure 8.21, cyanobacteria scums initially occurred around June, with the locations of occurrences mainly concentrated in the central and the southern part and much less frequently in the northern coastal regions of the lagoon. In summer, cyanobacteria scums frequently occurred in almost the entire lagoon. The scums were frequent in September, however they were mostly located in central and south-eastern parts. From October to November there was a gradual decrease in the number of cyanobacteria scums and they were more frequent in the central part close to the Nemunas river delta.

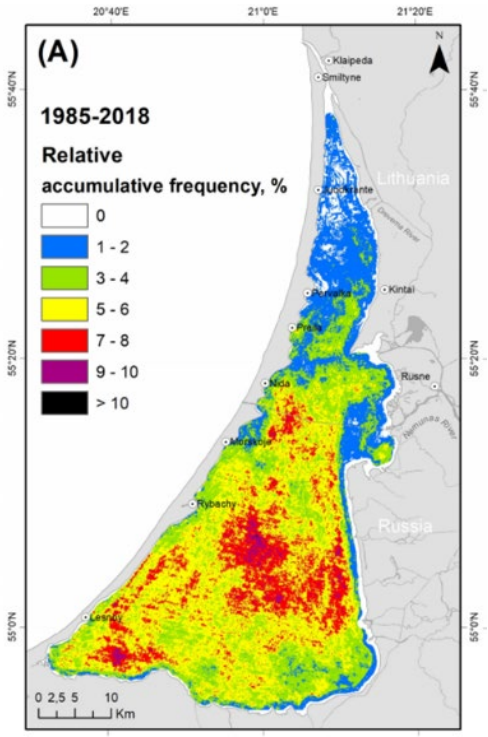

Figure 8.21. The relative accumulative frequency of cyanobacteria scum events (% of the total number of events) during the period of June–November from 1985 to 2018 (from Vaiciute et al., 2021 Fig. 5A).

An example of spatial differences of phytoplankton concentrations and distribution was reported in Figure 8.22, related to in situ activities performed during FP.7 INFORM project.

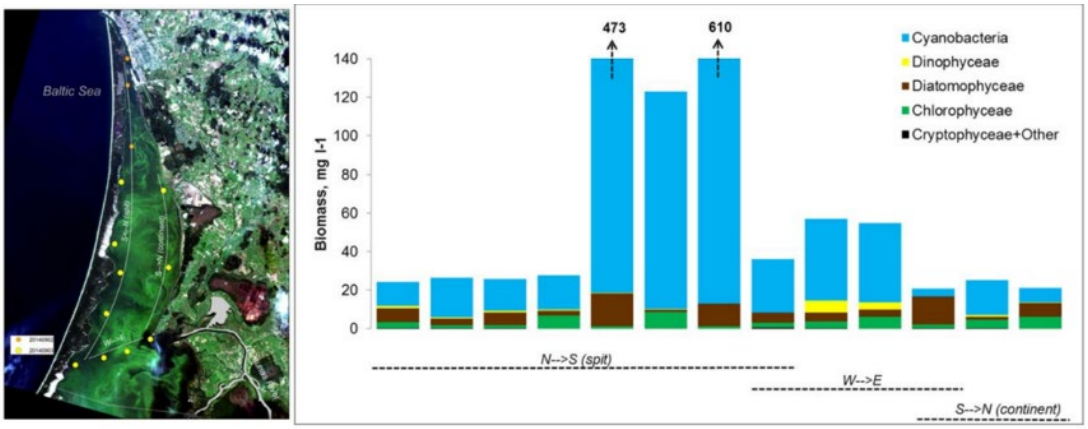

Figure 8.22. Spatial distribution of phytoplankton biomass (mg l^{-1}) in the Curonian Lagoon during 2-3 September 2014 (from INFORM DEL 4.6 Testing campaign in situ data).

The composition and abundance of phytoplankton and cyanobacteria in particular influence the Remote Sensing Reflectances (R*rs*) of the water, as reported in Bresciani et al. (2014) and in Figure 8.23: the *in situ* R*rs* change based on Chl-a concentrations and scum accumulation in particular in the RED-NIR region. The mean specific absorption coefficient of phytoplankton a*ph(λ) gathered from historical data collected in the Curonian Lagoon clearly show the high absorption due to cyanobacteria (Figure 8.24).

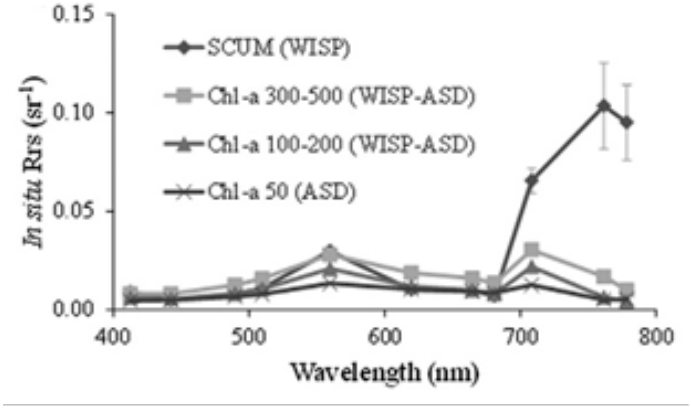

Figure 8.23: Rrs values measured in situ, resampled on MERIS bands, for different Chl-a concentrations (mg m^{-3}) and in association with a scum event. The spectra were acquired in 2009, 2011 and 2012 using ASD or WISP, or both (from Bresciani et al., 2014 Fig. 3a).

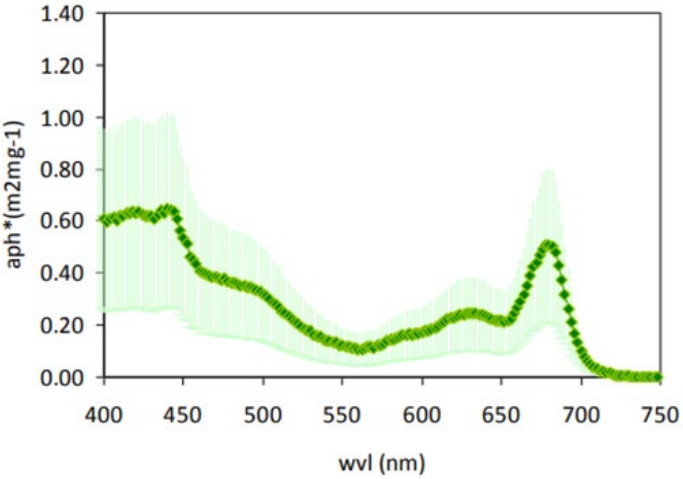

Figure 8.24. The mean specific absorption coefficient (with standard deviation) due to phytoplankton measured in Curonian Lagoon (from INFORM DEL 4.2 Existing in situ data and uncertainty quantification, airborne hyperspectral and synthetic satellite images).

Vaiciute et al. (2015) found empirical evidence that river discharge, the presence of phytoplankton, salinity, water temperature and wind determine the spatial and temporal CDOM concentration in the Curonian Lagoon. The mean CDOM concentration in the spring-summer period is 1.47±0.70 m^{-1}. During spring normally, the highest mean CDOM concentration was observed close to the rivers, Nemunas and Deimena, and lowest mean CDOM concentration was observed in the south-western part of the lagoon. Similar to the spring period, the mean CDOM concentration was higher in the regions where the rivers mainly influence water properties but the lowest mean CDOM concentration was observed in the northern part, where the Curonian lagoon is connected with the brackish waters of the Baltic Sea.

In the FP.7 INFORM project the historical data of CDOM collected in the Curonian Lagoon was used to evaluate the relation between slope and absorption of CDOM in different years and regions of the lagoon (Figure 8.25).

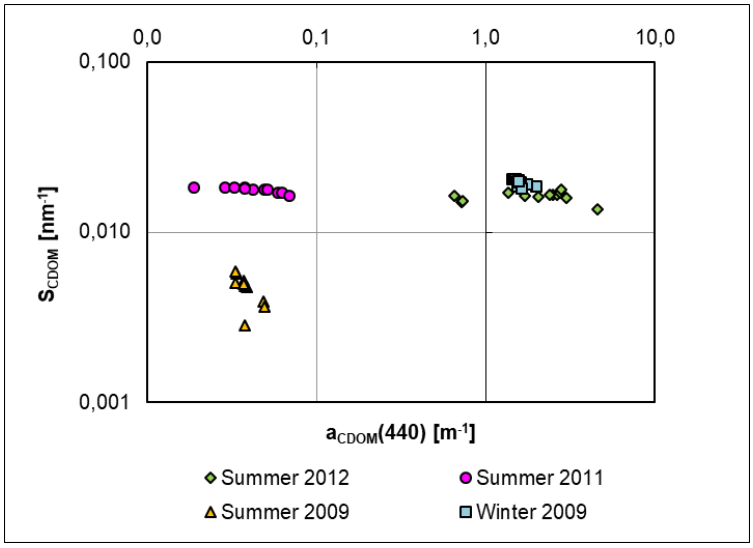

Figure 8.25. Seasonal slopes and absorption coefficients at 440 for CDOM.

Nutrient loads and runoff from the catchment

The Nemunas river catchment area (97924 km^2) is shown in figure 8.26. Agricultural activities affect hydrology and nutrient cycling within croplands by altering filtration, groundwater recharge, base flow, and run-off from catchments (Todd et al., 2007). The annual nutrient loads from the Nemunas river varied by up to 50% (2012-2016) and their concentrations underwent strong seasonality, with summer N and Si limitation (Vybernaite-Lubiene et al., 2018).

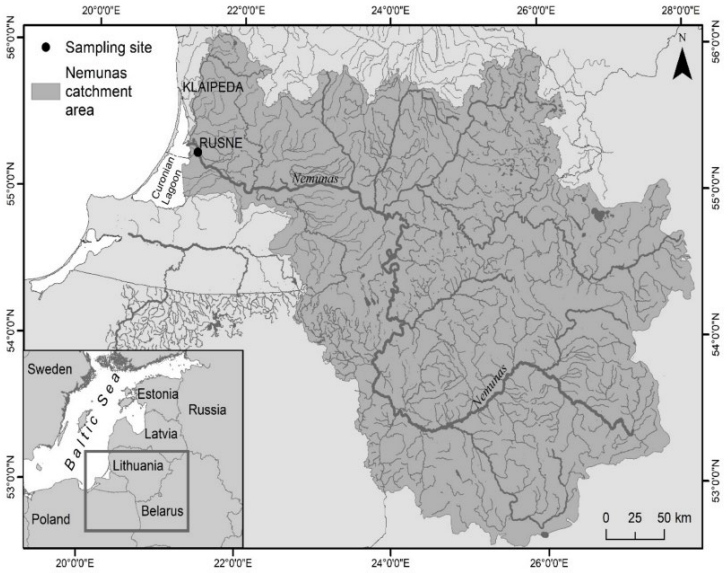

Figure 8.26. Map of the Nemunas river catchment area (97924 km^2; dark grey area) (from Vybernaite-Lubiene et al., 2018 Fig.1).

In Table 8.1 a summary of the published average annual discharge (from 16 to 21 km3 yr^{-1}) and nutrient loads (total nitrogen in the range between 37 and 58x10^3 t yr^{-1}; total phosphorous in the range 1.5 – 5.4x10^3 t yr^{-1}) to the Baltic Sea or at the mouth of the Nemunas river during the 1980-2016 period is reported (Vybernaite-Lubiene et al., 2018). Total silica was estimated in the range 50-70x10^3 t yr^{-1} during the 2012–2016 period (Vybernaite-Lubiene et al., 2018). The discharge from the Nemunas River displayed seasonal and interannual variability (2012-2016), with higher flows generally measured during colder months and lower flows measured during warmer months (Vybernaite-Lubiene et al., 2018, Fig. 8.27).

Table 8.1. Published average annual discharge and nutrient loads to the Baltic Sea or at the mouth of the Nemunas river during the 1980-2016 period. References: Stålnacke et al., 1999; Šileika et al., 2006 and 2013; Helsinki Commission, 2015; Vybernaite-Lubiene et al., 2018. (From Vybernaite-Lubiene et al., 2018).

Period	Flow ($km^3\ yr^{-1}$)	Nutrient Loads ($t \cdot yr^{-1}$)					DIN:DIP
		NO_3^-	NH_4^+	TN	DIP	TP	
1980–1993	20.5	31,650		58,340	4140	5410	8
1986–1991		9702	8601		4573		4
1992–1996		20,604	5983		969		27
1997–2002	16.6 *	25,048	2202		636		43
1997–2008	16.6 *			46,335		2635	
2000–2006	15.9 *			37,620			
2008–2010	18.3 *			41,546		1834	
2012–2016	16.4	21,429	995	44,208	561	1547	40

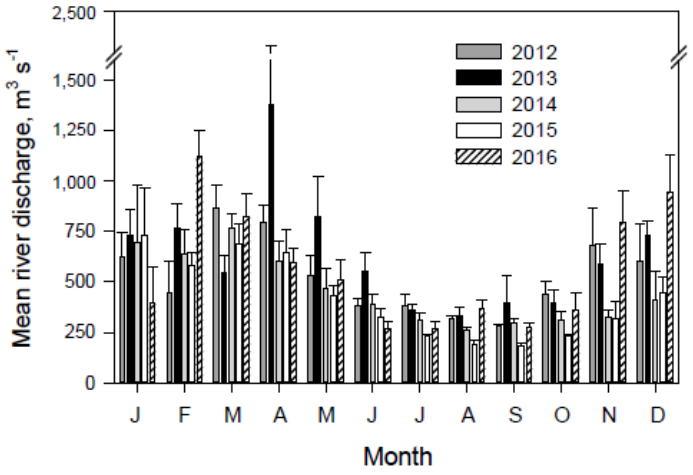

Figure 8.27. The monthly mean Nemunas River flow during 2012–2016 (from Vybernaite-Lubiene et al., 2018 Fig. 2a).

In the period 2012-2016, at the closing section of the river, the dissolved inorganic nitrogen and silica concentrations showed a strong seasonality, with spring/summer minima and autumn/winter peaks. Seasonal and interannual variations were shown by dissolved inorganic phosphorous (DIP) concentrations (Vybernaite-Lubiene et al., 2018). Only nitrate loads increased significantly, a trend that is opposite to the predicted trend and desired political actions (Bauer, 2015). A similar total N export from the river watershed compared to historical data (1986–2002) was due to agricultural practices change, while wastewater treatment plant (Figure. 8.28) improvements led to a ~60% decrease of P loads (Vybernaite-Lubiene et al., 2018).

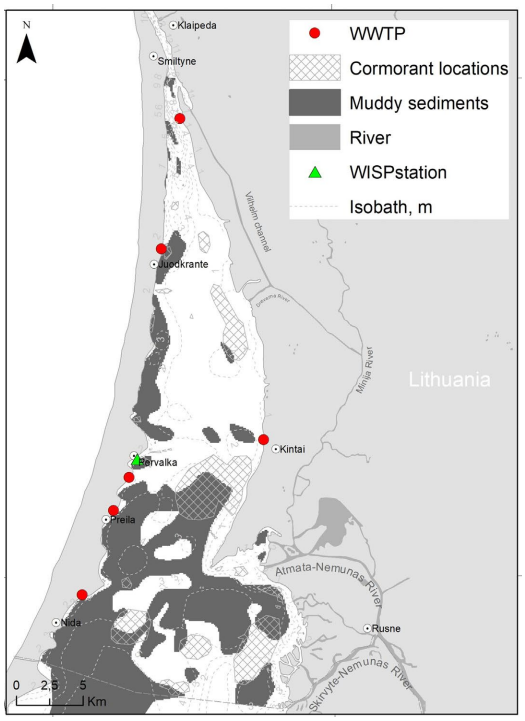

Figure 8.28. Maps of the wastewater treatment plants (WWTP; red dots) in the Lithuanian part of the Curonian Lagoon (from Vaiciute et al., 2021).

Agriculture and the associated conversion of pastures into croplands remain the main contributors of N loads transported by the Nemunas river according to recent inventories (Bauer, 2015). Nitrogen accumulation in soils due to intensive application of N fertilisers was favoured during the Soviet Union period thanks to the low cost of fertilisers. Such elevated background input may mask the expected positive effects of more sustainable agricultural practices (e.g., nutrient reduction). The changes in agricultural practices coincided with an increase in new subsidies for crops, causing an increase in fertiliser applications, after the entrance of Lithuania into the European Union (Vybernaite-Lubiene et al., 2018). A major fraction of this N (and P) is generated in the Belarus portion of the Nemunas catchment, while a minor fraction has a natural origin (Korth et al., 2013). Several studies have demonstrated that 14–88% of the total nitrogen loads and 27–89% of the total phosphorous loads were retained during their transport through the large Baltic lagoons (Grelowski et al., 2000; Vybernaite-Lubiene et al., 2017). Within lagoons, retention can be sometimes offset by cyanobacterial blooms, which result in large export of algal cells, and may induce bottom anoxia and favour P release from anoxic sediment and its transport to the Baltic Sea (Petkuviene et al., 2016; Vybernaite-Lubiene et al., 2017; Zilius et al., 2018).

8.5 Identification of under sampled regions

8.5.1 Satellite (Sentinel 2) and in situ match up analysis

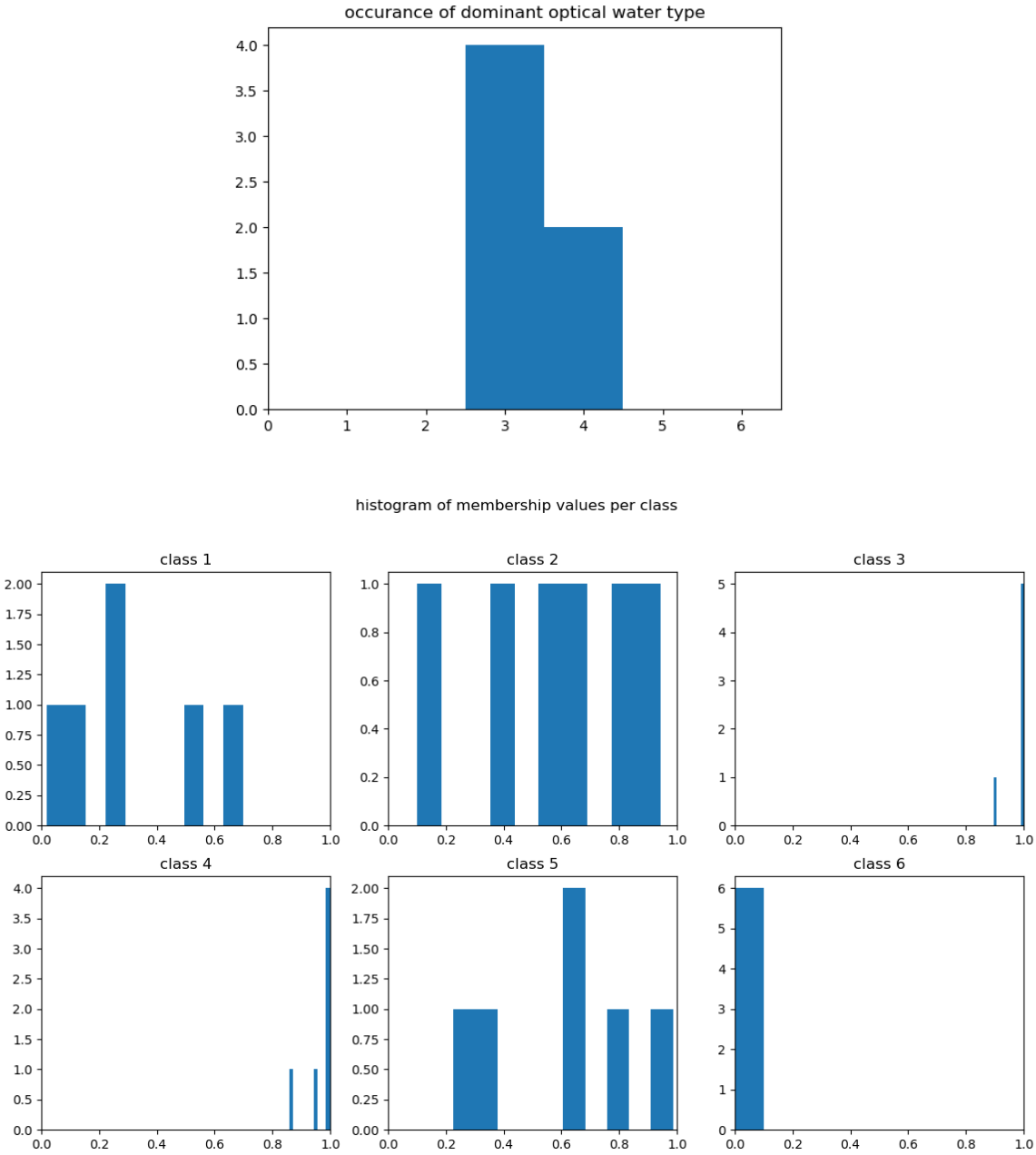

Figure 8.29: (top) Dominant optical water type and (bottom) histogram of membership values per class obtained for Curonian Lagoon.

8.6 Proposed ideal sampling time for year 2 (2021) in the Curonian Lagoon

- Time of sampling – July 2021
- Sampling platform availability – logistics arranged
- Campaign participants – CNR*, Klaipeda University

Table 8.2: Sentinel 3 passes over Curonian Lagoon in July 2021

	July (date)	July (time) UTC	August (date)	August (time) UTC
SENTINEL3	daily	08:30 – 09:30	daily	08:30 – 09:30

Table 8.3: Sentinel 2 passes over Curonian Lagoon in July 2021

Satellite platform	Orbit	Date	Time (UTC)
SENTINEL2A	31493	2021/07/03	9:45
SENTINEL2A	31536	2021/07/06	9:55
SENTINEL2A	31579	2021/07/09	10:05
SENTINEL2A	31636	2021/07/13	9:45
SENTINEL2A	31679	2021/07/16	9:55
SENTINEL2A	31722	2021/07/19	10:05
SENTINEL2A	31779	2021/07/23	9:45
SENTINEL2A	31822	2021/07/26	9:55
SENTINEL2A	31865	2021/07/29	10:05
SENTINEL2B	22556	2021/07/01	9:55
SENTINEL2B	22599	2021/07/04	10:05
SENTINEL2B	22656	2021/07/08	9:45
SENTINEL2B	22699	2021/07/11	9:55
SENTINEL2B	22742	2021/07/14	10:05
SENTINEL2B	22799	2021/07/18	9:45
SENTINEL2B	22842	2021/07/21	9:55
SENTINEL2B	22885	2021/07/24	10:05
SENTINEL2B	22942	2021/07/28	9:45
SENTINEL2B	22985	2021/07/31	9:55

8.7 Covid19 Mitigation: proposed essential measurements and USTIR support

University of Stirling will provide support in terms of instrumentation and post-sampling analysis (for sites that need support). In year 2 (2021) participation by USTIR in the sampling campaigns will be subjected to Covid19 travel restrictions. However, the plan is to replicate a small percentage of samples for Chl-a, TSM, PC and particulate absorption from all sites. Shipping of the samples to USTIR will be arranged accordingly. USTIR will arrange a shipment and a rota of required instrumentation, in association with FC.ID, across the different sites in Europe. Intercomparison experiments therefore are planned in year 3 (2022) with a possibility to participate onboard with a suite of USTIR instrumentation across the sites in the UK and Europe.

Table 8.4: proposed essential measurements and USTIR support. Sampling will be carried out in collaboration with Klaipeda University, Lithuania.

	Parameters to be measured (essentials in bold)	**Instrumentation/ Sample Analysis 2021**	**Instrumentation/ Sample Analysis 2022**
Biogeochemistry	Chlorophyll a, Chl-a	CNR	CNR
	Phycocyanin, PC	CNR	CNR
	Total Suspended Matter, TSM	CNR	CNR
AOPs	**Remote sensing reflectance, R_{rs}**	CNR (WISP) USTIR (TriOS)	CNR (WISP) USTIR (TriOS)
	Diffuse attenuation coefficient, K_d	CNR (Satlantic)	CNR (Satlantic)
	Secchi disk depth, Z_{SD}	CNR	CNR

IOPs	**Total absorption coefficient, a**	---	---
	Absorption coefficient of phytoplankton, a_{ph}	CNR	CNR
	Absorption coefficient of non-algal particles, a_{nap}	CNR	CNR
	Coloured dissolved organic matter, CDOM	CNR	CNR
	Backscattering coefficient, b_b	CNR	CNR
	Beam attenuation coefficient, c	---	---
Physical Parameters	Water temperature	CNR	CNR
	Salinity	CNR	CNR
	Turbidity	CNR	CNR
	Water depth	CNR	CNR
Atmospheric parameters	Wind speed	CNR	CNR
	Aerosol Optical Thickness, AOT	CNR (Microtops) USTIR (Microtops)	CNR (Microtops) USTIR (Microtops)

8.8 References

Bartoli M, Zilius M, Bresciani M, Vaiciute D, Vybernaite-Lubiene I, Petkuviene J, Giordani G, Daunys D, Ruginis T, Benelli S, Giardino C (2018). Drivers of cyanobacterial blooms in a hypertrophic lagoon. Frontiers in Marine Science 5, 434.

Bartoli M, Nizzoli D, Zilius M, Bresciani M, Pusceddu A, Bianchelli S, ... & Viaroli P (2021). Denitrification, Nitrogen Uptake, and Organic Matter Quality Undergo Different Seasonality in Sandy and Muddy Sediments of a Turbid Estuary. Frontiers in microbiology 11, 3524.

Bauer A (2015). Status of Nutrient Book keeping in the Baltic Sea Countries. Report Document Texte 95/2015. 2105. Available online: http://www.umweltbundesamt.de/publikationen/status-of-nutrient-bookkeeping-inthe-baltic-sea.pdf

Dailidienė I, Davulienė L (2008). Salinity trend and variation in the Baltic Sea near the Lithuanian coast and in the Curonian Lagoon in 1984–2005. J. Mar. Syst. 74, 20–29.

Daunys D (2001). Patterns of the bottom macrofauna variability and its role in the shallow coastal Lagoon. Summary of PhD dissertation, Klaip da University.

Ferrarin C, Razinkovas A, Gulbinskas S, Umgiesser G, Bliudziute L (2008). Hydraulic regime-based zonation scheme of the Curonian Lagoon. Hydrobiologia 611, 133–146.

Gasiūnaitė ZR (2000). Coupling of the limnetic and brackishwater plankton crustaceans in the Curonian lagoon (Baltic Sea). Int Rev Hydrobiol 85, 653–662.

Gasiūnaitė ZR, Daunys DS, Razinkovas A (2008). The Curonian Lagoon. Chapter 9 in: *Ecology of Baltic coastal waters*. Schiewer (eds) (2008). Berlin: Springer.

Grelowski A, Pastuszak M, Sitek S, Witek Z (2000). Budget calculations of nitrogen, phosphorus and BOD5 passing through the Oder estuary. J. Mar. Syst. 5, 221–237.

Helsinki Commission (2015). Updated Fifth Baltic Sea pollution load compilation (PLC-5.5). In Baltic Sea Environment Proceedings; Helsinki Commission: Helsinki, Finland, 2015.

Idzelytė R, Kozlov IE, Umgiesser G (2019). Remote sensing of ice phenology and dynamics of Europe's largest coastal lagoon (The Curonian Lagoon). Remote Sensing 11(17), 2059.

Idzelytė R, Mėžinė J, Zemlys P, Umgiesser G (2020). Study of ice cover impact on hydrodynamic processes in the Curonian Lagoon through numerical modeling. Oceanologia 62(4), 428-442.

Jakimavičius (2012). Doctor thesis, Kaunas, 2012.

Jurevičius R (1959). Hydrochemical characteristic of the Kurši Marios Lagoon (in Russian with German summary). In: Jankevi ius K, Gasi nas I, Gediminas A, Gudelis V, Kublickas A, Maniukas I (eds) Kurši Marios. Pergale˙, Vilnius, pp 69–108.

Korth F, Fry B, Liskow I, Voss M (2013). Nitrogen turnover during the spring outflows of the nitrate-rich Curonian and Szczecin lagoons using dual nitrate isotopes. Mar. Chem. 154, 1–11.

Petkuviene J, Zilius M, Lubiene I, Ruginis T, Giordani G, Razinkovas-Baziukas A, Bartoli M, (2016). Phosphorus Cycling in a Freshwater Estuary Impacted by Cyanobacterial Blooms. Estuar. Coast 39, 1386–1402.

Pustelnikovas O (1998). Geochemistry of Sediments of the Curonian Lagoon (Baltic Sea). Institute of Geography, Vilnius.

Razinkovas A, Bliudziute L, Erturk A, Ferrarin C, Lindim C, Umgiesser G, Zemlys P (2005). Curonian lagoon: a modelling study – Lithuania. In: Russo RC (ed) Modeling nutrient loads and response in river and estuary systems. Report No. 271., Committee on the Challenges of Modern Society, North Atlantic Treaty Organization, Brussels, pp 194–222.

Razinkovas A, Pilkaitytė R (2002). Factors limiting phytoplankton development in the Curonian lagoon (in Lithuanian). Sea Environ 1, 39–46.

Šileika AS, Stålnacke P, Kutra S, Gaigalis K, Berankiene L (2006). Temporal and spatial variation of nutrient levels in the Nemunas River (Lithuania and Belarus). Environ. Monit. Assess. 122, 335–354.

Šileika AS, Wallin M, Gaigalis K (2013). Assessment of nitrogen pollution reduction options in the river Nemunas (Lithuania) using FyrisNP model. J. Environ. Eng. Landsc. 21, 141–151.

Stålnacke P, Grimvall A, Sundblad K, Tonderski A (1999). Estimation of riverine loads of nitrogen and phosphorus to the Baltic Sea, 1970–1993. Environ. Monit. Assess. 58, 173–200.

Todd RW, Cole NA, Harper LA, Flesch TK (2007). Flux-gradient estimates of ammonia emissions from beef cattle feed yard pens. Am. Soc. Agric. Biol. Eng.

Umgiesser G, Zemlys P, Erturk A, Razinkova-Baziukas A, Mėžinė J, Ferrarin C (2016). Seasonal renewal time variability in the Curonian Lagoon caused by atmospheric and hydrographical forcing. Ocean Science 12(2), 391-402.

Vaičiūtė D, Bučas M, Bresciani M, Dabulevičienė T, Gintauskas J, Mėžinė J, ... & Bartoli M (2021). Hot moments and Hotspots of cyanobacteria hyperblooms in the Curonian Lagoon (SE Baltic Sea) revealed via remote sensing-based retrospective analysis. Science of The Total Environment 769, 145053.

Vybernaite-Lubiene I, Zilius M, Giordani G, Petkuviene J, Vaiciute D, Bukaveckas PA, Bartoli M (2017). Effect of algal blooms on retention of N, Si and P in Europe's largest coastal lagoon. Estuar. Coast Shelf Sci. 194, 217–228.

Vybernaite-Lubiene I, Zilius M, Saltyte-Vaisiauske L, Bartoli M (2018). Recent trends (2012–2016) of N, Si, and P export from the Nemunas River Watershed: Loads, unbalanced stoichiometry, and threats for downstream aquatic ecosystems. Water 10(9),1178.

Žaromskis R (1996). Oceans, Seas, Estuaries (in Lithuanian). Debesija, Vilnius.

Zilius M, Bartoli M, Bresciani M, Katarzyte M, Ruginis T, Petkuviene J, Lubiene I, Giardino C, Bukaveckas PA, de Wit R, Razinkovas-Baziukas A (2014). Feedback mechanisms between cyanobacterial blooms, transient hypoxia, and benthic phosphorus regeneration in shallow coastal environments. Estuaries and coasts 37(3), 680-94.

Zilius M, Vybernaite-Lubiene I, Vaiciute D, Petkuviene J, Zemlys P, Liskow I, ... & Bukaveckas PA (2018). The influence of cyanobacteria blooms on the attenuation of nitrogen throughputs in a Baltic coastal lagoon. Biogeochemistry 141(2), 143-165.

9 Summary

Table 9.1 represents the summary of the sampling campaigns planned for years 2 (2021) and 3 (2022).

Table 9.1: Sampling campaigns planned for years 2 (2021) and 3 (2022)

	Sampling 2021	**Sampling 2022**
Danube Delta	May/June	July/September
Elbe Estuary	June 28-July 3	April/May
Curonian Lagoon	July	May
Venice Lagoon	July/August	October/November
Tagus Estuary	September/October	April
Plymouth Sound	September/October	April/May

Table 9.2 and 9.3 represent the summary of the sampling strategy proposed for years 2 (2021) and 3 (2022) respectively. Intercomparison experiments are planned in year 3 (2022) with a possibility to participate onboard with a suite of USTIR instrumentation across the sites in the UK and Europe.

Table 9.2: Summary of the sampling strategy proposed for year 2 (2021)							
Category	Parameter	Plymouth	Curonian	Tagus	Venice	Danube	**Elbe**
Biogeochemistry	Chl-a	PML	CNR (spec.)	FC.ID (HPLC/spec.)	CNR (HPLC)	GeoEcoMar (spec.)	HZ Hereon (HPLC)
	PC	---	CNR	FC.ID	---	GeoEcoMar-USTIR	---
	TSM	PML	CNR	FC.ID	CNR	GeoEcoMar	HZ Hereon
AOPs	R_{rs}	PML (HyperSAS)	CNR(WISP), USTIR (TriOS)	FC.ID (TriOS) USTIR (TriOS)	CNR (WISP-3)	GeoEcoMar (TriOS)	HZ Hereon (TriOS) USTIR (TriOS)
	K_d	USTIR (USSIMO)	CNR (Satlantic)	FC.ID (PAR) USTIR (USSIMO)	USTIR (USSIMO)	USTIR (USSIMO)	USTIR (USSIMO)
	Z_{SD}	PML	CNR	FC.ID	CNR	GeoEcoMar	HZHereon
IOPs	a	USTIR (ac-s)*	---	USTIR (ac-s)*	---	---	HZ Hereon (ac-s)
	a_{ph}	PML (IS)	CNR (T)	FC.ID (T-R)	CNR-USTIR	GeoEcoMar-USTIR	HZ Hereon (IS)
	a_{NAP}	PML (IS)	CNR (T)	FC.ID (T-R)	CNR-USTIR	GeoEcoMar-USTIR	HZ Hereon (IS)
	CDOM	PML	CNR	FC.ID	CNR	GeoEcoMar	HZ Hereon
	b_b	PML (eco-bb3)	CNR (Hydroscat-6)	USTIR (sc-6)	---	USTIR (sc-6)	HZ Hereon (sc-6)
	c	USTIR (ac-s)*	---	USTIR (ac-s)*	---	---	HZ Hereon (ac-s)
Physical parameters	Water temperature	PML	CNR	FC.ID	CNR	GeoEcoMar	HZ Hereon (CTD)
	Salinity	PML	CNR	FC.ID	CNR	GeoEcoMar	HZ Hereon
	Turbidity	PML	CNR	FC.ID	CNR	GeoEcoMar	HZ Hereon
	Water depth	PML	CNR	FC.ID	CNR	GeoEcoMar	HZ Hereon
Atmospheric parameters	Wind speed	PML	CNR	FC.ID	CNR	GeoEcoMar	HZ Hereon
	AOT	PML (microtops) USTIR (microtops)	CNR (microtops) USTIR (microtops)	USTIR (microtops)	CNR (CIMEL)	USTIR (microtops)	USTIR (microtops)

Table 9.3: Summary of the sampling strategy proposed for year 3 (2022)							
Category	**Parameter**	**Plymouth**	**Curonian**	**Tagus**	**Venice**	**Danube**	**Elbe**
Biogeochemistry	Chl-a	PML	CNR (spec.)	FC.ID (HPLC/spec.)	CNR (HPLC)	GeoEcoMar (spec.)	HZ Hereon (HPLC)
	PC	---	CNR	FC.ID	---	GeoEcoMar-USTIR	---
	TSM	PML	CNR	FC.ID	CNR	GeoEcoMar	HZ Hereon
AOPs	R_{rs}	PML (HyperSAS)	CNR(WISP), USTIR (TriOS)	FC.ID (TriOS) USTIR (TriOS)	CNR (WISP-3)	GeoEcoMar (TriOS)	HZ Hereon (TriOS) USTIR (TriOS)
	K_d	USTIR (USSIMO)	CNR (Satlantic)	FC.ID (PAR) USTIR (USSIMO)	USTIR (USSIMO)	USTIR (USSIMO)	USTIR (USSIMO)
	Z_{SD}	PML	CNR	FC.ID	CNR	GeoEcoMar	HZ Hereon
IOPs	a	PML (ac-s) USTIR (ac-s)	USTIR (ac-s)	USTIR (ac-s)	CNR (ac-s) USTIR (ac-s)	USTIR (ac-s)	HZ Hereon (ac-s) STIR (ac-s)
	a_{ph}	PML (IS)	CNR (T)	FC.ID (T-R)	CNR-USTIR	GeoEcoMar-USTIR	HZ Hereon (IS)
	a_{NAP}	PML (IS)	CNR (T)	FC.ID (T-R)	CNR-USTIR	GeoEcoMar-USTIR	HZ Hereon (IS)
	CDOM	PML	CNR	FC.ID	CNR	GeoEcoMar	HZ Hereon
	b_b	PML (eco-bb3)	CNR (Hydroscat-6)	USTIR (sc-6)	---	USTIR (sc-6)	HZ Hereon (sc-6)
	c	PML (ac-s) USTIR (ac-s)	USTIR (ac-s)	USTIR (ac-s)	CNR (ac-s) USTIR (ac-s)	USTIR (ac-s)	HZ Hereon (ac-s) STIR (ac-s)
Physical parameter	Water temperature	PML	CNR	FC.ID	CNR	GeoEcoMar	HZ Hereon (CTD)
	Salinity	PML	CNR	FC.ID	CNR	GeoEcoMar	HZ Hereon
	Turbidity	PML	CNR	FC.ID	CNR	GeoEcoMar	HZ Hereon
	Water depth	PML	CNR	FC.ID	CNR	GeoEcoMar	HZ Hereon
Atmospheric parametrs	Wind speed	PML	CNR	FC.ID	CNR	GeoEcoMar	HZ Hereon
	AOT	PML (microtops) USTIR (microtops)	CNR (microtops) USTIR (microtops)	USTIR (microtops)	CNR (CIMEL)	USTIR (microtops)	USTIR (microtops)